DESIGN OF PRINTED PLANAR ANTENNA ARRAY WITH INTEGRATED FEED NETWORK

BY

SAEED AHMED AL DWEIK

A Thesis Presented to the

DEANSHIP OF GRADUATE STUDIES

KING FAHD UNIVERSITY OF PETROLEUM & MINERALS

DHAHRAN, SAUDI ARABIA

In Partial Fulfillment of the
Requirements for the Degree of

MASTER OF SCIENCE

In

ELECTRICAL ENGINEERING

MAY 2014

KING FAHD UNIVERSITY OF PETROLEUM & MINERALS

DHAHRAN- 31261, SAUDI ARABIA

DEANSHIP OF GRADUATE STUDIES

This thesis, written by **SAEED AHMED AL DWEIK** under the direction his thesis advisor and approved by his thesis committee, has been presented and accepted by the Dean of Graduate Studies, in partial fulfillment of the requirements for the degree of **MASTER OF SCIENCE IN ELECTRICAL ENGINEERING.**

Dr Mohammad S. Sharawi

(Advisor)

Dr. Ali Ahmad AL-Shaikhi
Department Chairman

Dr. Sheikh Sharif Iqbal
(Member)

Dr. Salam A. Zummo
Dean of Graduate Studies

Dr. Oualid Hammi
(Member)

27/5/14

Date

عمادة الدراسات العليا
DEANSHIP OF GRADUATE STUDIES

DESIGN OF PRINTED PLANAR ANTENNA ARRAY WITH INTEGRATED FEED NETWORK

SAEED AHMED AL DWEIK

ELECTRICAL ENGINEERING

MAY 2014

KING FAHD UNIVERSITY OF PETROLEUM & MINERALS
DHAHRAN- 31261, SAUDI ARABIA

DEANSHIP OF GRADUATE STUDIES

This thesis, written by **SAEED AHMED AL DWEIK** under the direction his thesis advisor and approved by his thesis committee, has been presented and accepted by the Dean of Graduate Studies, in partial fulfillment of the requirements for the degree of **MASTER OF SCIENCE IN ELECTRICAL ENGINEERING.**

_____
Dr Mohammad S. Sharawi
(Advisor)

_____
Dr. Ali Ahmad AL-Shaikhi
Department Chairman

_____
Dr. Sheikh Sharif Iqbal
(Member)

_____
Dr. Salam A. Zummo
Dean of Graduate Studies

_____
Dr. Oualid Hammi
(Member)

_____
Date

To My Mother and Father and Sisters and Brother

ACKNOWLEDGMENTS

With the name of Allah, the most Beneficent, the most Merciful Blessings and grace on Prophet Muhammad (PBUH).

First of all, I would like to thank my family, especially my mother, for their support and prayers. Without their prayers, I would not have been able to get admit in an international institute to earn a post-graduate degree. I would also like to thank Dr. Mohammad S. Sharawi for allowing me to pursue my master's thesis with him and providing complete support and guidance to accomplish my thesis requirements.. In addition to my supervisor, I would also like to thank my thesis committee members, Dr. Oualid Hammi and Dr. Sheikh Sharif Iqbal to rigorously review my thesis work.

TABLE OF CONTENTS

LIST OF TABLES

LIST OF FIGURES

ABSTRACT

Full Name : [Saeed Ahmed AL Dweik]

Thesis Title : [Design Of Printed Planar Antenna Array With Integrated Feed Network]

Major Field : [Electrical Engineering]

Date of Degree : [May 2014]

In this Thesis, an antenna array which is integrated with a feeding network on the same metalized PCB is designed, analyzed, and modeled then fabricated in order to be fixed in the wing structure of a UAV. The planar antenna array is chosen due to its high gain and ability to perform beam scanning. The integration of this array in the UAV structure will reduce drag and enhance the communication process.

In this work, a 2x6 planar antenna is designed on a 3 layer RO4350 substrate to obtain good efficiency. The overall dimensions of the integrated array were 459.04x161x1.27mm^3. The integrated feed network consisted of digitally programmable RF phase shifter and IC type power combiner. The antenna array maximum gain was 12dB, with an efficiency of 75% the gain will be 15.5dB, also the insertion for the antenna array gain becomes 15.5dB.

In addition to the feed network design presented, the new idea for implementing feed network with six phase shifters to supply twelve patch antenna elements is introduced to minimize the complexity of the feed network. Three methods were proposed by providing minimum number of phase shifters to feed the twelve elements for the antenna array, A comparison between them in terms of complexity and coverage is provided.

ملخص الرسالة

الاسم الكامل:سعيد أحمد عطا الدويك

عنوان الرسالة: تصميم مصفوفة هوائيات متكاملة مع شبكة تغذية

التخصص: الهندسة الكهربائية

تاريخ الدرجة العلمية: 13 مايو 2014

في هذه الرسالة مصفوفة هوائيات متكاملة مع شبكة تغذية بنفس الدائرة سيتم تصميمها و تحليلها ثم تصنيعها لكي يتم تثبيتها على جناح الطائرة بدون طيار. مصفوفة هوائيات ثنائية الأبعاد هي إختيرت لقدرتها التضخيميه ولقدرتها على تحريك الطيف الكهرومغناطيسي نحو إتجاهات معينة. وضع الهوائي داخل جناح الطائرة يقلل من التأثير الإحتكاكي للهوائي و بتالي يطيل من عمر الهوائي.

في هذا العمل مصفوفة هوائيات مكونة من2x6 عنصر هي صممت على لوح ثلاثي الطبقات و الذي شكل من مادة RO4350 و ذلك للحصول على هوائي ذات كفاءة عالية. الحجم الكلي للهوائي هو($459.04x161x1.27mm^3$). شبكة التغذية تتألف من دائرة متكاملة لتغير طور الإشارة و من دائرة متكاملة لتجميع الإشارات. الهوائي ذات الكفاءة المنخفضة يمكنه تزويد قدرة مقدارها (12dB) ولكن بعد تحسن الكفاءة لمقدار (75%) تم الحصول على قدرة للهوائي بمقدار(15.5dB). و الشبكة تقلص الإشارة الداخلة بمقدار (15.5dB).

تصميم جديد لشبكة التغذية و ذلك بتقليص عدد الدوائر المتكاملة و المستعملة لتغيير طور الإشارة إلى ست و حدات لتزويد إثنا عشر مصفوفة و ذلك لتقليص تعقيد الشبكة. يمكن بناء هذه الشبكة باستعمال أقل عدد ممكن من الدوائر و ذلك ياستعمال أربعة طرق. و يكمن تصميم شبكة تغذية باستعمال دائرتين متكاملتين.

CHAPTER 1

INTRODUCTION

Unmanned air vehicles (UAV) are widely used for exploration purposes that need remote sensing and monitoring for large areas. UAVs can be used in many sectors, but mainly they are used in military and civilian applications. They can be used in research purposes and meeting the increased demand for mapping areas of interest [1].

Since these UAVs are moving without pilot or operator, they should be able to move independently or in other word with some degree of autonomy in order to perform the assigned tasks efficiently. UAVs are controlled by automated blocks that can direct the vehicle to the right path and control its speed, altitude, centre of gravity and acceleration [2].

However, although a UAV can be controlled by an automated system, that can be controlled and motioned by an earth station operator to guide its behavior, update a target, handle the feedback signal or manage any unexpected action in real time of motion. The communication between the earth station and the vehicle is performed by using two different links, an uplink (control link) and downlink (data link). In general the uplink has narrower operating band width than the downlink, and in down link communication, sensory information is sent to the earth station [2].

The range of data link can be improved by using antenna arrays which can provide large amount of gain. Such arrays will increase the directivity of the antenna so narrower beams will be produced. Thus, the antenna array can increase the signal to noise ratio (SNR) and the throughput

for the overall system. Also phased array antennas play vital role in beam scanning for the radiation pattern of the antenna to follow and track a specific signal of interest. The antenna array can provide null steering with the radiation pattern provided by the antenna to overcome the interference signals coming from undesired sources [1].

This work proposes an antenna array which is integrated with its feed network in a single metalized sheet, and to be located on the wing structure of a UAV. Low profile antennas can overcome mechanical damages for UAV structures and also extra load can be fixed on the wing due to the light weight of the antenna. Moreover freedom in movement for UAV can be provided due to the lightness of the integrated unit. The antenna life time will be improved when it is located on the UAV wing structure that is because the antenna is located in safe environment [2].

The feed network is a major block that receives and processes the radio frequency (RF) input signal then distribute it among the different branches of the array. The feed network is composed of microstrip lines that are connected to power combiners/splitters before feeding the phase shifters. Phase shifters are the fundamental components in beam scanning process for the radiation pattern. The phase shifter changes the progressive phase between radiating elements in order to steer the beam to certain coordinates.

The impact of compact digitally controlled phase shifters that can be efficiently integrated with printed planar antenna array has hindered the use of phased array antenna in many applications, especially for those that are related to exploration purposes [1].

The work presented is divided into three stages. The first stage consists of the modeling and design of a 12 element planar printed patch antenna array using a 3-D full wave electromagnetic field solver. In addition the modeling and design of an RF feed network with 12 digitally

controlled phase shifters is included in this stage. The feed network was designed and optimized using Microwave Office (MWO).

The second stage consists of the layout of the antenna array as well as the feed network on a 3-layer PCB. The fabrication and testing of the antenna array performance and beam steering capability is included in this phase. Two measurement stages are required, laboratory testing for S-parameters measurements, and antenna pattern testing for gain pattern and beam steering verification. The third stage is concerned with coming up with a low complexity feed network with minimum number of phase shifters and assess its performance.

1.1 Work Objectives

The objectives of this work are:

1. To design, simulate and implement a planar antenna array of 12-elements on a single board and with a single antenna efficiency of at least 75%. This antenna is to be installed within the wing structure of a small UAV to enhance its communication link performance.
2. To design, simulate and implement a digitally controlled RF feed network to provide beam steering capability to the 12 element antenna array.
3. To integrate the antenna array and its feed network on a single PCB with minimum weight and characterize its performance.
4. To come up with a minimum number phase shifter design that can provide beam steering capabilities that cover the foot print areas below the UAV wing for minimum cost architecture.

1.2 Thesis Organization

This thesis is organized and presented in seven chapters. Chapter 1 includes, Introduction, thesis objectives and the thesis organization. Chapter 2 includes the theoretical background. Chapter 3 presents the literature review. Chapter 4 shows the design methodology. Chapter 5 presents simulation and measurement results. Chapter 6 investigates the minimum number of phase shifters that can be used in the proposed feed network. Finally Chapter 7 includes the conclusion and future work.

CHAPTER 2

THEORITICAL BACKGROUND

An Antenna is considered as the eye or ear for all communication systems [3]. The antenna plays vital role in the communication process which means that any wireless communication system cannot work without an antenna for transmission and reception. So many definitions were given to it. An antenna is defined by Webster's Dictionary as "a rod or wire for radiating or receiving radio waves". While in IEEE standard it is defined as "a means for radiating or receiving radio waves"[4]. The antenna is defined also as a transducer that is used to transfer between two energy forms electrical and electromagnetic.

Mainly our goal is to have an antenna with maximum gain, small size with wide bandwidth. In general, the radiation pattern, gain and the operating bandwidth can be considered as the main parameters for any antenna in any application. The organization of this chapter is as follows, we will start with antenna parameters, then a little about the microstrip patch antenna, antenna arrays, basics of power splitter/combiner, phase shifters and finally the basics of microcontrollers (Ardino Mega 2560).

2.1 Antenna Parameters

In this section the antenna parameters, and their definitions are discussed.

2.1.1 Radiation Pattern

It is defined as a mathematical function or graphical representation for the radiation properties of an antenna where this parameter can be considered in the far field space as can be shown in Figure 2.1[3]. Radiation properties that can be described by the radiation pattern are power density, field intensity, wave polarization, directivity and the gain.

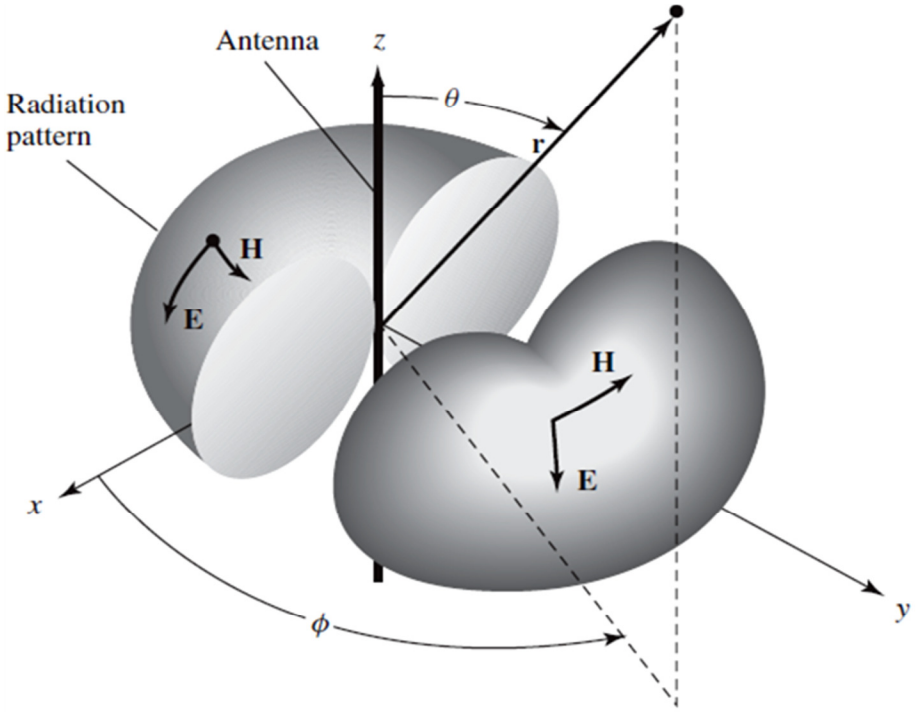

Figure 2.1: Radiation Pattern [3]

2.1.2 Reflection Coefficient

The reflection coefficient is defined as ratio between the amplitude of the reflected voltage wave (Vo-) to the amplitude of the incident voltage wave(Vo+) as shown in equation (2.1) [5].

$$\Gamma = \frac{Vo^-}{Vo^+} = |S_{11}| \quad (2.1)$$

2.1.3 Half Power Beamwidth (HPBW).

The half power beamwidth is defined as the surface that includes the direction of the maximum of a radiation pattern limited by 3dB point [4]. It is also can be describe as the angle between the two points that are 3dB (in dB scale) less than the maximum point in the radiation field as can be shown in Figure 2.2. HPBW is considered as a very important parameter to describe the performance of any antenna. For the two dimension a normalized field pattern as shown in Figure 2.3. The two dimensional normalized power pattern is shown in Figure 2.4.

2.1.4 Directivity.

The directivity is the ratio between the radiation intensity in a certain direction to the average radiation intensity [4]. The average radiation intensity is the total power radiated from antenna divided by 4π. In other word the directivity for a directive antenna the ratio between the radiation intensity in a certain direction to the radiation intensity that is produced by an isotropic antenna. Equation 2.3 can be used for calculating the directivity.

$$D = \frac{U_{Max}}{U_o} = 4\pi \frac{U_{Max}}{P_{rad}} \quad (2.3)$$

Where D is the Directivity, U_{max} is the maximum radiation intensity (W/unit solid angle), U_o is the radiation intensity of isotropic source (W/unit solid angle), P_{rad} is the total radiated power (W).

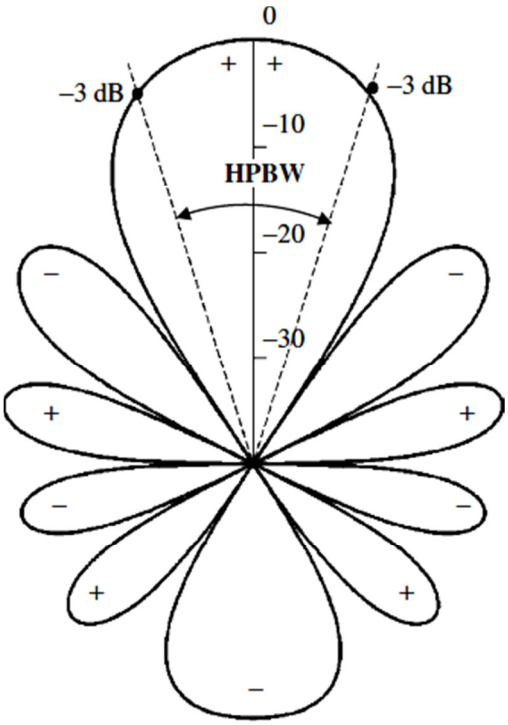

Figure 2.2: The half power beam width 2-D normalized power pattern in dB [3]

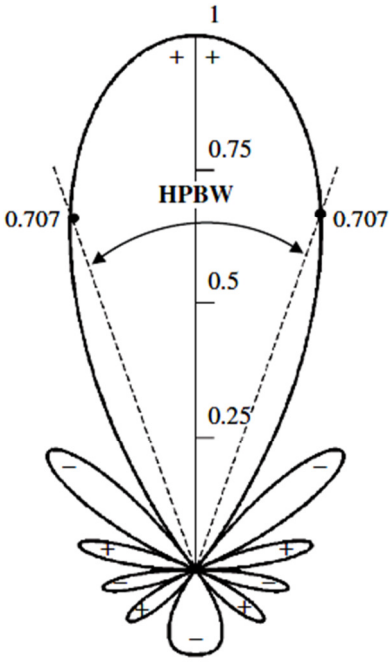

Figure 2.3: Normalized field pattern in linear scale [3]

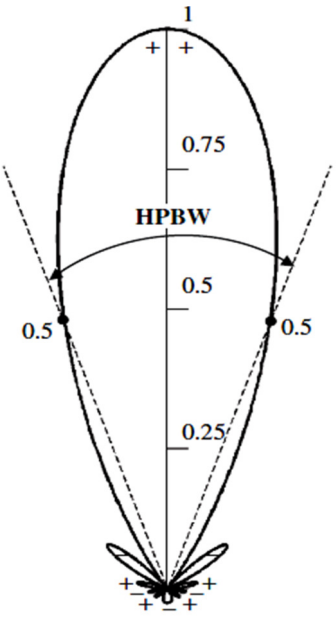

Figure 2.4: Normalized power pattern in linear scale [3]

2.1.5 Antenna Efficiency.

The antenna is the ratio between the provided power to the antenna to that actually radiated. It is a measure of antenna losses.

The losses in antenna can be classified into two categories

1. Losses due to reflection.
2. Conduction and dielectric losses.

The total efficiency is shown in equation (2.4)

$$e_o = e_r e_{cd} \tag{2.4}$$

Where, e_o is the total efficiency, e_r is the reflection efficiency which is showing the mismatch effect = $(1-|\Gamma|^2)$, e_{cd} is the antenna radiation efficiency (due to conduction and dielectric losses).

2.1.6 Gain.

The gain is a very important parameter that has to be considered when evaluating any antenna. The antenna gain is the ratio of field intensity in certain direction to the field intensity that would be produced by an isotropic source due to the same input [4]. The radiation intensity corresponding to the isotropically radiated power is equal to the power accepted (input) by the antenna divided by 4π [4]. The gain is equal to the directivity multiplied by the efficiency as shown in equation (2.8).

$$G = 4\pi \frac{U_{max}}{P_{in}} \tag{2.5}$$

If we replace U_{max} by $\frac{DP_{rad}}{4\pi}$

Then

$$G = D\frac{P_{rad}}{P_{in}} \tag{2.6}$$

$$e_{cd} = \frac{P_{rad}}{P_{in}} \tag{2.7}$$

So equation (2.6) will be

$$G=e_{cd}D \tag{2.8}$$

2.2 Microstrip Antennas

In many applications related to aircraft and space navigation, antennas with low profile, ease of installation and low fabrication costs are required. So, to satisfy these requirements, Microstrip antennas are usually chosen. In addition to these features, microstrip antennas can fit with planar and non-planar surfaces, are easy to design and analyze, can be integrated easily with other microstrip circuits and can provide linear and circular polarization. But such antenna suffers from, low efficiency, low power, narrow bandwidth and polarization impurity.

A Microstrip patch antenna consists of a thin metal layer called the patch on top of a substrate material (a dielectric) and a bottom metallic layer. The bottom metal plate is extended more than

the top one (i.e patch) to form what we can call a ground plane. The top metallic patch will operate as a radiating element as shown in Figure 2.5.

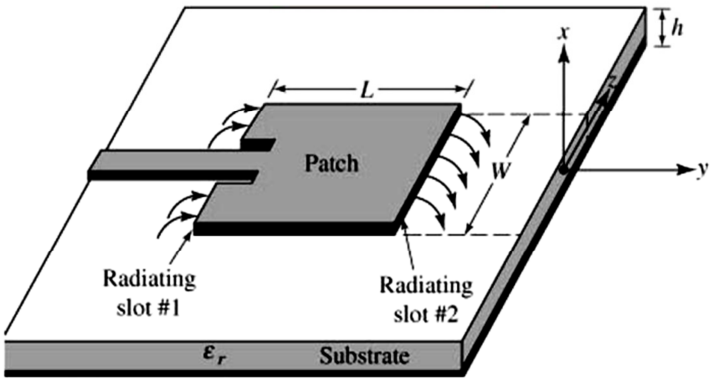

Figure 2.5: Basic structure of a microstrip antenna [3]

The dimensions of the patch antenna are proportional to the frequency of operation, so for this reason this type of antenna can be considered as a resonant antenna. Patch antennas can be manufactured in many shapes such as square, rectangular, circular, elliptical, triangular, circular ring and disc sector. The patch antenna is designed to have its radiation pattern normal to the patch or in other words, at broadside. This can be achieved by certain selection of the mode of operation for the radiating element. Using a different excitation mode, the patch can radiate at the end fire direction.

The substrate layer which is sandwiched between two parallel plates (radiating patch and ground plane) is made up of dielectric material with dielectric constant that varies between ($2<\varepsilon<12$) and with thickness that varies between ($0.003\lambda_0<h<0.05\lambda_0$), where λ_o is the free space wavelength [4].

After exciting the patch antenna, charge will be accumulated at the bottom of the patch and the ground plane as well. Attraction and repulsive forces between charges under the bottom of patch and the ground plane will push the charges towards the edges of the patch. These are the source of fringing fields. The radiation created from the patch antenna can be done due to the fringing field as can be shown in Figure 2.6.

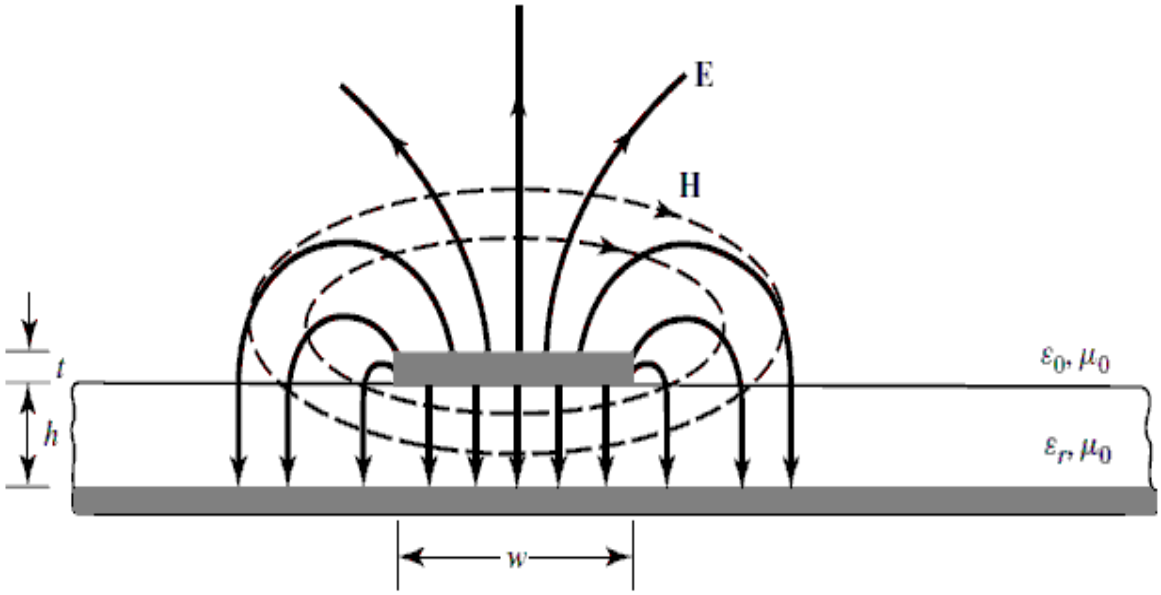

Figure 2.6: : Basic Concept for fringing field [4].

The ratio between the patch length to height is increased as the fringing field decreases. The wavelength in the microstrip line can be given by [4].

$$\lambda = \frac{\lambda_o}{\sqrt{\epsilon_{r_{eff}}}} \tag{2.9}$$

The effective permittivity (ε_{reff}) of microstrip line can be given by the following equation [4]

$$\varepsilon_{reff} = \frac{\varepsilon_r + 1}{2} + \frac{\varepsilon_r - 1}{2}\left(1 + 12\frac{h}{w}\right)^{-\frac{1}{2}} \qquad (2.10)$$

Where the wavelength in free space is, ε_r is the dielectric constant for substrate material, ε_{reff} is the effective dielectric constant, w is the width of the patch antenna, and h is the substrate height. Microstrip antenna behavior can be explained in many ways, but mainly three methods are widely used:

1- Transmission line method.

2- Cavity model.

3- Full wave method.

The transmission line method will be discussed in the next section, from which design formula can be derived, that can be used and then optimized using full wave field solvers.

2.3 Transmission Line Model

In this section the microstrip transmission line model will be used in order to find the required dimensions of a patch antenna (width and length). It is important to define the frequency of operation, dielectric constant for the substrate material used and the substrate height. To design a patch antenna for a specific frequency, the following procedure should be followed [5]:

- Find the width of the patch by using

$$w = \frac{1}{2 f_r \sqrt{\mu_o \varepsilon_o}} \sqrt{\frac{2}{\varepsilon_r + 1}} = \frac{\upsilon_o}{2 f_r} \sqrt{\frac{2}{\varepsilon_r + 1}} \qquad (2.11)$$

Where υo is the free space velocity, fr is the resonant frequency, ε_r is the dielectric constant for the substrate material.

- Find the effective dielectric constant from equation 2.10
- Find the change in length due fringing from [5]:

$$\frac{\Delta L}{h} = 0.412 \frac{\left(\varepsilon_{reff} + 0.3\right)\left(\frac{w}{h} + 0.264\right)}{\left(\varepsilon_{reff} - 0.258\right)\left(\frac{w}{h} + 0.8\right)} \qquad (2.12)$$

Then,

- find the length of the patch (L) [5]:

$$L = \frac{1}{2 fr \sqrt{\varepsilon_{reff} \mu_o \varepsilon_o}} - 2\Delta L \qquad (2.13)$$

$$L_{eff} = L + 2\Delta L \qquad (2.14)$$

Where ΔL is the length extension for the patch dimension.

2.4 Antenna Arrays

With the growth of communication systems in recent decades, it has been required to increase the directivity for the wave propagating in free space in order to increase the range of the communication system. This can be achieved by using antenna arrays instead of individual ones to increase the antenna gain and its directivity as well. Single radiators produce signals with wide beam width and low directivity. So to overcome this problem, assembly of elements in an arranged way will produce an array. By using antenna arrays, the produced beam will be more directive compared to that produced by a single element at the expense of the size of the antenna. The most directive antenna can be achieved if and only if, the fields from each radiator in the array are added up in the desired direction, and in the same time cancel out in other directions. The radiation pattern of the array can be controlled by one of the following techniques:

1. The shape of array configuration (linear, planar, circular and spherical).
2. Interspace distance between adjacent elements.
3. Excitation amplitude for each element.
4. Excitation phase for each element.
5. The radiation pattern of the individual element.

The overall field of an array antenna can be formed using equation (2.15)

$$E(\text{Total})=E(\text{Single element at reference point})\text{x}[\text{Array Factor}] \qquad (2.15)$$

Which means the array radiation pattern is equal to the radiation pattern of the single antenna element times the array factor. That is a function of the array geometry and excitation and is valid when low coupling is achieved.

2.5 Uniform Array Antenna

To create a uniform array antenna, the excitation amplitude for all the source elements should be equal as well as the inter space distance between the elements of array. However, the array can be classified according to the geometry structure of the uniform array such as linear array antenna (one dimension), planar array (two dimension), and circular [4].

2.5.1 Linear Antenna Array

The antenna elements are arranged in one dimension in this configuration. In this array, the inter space distance between adjacent elements is the same, and all radiating elements of the array have the same amplitude.

As the inter space distance between adjacent elements decreases to less than λ/2, the half power beam width will get wider and the directivity will be smaller [3]. As the inter space distance is larger than λ/2, side lobes increase to values near to the maximum lobe which decreases the power efficiency. Figure 2.7 shows a linear antenna array placed along the x-axis with inter-element spacing of d_x.

The array factor for an antenna array with linear geometry can be written as,

$$AF = 1 + e^{j\psi} + e^{j2\psi} \ldots + e^{jN\psi} \qquad (2.16)$$

Where

$$\psi = kd\cos\theta + \beta \tag{2.17}$$

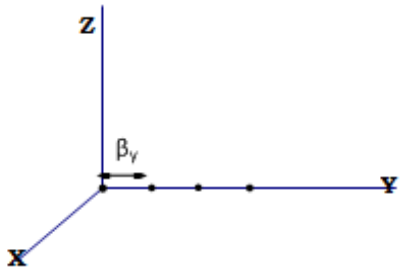

Figure 2.7: Linear Array constellation diagram

Where k is the wave number, $k=\frac{2\pi}{\lambda}$, d is the distance between two adjacent elements in the array (in our case it is λ/2), β is progressive phase between adjacent elements, ψ is the phase difference of fields between adjacent elements and N is the number of elements in the array.

After simplifications (2.16) can be written as [4]

$$AF = \frac{1}{N}\frac{\sin\frac{N\psi}{2}}{\sin\frac{\psi}{2}} \tag{2.18}$$

The progressive phase for array elements can be considered as a critical factor to steer the beam to any desired direction. To illustrate this, three cases can be considered.

- **Case-1 Broadside Array**

In this case, the maximum lobe of the radiated beam from the antenna array is directed to the normal direction with respect to the axis of radiation as can be shown in the Figure 2.8.

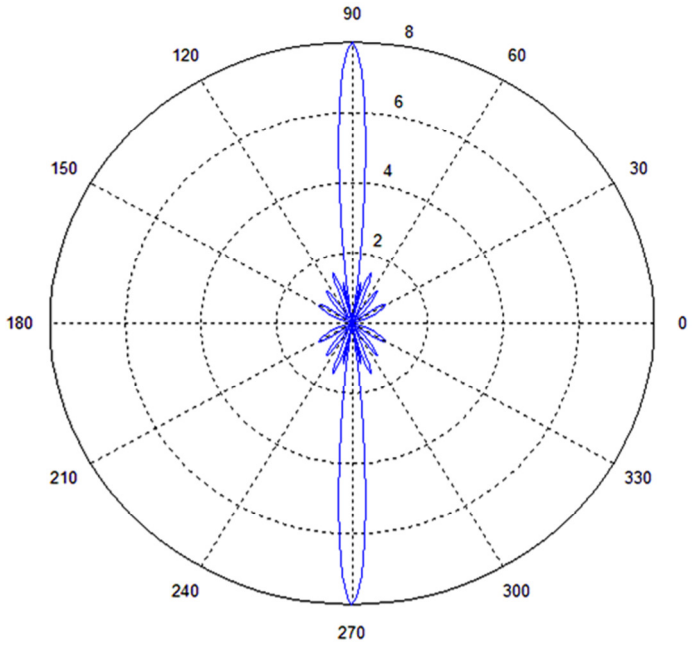

Figure 2.8: Radiation pattern for Broadside array (Sources in phase)

To avoid grating lobes in other directions, the distance between adjacent elements should not be multiple of wavelength (nλ). To achieve broadside radiation, one need to find the value of the progressive phase that will point the beam towards θ=90 (i.e if array is placed at z axis then the broadside will be at x-y plane), thus

$$\psi = kd \cos \theta + \beta = 0$$

So for broadside β=0

Substitute in equation (2.18)

$$AF = \frac{1}{N} \frac{\sin \frac{Nkd \cos\theta}{2}}{\sin \frac{kd \cos\theta}{2}} \qquad (2.19)$$

- **Case-2 End Fire Array**

In this case, the direction of the beam radiated from antenna array can be steered toward the axis of antenna array or in other word to $\theta = 0$ or $\theta = 180$. As shown in Figure (2.9) if the maximum required is to be directed toward θ=0

θ=0 ⟹ β=-kd

$$\psi = kd(\cos\theta - 1) \qquad (2.20)$$

θ=180 ⟹ β=kd

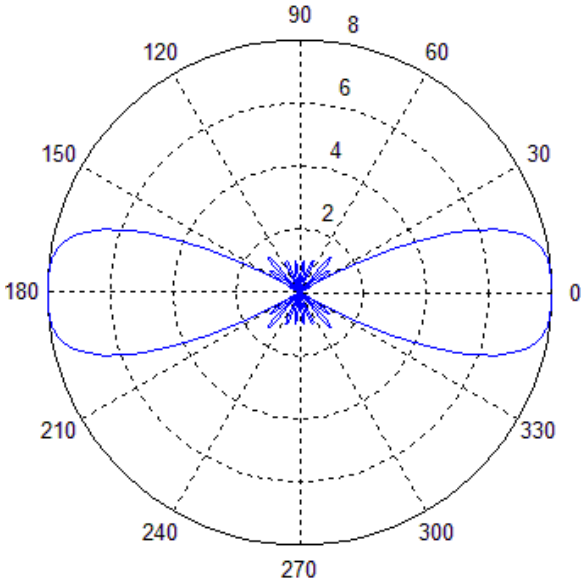

Figure 2.9 : Radiation pattern for end fire array

and (2.18) will be

At θ=0

$$AF = \frac{1}{N} \frac{\sin \frac{Nkd(\cos\theta - 1)}{2}}{\sin \frac{kd(\cos\theta - 1)}{2}} \tag{2.22}$$

at θ=180

$$AF = \frac{1}{N} \frac{\sin \frac{Nkd(\cos\theta + 1)}{2}}{\sin \frac{kd(\cos\theta + 1)}{2}} \tag{2.23}$$

- **Case-3 Phased Array**

In this case, the direction of the beam radiated from antenna array can be steered toward any point according to the value of the phase excitation between the antenna elements as in Figure 2.10. The phase excitation mainly depend on the initial value of theta θ_0.

$\theta = \theta_0$. $\beta = -kd \cos\theta_0$.

and (2.18) will becomes

At $\theta=\theta_o$

$$AF = \frac{1}{N} \frac{\sin \frac{Nkd(\cos\theta - \cos\theta_o)}{2}}{\sin \frac{kd(\cos\theta - \cos\theta_o)}{2}} \tag{2.24}$$

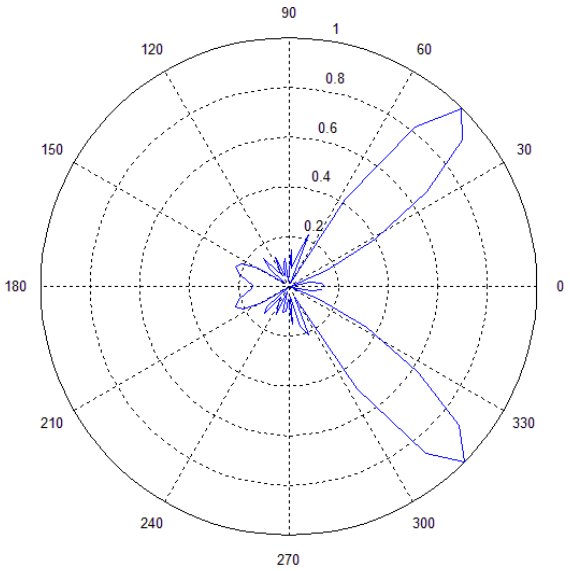

Figure 2.10 : Radiation pattern for phased array antenna at θo=45^{o}

2.5.2. Planar Antenna Array

The elements of antenna array can be assembled in a rectangular configuration to compose what is called a planar array. The beam produced by the planar array has two degrees of freedom. In other words, - the beam scanning for any field produced by the planar antenna array have coordinates in theta and phi as well. The progressive phase for the planar array changes in the two dimensions (i.e x and y) independently. Figure 2.11 shows the geometry of a planar array [4].

For a planar array the normalized array factor can be written as [4],

$$AF = \frac{1}{M}\left(\frac{\sin\frac{M\psi_x}{2}}{\sin\frac{\psi_x}{2}}\right)\frac{1}{N}\left(\frac{\sin\frac{N\psi_y}{2}}{\sin\frac{\psi_y}{2}}\right) \qquad (2.25)$$

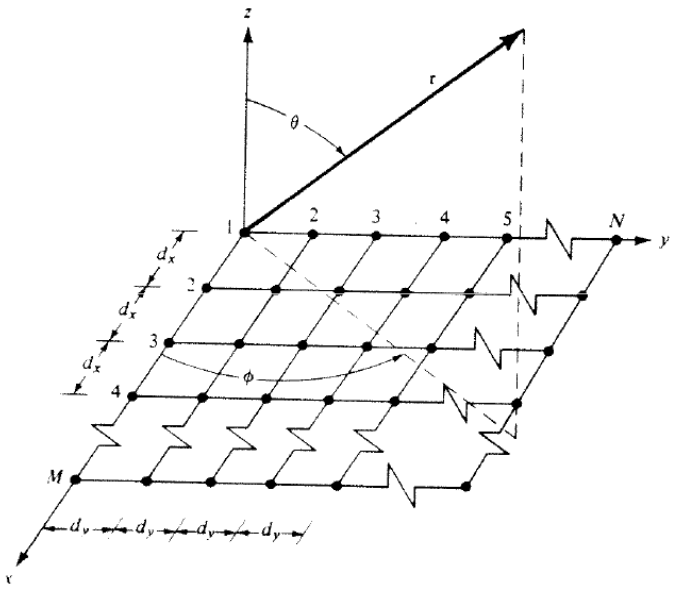

Figure 2.11: Planar array configuration [4].

$$\psi_x = kd_x \sin\theta \cos\phi + \beta_x \tag{2.26}$$

$$\psi_y = kd_y \sin\theta \cos\phi + \beta_y \tag{2.27}$$

$$\beta_x = -kd_x \sin\theta_o \cos\phi_o \tag{2.28}$$

$$\beta_y = -kd_y \sin\theta_o \sin\phi_o \tag{2.29}$$

2.6 Power Combiner/Splitter

The power combiner/splitter is a microwave passive device which can be used for power combining or power splitting. The power combiner can combine multiple input signals into individual ones, while the power splitter divides the input signal into multiple output signals. The combiner/splitter can be three terminals, four terminal or more. The example of three-terminal

can have a T shape, which means one input and two outputs. Four terminal power combiner/splitter like a hybrid network can produce identical output power (In case of power splitter) but with difference in phase between the two outputs, either 90 or 180 depending on the type of the hybrid network. Some basic properties of three-terminal and four-terminal networks will be discussed in the following sections based on [6].

2.6.1 Three-Terminal Networks (T-Junction)

By utilizing the scattering matrix, the properties of these networks can be defined. As shown in the Figures 2.12, the three terminal network can operate as a power splitter (Figure 2.12) when the input signal is divided into two signals with same phase. The three-terminal network can operate as a power combiner when the input signals are combined to have one signal at the output as shown in Figure 2.13.

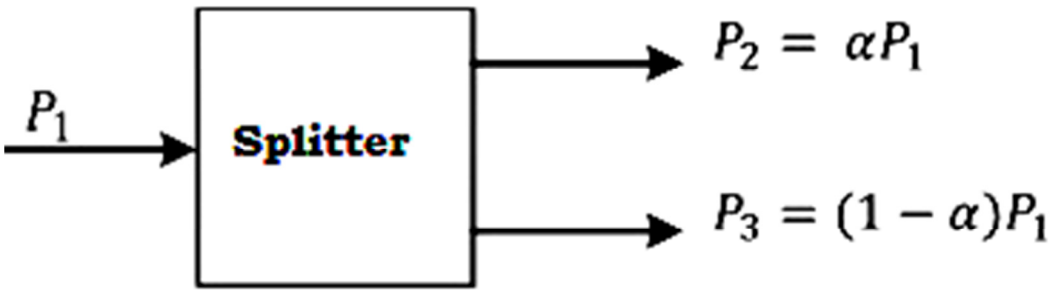

Figure 2.12 Power Splitter [6]

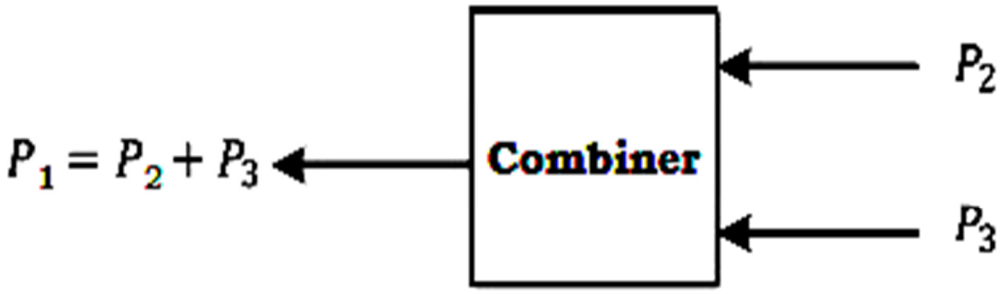

Figure 2.13 Power Combiner [6]

The scattering matrix for a three port network (T-Junction) will be represented as [6]

$$[S] = \begin{bmatrix} S11 & S12 & S13 \\ S21 & S22 & S23 \\ S31 & S32 & S33 \end{bmatrix} \tag{2.30}$$

If three port network is nonreciprocal, then $S_{xy} \neq S_{yx}$. And if all terminals are matched properly then $S_{xx}=0$, and the network is lossless then,

$$[S] = \begin{bmatrix} 0 & S12 & S13 \\ S21 & 0 & S23 \\ S31 & S32 & 0 \end{bmatrix} \tag{2.31}$$

If the network is lossless network, [*S*] should be unitary then

$$S^*_{31}S_{32}=0 \tag{2.32}$$

$$S^*_{21}S_{23}=0 \tag{2.33}$$

$$S^*_{12}S_{13}=0 \tag{2.34}$$

$$|S_{12}|^2+|S_{13}|^2=1 \quad (2.35)$$

$$|S_{21}|^2+|S_{23}|^2=1 \quad (2.36)$$

$$|S_{31}|^2+|S_{32}|^2=1 \quad (2.37)$$

These equations (2.32) to (2.37) can satisfied in one of two ways

$S_{12}=S_{23}=S_{31}=0$, $|S_{21}|=|S_{32}|=|S_{13}|=1$.

or

$S_{21}=S_{32}=S_{13}=0$, $|S_{12}|=|S_{23}|=|S_{31}|=1$

2.6.2 Four Terminals Networks

When all terminals are matched and the matrix is reciprocal then the scattering (4x4) matrix can be written as [6]:

$$[S]=\begin{bmatrix} 0 & S12 & S13 & S14 \\ S12 & 0 & S23 & S24 \\ S13 & S23 & 0 & S34 \\ S14 & S24 & S34 & 0 \end{bmatrix} \quad (2.38)$$

Multiply row1 and row 2 then

$$S^*_{13}S_{23}+S^*_{14}S_{24}=0 \quad (2.39)$$

Multiply row3 and row 4 then

$$S^*_{14}S_{13}+S^*_{24}S_{23}=0 \quad (2.40)$$

Multiply (2.39) by S^*_{24} and (2.40) by S^*_{13} and subtract them:

$$S^*_{14}\,(|S_{13}|^2-|S_{24}|^2)=0 \quad (2.41)$$

Similarly multiply row 1 and row 3 and the multiplication of row 2 and row 4,

then

$$S^*_{12}S_{23}+S^*_{14}S_{34}=0 \tag{2.42}$$

$$S^*_{14}S_{12}+S^*_{34}S_{23}=0 \tag{2.43}$$

Multiply (2.42) by S_{12} and (2.43) by S_{34}:

$$S_{23}\,(|S_{12}|^2-|S_{34}|^2)=0 \tag{2.44}$$

Equations (2.41) and (2.44) can be satisfied if and only if

$$S_{23}=S_{14}=0 \tag{2.45}$$

Self product of the rows of the unitary scattering matrix (2.38) will provide the following equations:

$$|S_{12}|^2+|S_{13}|^2=1 \tag{2.46}$$

$$|S_{12}|^2+|S_{24}|^2=1 \tag{2.47}$$

$$|S_{13}|^2+|S_{34}|^2=1 \tag{2.48}$$

$$|S_{24}|^2+|S_{34}|^2=1 \tag{2.49}$$

It can be shown from these equations that $S_{13}= S_{24}$

If we choose $S_{12}=S_{34}=\alpha$, $S_{13}=\beta\, e^{j\theta}$, $S_{24}= \beta e^{j\varphi}$.

After some simplifications then the symmetric and non-symmetric couplers have the following matrices.

1- Symmetric coupler: θ=φ=π/2

$$[S] = \begin{bmatrix} 0 & \alpha & j\beta & 0 \\ \alpha & 0 & 0 & j\beta \\ j\beta & 0 & 0 & \alpha \\ 0 & j\beta & \alpha & 0 \end{bmatrix} \tag{2.50}$$

2- Anti-symmetric coupler: θ=0, φ=π

$$[S] = \begin{bmatrix} 0 & \alpha & \beta & 0 \\ \alpha & 0 & 0 & -\beta \\ \beta & 0 & 0 & \alpha \\ 0 & -\beta & \alpha & 0 \end{bmatrix} \tag{2.51}$$

For 90^o Hybrid coupler $\alpha=\beta=\frac{1}{\sqrt{2}}$

$$[S] = \frac{1}{\sqrt{2}} \begin{bmatrix} 0 & 1 & 1 & 0 \\ 1 & 0 & 0 & j \\ j & 0 & 0 & 1 \\ 0 & j & 1 & 0 \end{bmatrix} \tag{2.52}$$

For 180^o Hybrid coupler

$$[S] = \frac{1}{\sqrt{2}} \begin{bmatrix} 0 & 1 & 1 & 0 \\ 1 & 0 & 0 & -1 \\ -1 & 0 & 0 & 1 \\ 0 & -1 & 1 & 0 \end{bmatrix} \tag{2.53}$$

2.7 Phase Shifters

To steer the beam of an antenna array to a certain direction, phase shifters are required to provide the progressive phases for various elements according to the array type. A phase shifter is a two terminal passive device. Usually it is a reciprocal network which can pass the signal in both ways. An ideal case for the phase shifter when the insertion loss is very low and the amplitude for all shifter states are the same. When designing/using a phase shifters, one needs to check the following metrics [7]:

1. The operation frequency and band width.
2. Phase shifter steps.
3. Insertion loss.
4. The speed of switching between different states.
5. The amount of power the phase shifter can handle.
6. The accuracy of switching circuits for the phase shifter.
7. The matching between the input terminal and the output terminal.

Phase shifters in general can be classified into two types analog and digital.

2.7.1 Analog Phase Shifters

In this type, the phase varies continuously according to the variation of the bias voltages. The shift depends on the value of control signals (bias voltage), as the control signal changes the phase shift changes. The varactor diode is the most common semiconductor device that can be used in analog phase shifters. Analog phase shifters can achieve huge value of phase shift and need less number of diodes than digital phase shifters, but it is less accurate than digital one and provides narrower bandwidths [8].

2.7.2 Digital Phase Shifters

In a digital phase shifter, separate set of phase states for the phase shifts can be achieved. In other words, the phase shifts occur in discrete states according to the corresponding values of the phase shifter inputs. Digital phase shifters have a feature of being more immune to the external noise. The LSB (least significant bit) or phase shifter step can be determined by the number of bits used for its control. For example a 4-bit phase shifter has a shift a phase step of 16 which is equal to 22.5^{o}, a 3-bit phase shifter has LSB equal to 45^{o} and a 6-bit phase shifter will has an LSB equal to 5.625^{o}. Digital phase shifters can be divided to two categories according to the manufacturing material, ferrite (require bias) and semiconductor based [9]. The phase shifters that are semiconductor based, can be divided into two types: transmission type and reflection type. The transmission type consists of two switches and two lines (L1 and L2) that have different lengths as can be shown in figure 2.14 [9].

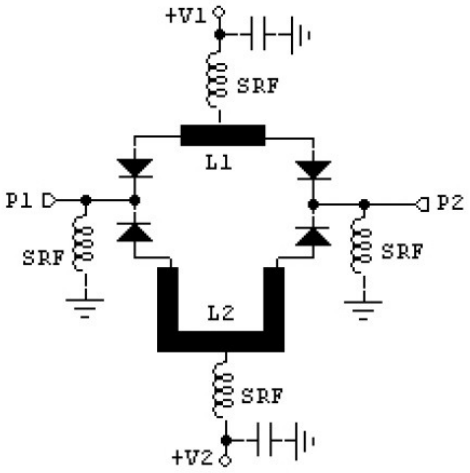

Figure 2.14: Digital Phase Shifter [9]

The features of the phase shifter mainly depend on the properties of the ferrite material used in its manufacturing. Ferrite phase shifters in general are preferable at frequencies higher than 5GHz that is because they can provide low loss, capability of handling high power ratings, high accuracy and excellent radiation performance. But the semiconductor based phase shifters can provide faster switching speed than the ferrite one. The semiconductor based phase shifters can provide smaller size and lighter weight than that can be provided by the ferrite based phase shifters [9]. Two states of phase shifts can be provided by using reflection type of phase shifters according to the position of the switch contact in order to determine the route of the incoming signal. Different paths were taken by the incident signal will provide different reflection coefficients for the each route in the reflective network. The input signal is routed in the circulator, then it passes to the reflective network, and then the signal will be reflected from the reflective network to the output port as can be shown in Figure 2.15 [9].

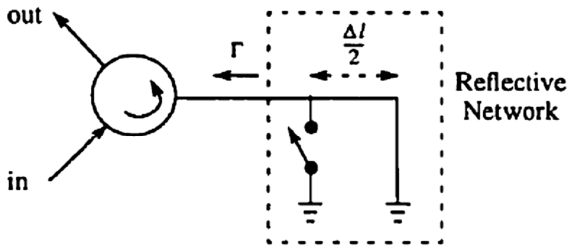

Figure 2.15: Reflection type phase shifter.[9]

2.8 The Arduino Microcontroller

The Arduino board is a block that can respond to input signal in a certain manner according to the program that it contains. It can handle and deal only with electrical signals, which means that to be connected to the real world, sensors or component that convert various phenomena to electrical signals should be connected to it [10]. In Figure 2.16 the Arduino Mega 2560 development kit is shown. Arduino Mega 2560, is used in this work. Our purpose to deal with a decision making block that can handle 51 (4 pins for each of the 12 phase shifters, V_{cc}, V_{EE} and ground) pins or more. Arduino Mega 2560 has 54 digital input/output pins (for which 15 of them can be used as pulse width modulation outputs) [11]. Also it has 16 analog inputs, 4 serial ports, crystal oscillator of 16MHz, USB connection and a power jacket.

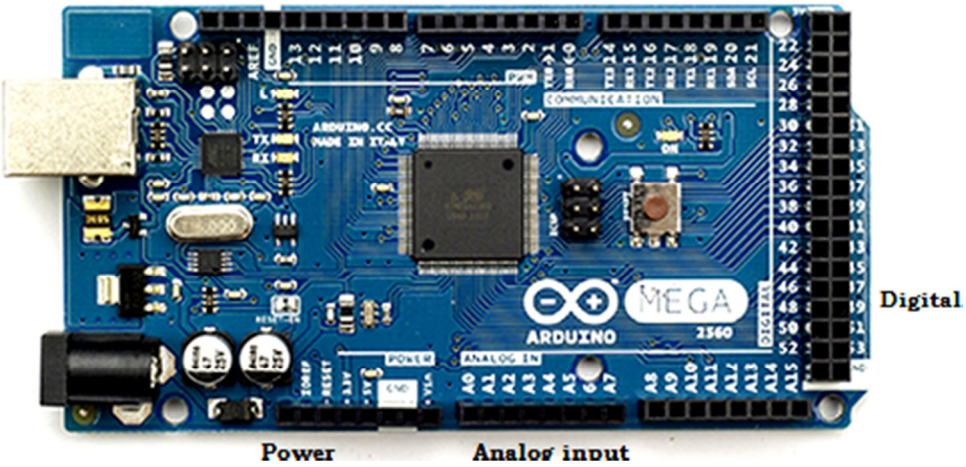

Figure 2.16: Arduino Mega 2560

CHAPTER 3

LITERATURE REVIEW

In this chapter, the literature review of similar works to our topic are discussed. The main objective of this chapter is to study previous literatures related to this work and compare them in order to identify contributions proposed in this work. The tree diagram in Figure 3.1 classifies the literature chosen in the survey in a systematic way. First, we classify them according to the antenna type in three branches:

1. Linear arrays.
2. Planar arrays.
3. Modified antenna shapes/single element.

Each one of these blocks was also subdivided into different blocks according to the application. Linear arrays can be divided into three branches:

1. Linear arrays for UAV applications.
2. Linear arrays for other applications.
3. Enhancements of linear arrays.

Planar arrays were subdivided into two branches:

1. Planar arrays used for UAV applications.
2. Planar array used for other applications.

Finally, the modified antennas/single element that were used for UAV applications contains two types of antennas:

1. Hexaferrite antenna
2. L-Shape monopole antenna.

3.1 Literature Related To Linear Array Antenna

Linear array antennas can provide better gain than what the single element can deliver and so better directivity. Moreover, it can provide beam scanning for the radiation field in one degree of freedom (theta) which indicates that limitation in the beam scanning process will be observed.

In [1],[12]-[14] linear phased array antennas for UAV applications were presented. While, [15]-[23] linear phased array antennas used for different applications in various frequency bands. Some enhancement for the linear array antenna performance in terms of reducing mutual coupling, side lobe level control were introduced in [24]-[28]. Some of these literatures will be discussed in details in the following sections.

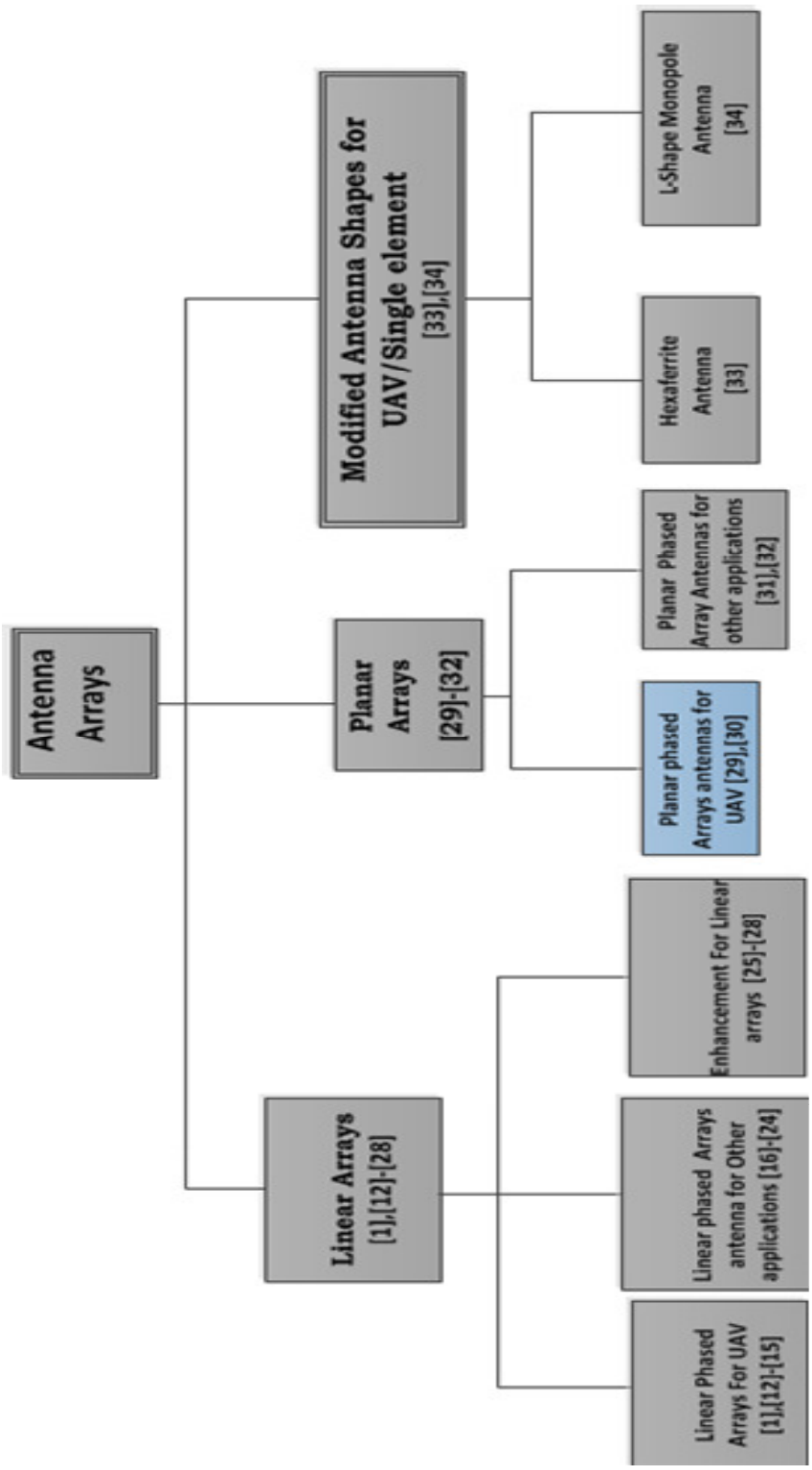

Figure 3.1 : Summary of the literature review

3.1.1. Linear Phased Array Antenna for UAV Applications.

A Linear array of four elements that were embedded separately in the wing structure of a UAV, was presented in [1]. The array was composed of four monopoles for which each element had a separate ground plane and they were connected directly to the feed network using RG-316 coaxial cables. The feed network was composed of connectorized phase shifters and power combiners connected in single box. The array was implemented using FR-4 Material substrate with 0.8mm thickness. The antenna operated in the ISM band with a centre frequency of 2.45GHz. The feeding cables were connected to RF phase shifter (HMC647LP3) and then connected to the power combiner (BP4U1+). The Phase shifter was controlled by a simple microcontroller which contained a program that sends the sequence of digital control to the phase shifters to achieve beam steering. The array with the wing of a small UAV is shown in Figure 3.2. In this work, discrete RF components were used and a linear array was implemented which ended up of increased weight and one degree of scanning freedom.

Figure 3.2: Antenna array in the wing structure in [1]

A low profile linear 8-element antenna array which can be installed in the UAV structure was presented in [12]. The phased array antenna used for communication between the UAV and

satellite operating in Ka band (26.5GHz-40GHz). In this work, at 30GHz exactly, the phased array antenna had 1GHz bandwidth. The beam coverage provided was between -30^{o} to +30^{o} and circular polarization was achieved. The maximum antenna gain can vary from 6.8dB to 8.6dB at the frequency of 30GHz. The patch antenna was implemented on Duroid RO 5880 substrate with height of 0.38mm, while the analog phase shifter and feeding network were installed on an Alumina substrate. The proposed analog phase shifter was composed of a hybrid coupler loaded with a varactor diode. The phase shifting is done by varying the bias voltage from 0V to 18 V, for which the maximum phase shift (272^{o}) can be obtained. The diagram of this implementation shown in Figure 3.3. This design provides one degree of freedom which means that the beam scanning can be provided in theta only. In this design, analog phase shifters were used, so large voltage levels are required for biasing, which cannot be applied for small UAV as per our application.

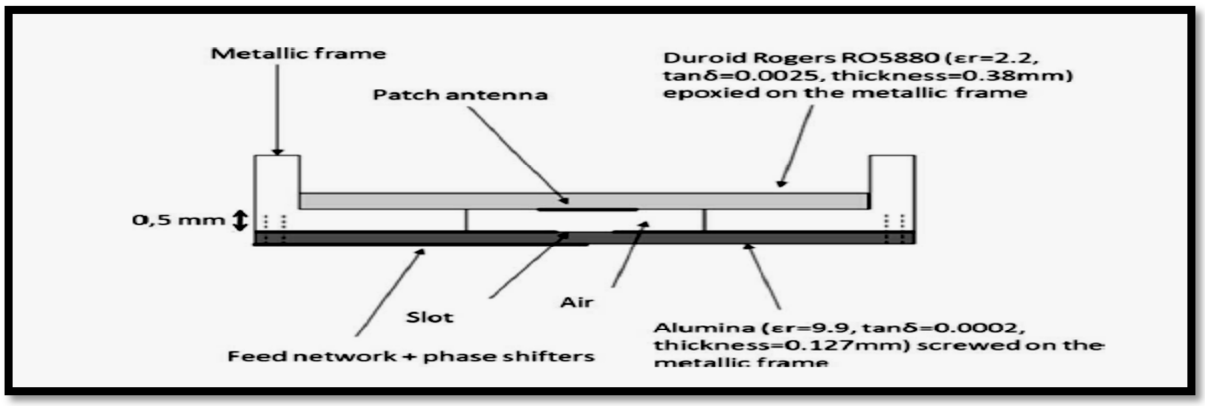

Figure 3.3: Linear array structure in [12]

3.1.2. Linear Phased Array Antennas for Other Applications

A Passive phased array antenna integrated with phase shifters and feed network in single metalized board was presented in [15]. The phase array antenna (PAA) operated at10 GHz with

beam scanning capability between ±50°. The proposed antenna array was composed of four branches, on each branch three cascaded patches were fed in series. On each branch, the patch elements were connected to each other through 50Ω microstrip-line. Each patch element was built on 6x4.55mm^2 area. The antenna provided a gain of 6 dB which is 3dB higher than the gain that can be provided by single patch element. The RF signals were distributed equally among the different branches. The proposed phase shifter with compressed size of (3 X 2.8mm^2) was manufactured based on artificial transmission line technique. This phase shifter was built on AL_2O_3 substrate with a small layer of BST (barium-strontium-titanate) on top of it. The bias voltage for the proposed phase shifter varies up to 50V in increment of 10V for each step as can be shown in Figure 3.4. This is very large variation and not practical for energy limited applications.

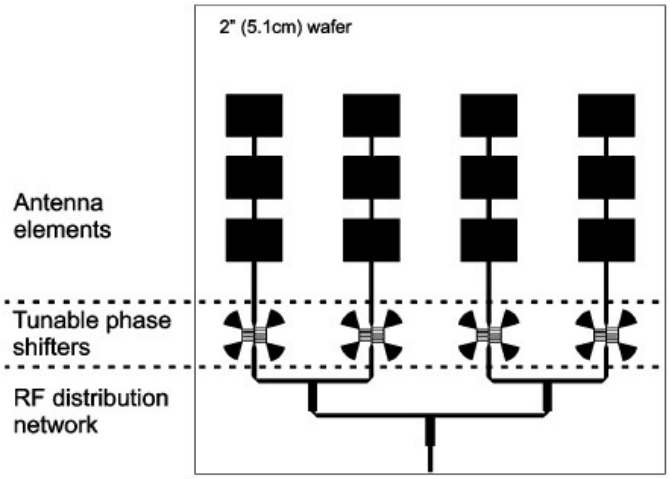

Figure 3.4: Antenna array and Feed network for [15]

In [19], a planar phase array with 4x4 elements array excited by a coplanar waveguide based phase shifter was presented. In this work, the proposed phased array antenna was composed of a planar array, phase shifters and feed network (λ/4 and power combiner). The antenna array constitutes of 4 columns, where each column contain four elements that are fed progressively. The PAA provided phase scanning for the range between -45^{o} to 45^{o} and it is operating on frequency of 20 GHz. The phase shifting can be done by changing the position of dielectric slab on gap of coplanar waveguide. The electrical permittivity changes as the distance from dielectric slab to coplanar waveguide changes so the dielectric permittivity is a function of distance. The substrate was built in IS640 material. The model is shown in Figure 3.5. Since it is linear array, so it provide only beam scanning in one dimension.

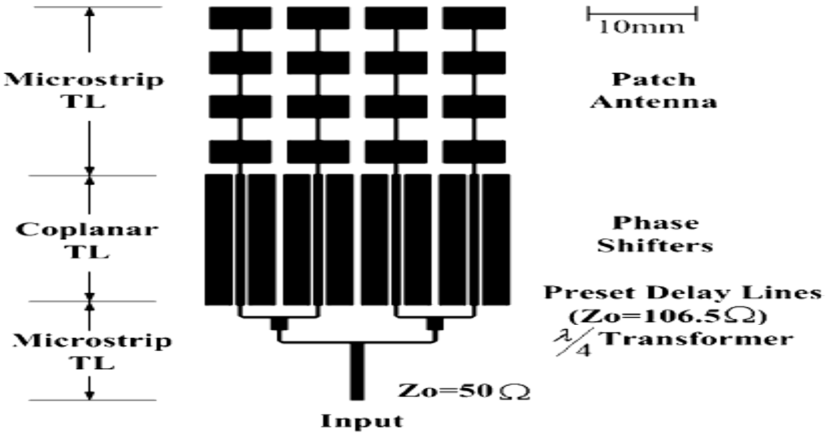

Figure 3.5: Antenna Array and Feed network In [19]

3.1.3 Enhancement For Linear Array

The reduction on the mutual coupling between the adjacent array elements due to the effect of reflected surface wave from the edge of substrate was introduced in [25]. In this work. This technique is mainly based on adjusting the substrate length to reduce the effect of surface wave reflected from the substrate edge. The mutual coupling was reduced by using this technique to 6.9 dB, while it was 20.84dB by adjusting the substrate length from $0.5\lambda_o$ to $0.7\lambda_o$. This experiment have been done using Taconic CER-10, which have dielectric constant of 10.8 and substrate thickness of 3.2mm.

3.2 Literature Related To Planar Array Antenna

3.2.1 Planar Phased Array Antenna for UAV Applications

A 12-element patch antenna array printed on a 396x116 mm^2 board operating in 2.45GHz frequency band was introduced in [29]. The printed array was to be used for UAV applications and fed by a dedicated feed network which contained 4 power combiner/splitter. The array antenna and the feed network were implemented on separate PCB boards. The feed network contained power combiners with no phase shifters. The array was printed in FR-4 board and with efficiency less than 50%. Figure 3.6 shows the antenna array loaded on the wing of the plane structure. In Figure 3.7, the 12 port power combiner board introduced in this work is shown.

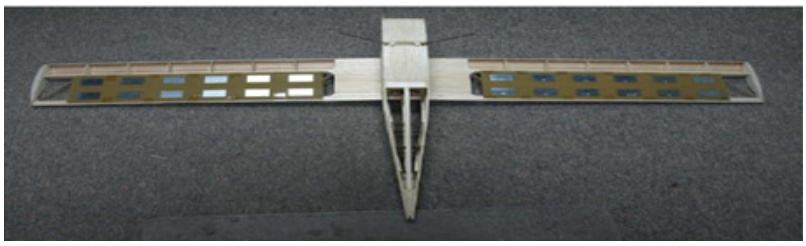

Figure 3.6: Antenna array loaded in the UAV structure in [29]

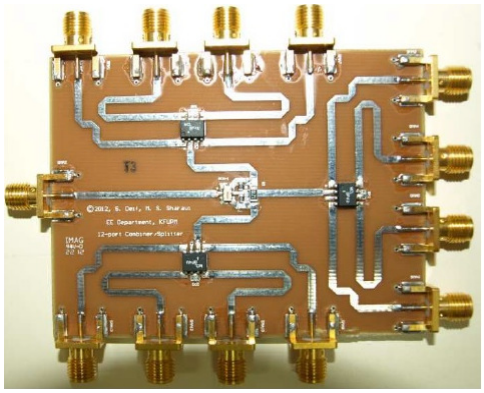

Figure 3.7: 12 ports Power combiner [29]

3.2.2 Planar Phased Array Antennas for Other Applications

In [31], 2D phased antenna array based on liquid crystal material is proposed. In this work 2x2 planar antenna array is presented. This phased array antenna is operating at 17.5 GHz. It contains 2 x 2 microstrip planar array, variable delay lines based on liquid crystal material, feeding network and dc biasing network.

3.3 Antennas for UAV Applications

In [33], a planar antenna fabricated on Co_2Z substrate for UAV applications was presented. In this work, the antenna constitute of two sloped radiating parts and two sloped and straight transmission lines. This antenna resonated exactly at 2.41 GHz, with more than 70 % efficiency .Where the antenna occupied area of 40x55mm^2. Small amount of gain can be provided by the single element antenna. The single element antenna cannot perform beam scanning for the radiation field. In Figure 3.8, the modified patch is shown.

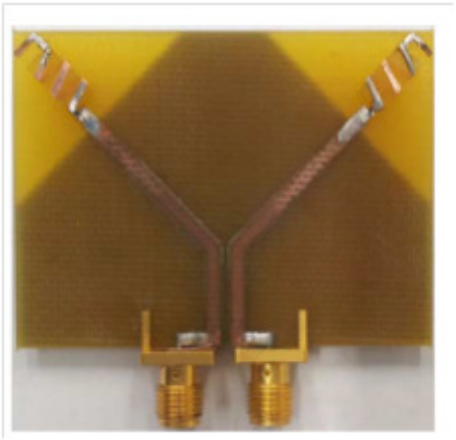

Figure 3.8: UAV antenna in [33]

3.4 Conclusion

In this chapter, a comprehensive literature review was conducted to see if an integrated planar array for UAV applications has been proposed before. It is clear that the proposed architecture is the first to appear and this gives the motivation for this work.

CHAPTER 4

DESIGN METHODOLOGY

In this chapter, the methods used for design and model implementations are discussed. This design is part of a system level that assists a flying UAV with automatic beams steering capability. The design procedure for the antenna array and the feed network will be explained in details. The general block diagram describing the project and its various parts is shown in Figure 4.1. The integrated array will be a part of a bigger system for automatic beam steering of the UAV data link beam. The decision making block will provide the appropriate phase excitation. In this chapter, we will describe the basic ideas for designing the feed network and the components used for this design. Then, the fundamental ideas for designing the antenna array are represented. Finally, the essential ideas for implementing the decision making block will be discussed.

In Figure 4.1 the components required for automatic beam steering process are shown. The first block is responsible for determining the position of the UAV consisting of an inertial measurement unit (IMU) and a global positioning system chip (GPS) which will send the digital signal to the decision making block. The decision making block (second block) consists of two blocks: tracking algorithm block and excitation phase calculator block. The decision making block will send digital signals to the array and to the ZigBee block. The signal sent to the array will set the phase shifters to certain values that are corresponding to the location of the UAV. Block 3 will send RF signal to the array for the communication with the earth station. The fourth block is explained in details as can be shown in Figure 4.2.The antenna proposed consists of

three layers all implemented in single unit. The upper layer contains the feed network, while the middle layer is the ground plane where the digital bias lines were implemented at the edge of the middle layer. Finally the bottom layer contains a 12 element printed antenna that is directly connected to the phase shifters through the three stacked layers as in Figure 4.2 via a pin feed mechanism.

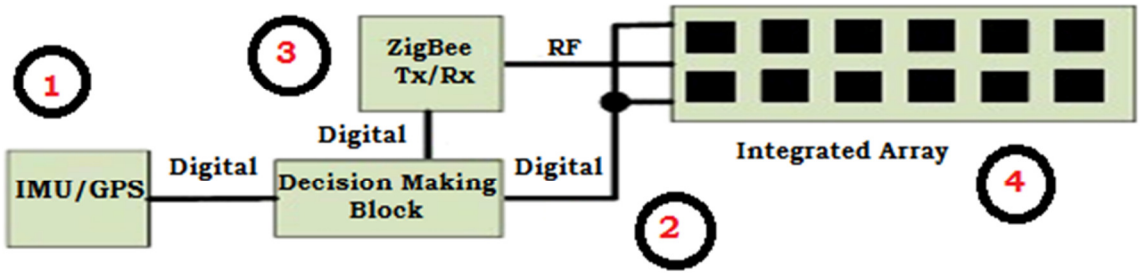

Figure 4-1: System Level architecture for automatic beam steering process

4.1. Feed Network Design

For the beam steering process, certain phase excitations for the radiating elements are required in order to direct the beam to a certain direction. Certain components are required to control the RF input signal and divide it, then distribute it among different branches. In each branch, a digital phase shifter can be used to change the phase of the incoming signal to the desired value that is required to excite the radiator in order to steer the beam to certain directions. The main components that are required to build the digitally controlled RF feed network for the 12-element array are:

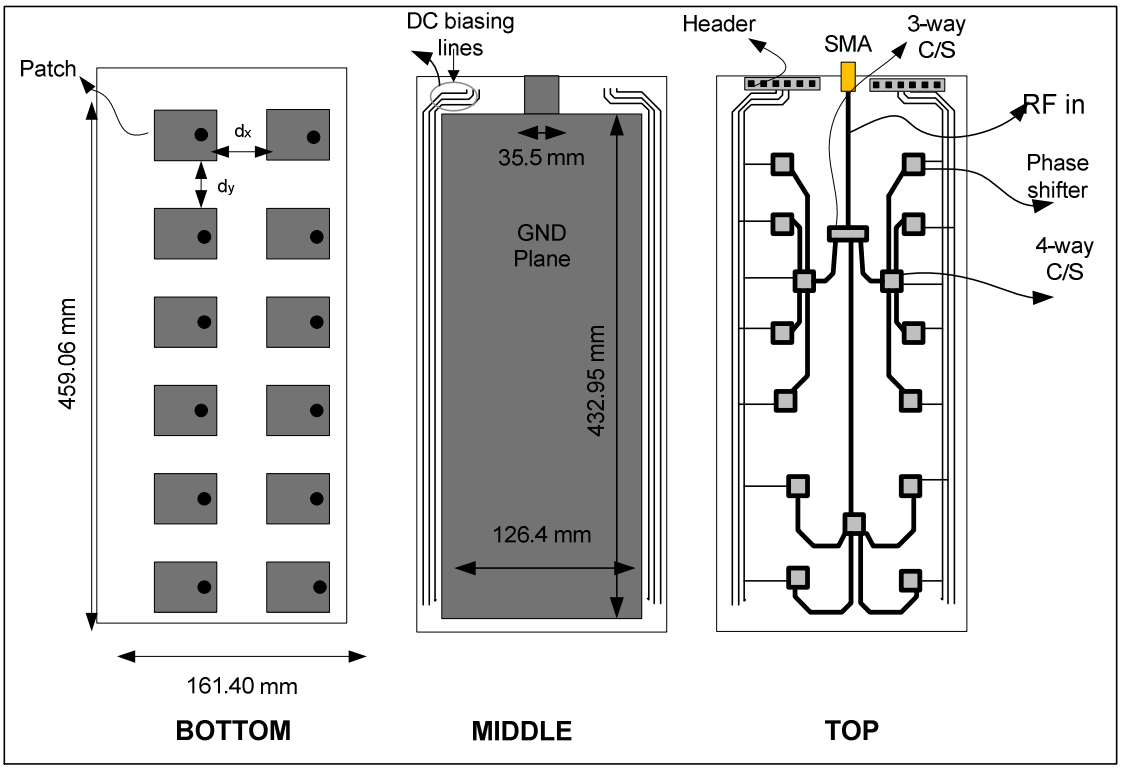

Figure 4.2: Layout for the three layer of the proposed antenna

1. One 3-way splitter/combiner (SCN-3-28).
2. Three 4-way splitter/combiner (BP4U1+).
3. Twelve digitally controlled RF phase shifters (MAPS-010144).
4. Two headers with 30 pins each (S5685-ND).

The feed network layer is built on an RO4350 substrate with 0.508mm thickness with dielectric constant of 3.66. The microstrip lines were optimized for 50Ω operation (w=1.1mm). The input incoming signal passes through the 3-way power combiner/splitter. The three outputs of the 3-way combiner are connected to individual 4-way combiners. The output of the 4-way combiner is connected to the phase shifter, which is directly installed at the bottom of the radiating element. In Figure 4.3 the layout of the fabricated feed network is shown. In Figure 4.4, the schematic

diagram for the feed network is shown. The microwave circuit simulations were conducted using microwave office (MWO) and the PCB using Altium designer [35].

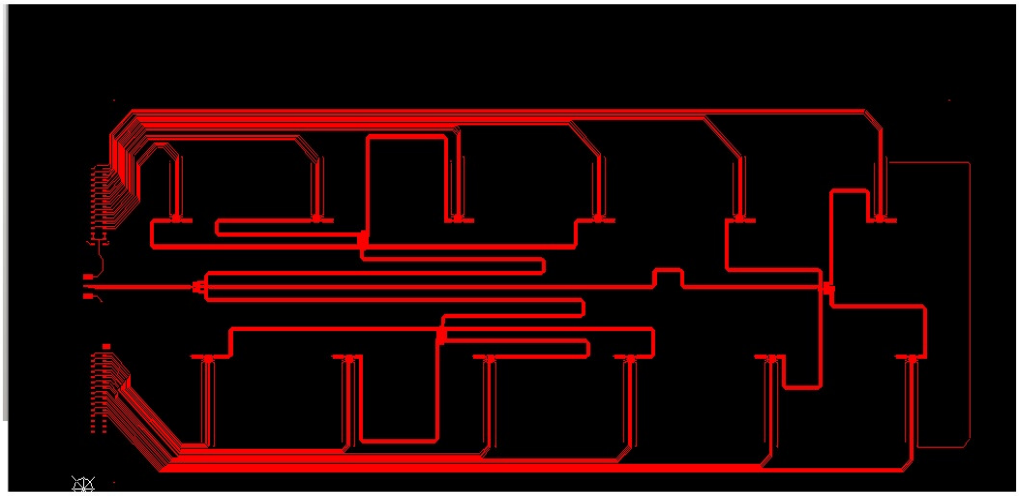

Figure 4.3: The foot print layout for the fabricated feed network

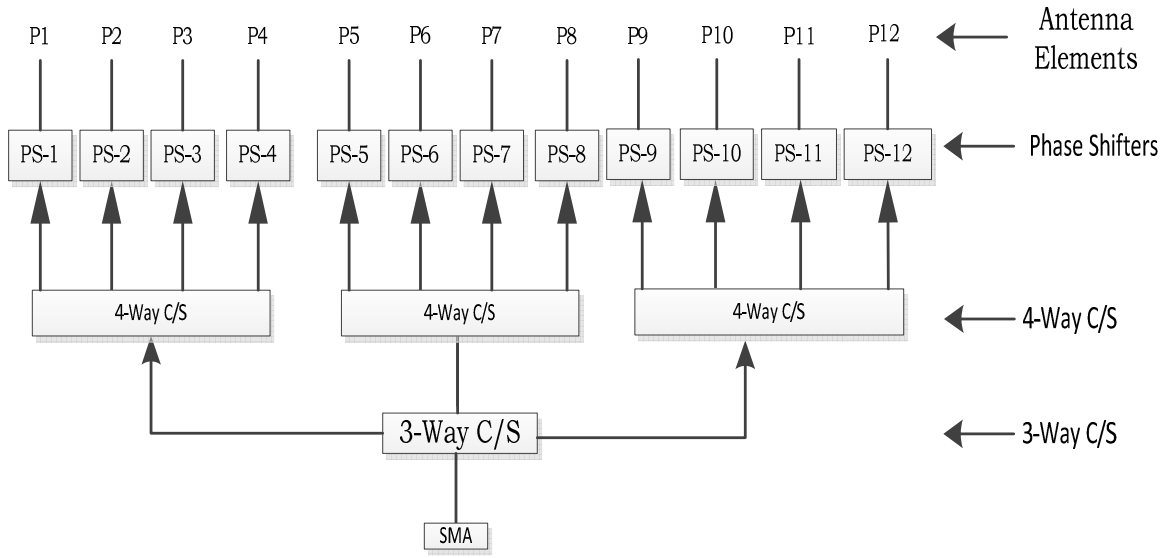

Figure 4.4: Feed network schematic diagram

4.1.1 3-Way Power Splitter/Combiner (SCN-3-28)

The main RF input signal is passed toward the 3-way power splitter/combiner, then it is divided among the branches by the power splitter device. This device has the following specifications [36]:

1. The frequency of operation for this device is between 1.6 GHz to 2.8 GHz.
2. The insertion loss for this combiner varies between 5.6dB to 6 dB.
3. The phase unbalance for this combiner between 5^{o} to 8^{o}.
4. The amplitude unbalance between 0.2dB to 0.6dB.

The pin diagram for the power combiner/splitter is shown in Figure 4.5 and its details are shown in Table 4.1.

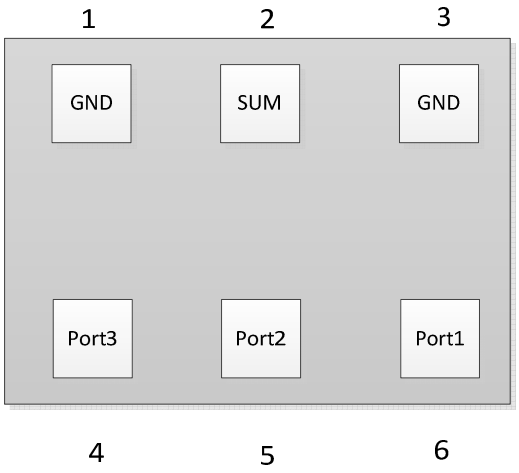

Figure 4.5: Pin Diagram For The 3-Way Power Combiner/Splitter

For this device, two 127 Ω resistors need to be connected between first and third ports while two 124 Ω between port 1 and port 2, port 2 and port 3.

Table 4.1 Pin diagram for the 3-way power combiner/splitter

Description	Pin Number
Sum Port	2
Port-1	6
Port-2	5
Port-3	4
Ground	1,3
Port 1-2, 2-3	Two External Resistors 124Ω
Port 1-3	External Resistors 127Ω

4.1.2 4-Way Power Splitter/Combiner (BP4U1+)

The output of the 3-way combiner is passed toward the 4-way power splitter/combiner, then it will be divided among four antennas [37].

1. The frequency of operation for this device is between 1.8 GHz to 3 GHz.
2. The insertion loss for this combiner varies between 6.7dB to 7.7 dB.
3. The phase unbalance for this combiner is around 28^{o}.
4. The amplitude unbalance for this device is around 1.3dB. The pin diagram for the power combiner/splitter is shown in Figure 4.6 and is described in Table 4.2.

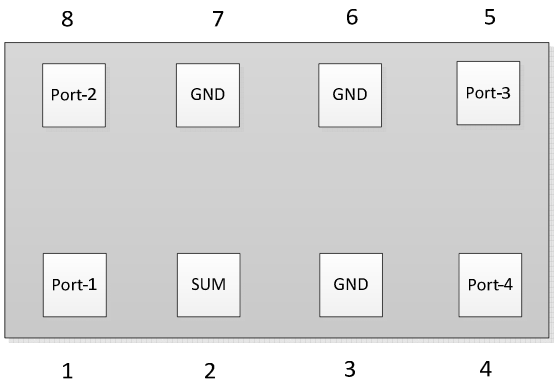

Figure 4.6: Pin diagram for the 4-way power combiner/splitter

Table 4.2 Pin diagram for the 4-way power combiner/splitter

Description	**Pin Number**
Sum Port	2
Port-1	1
Port-2	8
Port-3	5
Port-4	4
Ground	3,6,7

4.1.3 Digitally Controlled Phase Shifter (MAPS-010144)

The 4-bit digitally controlled phase shifter is considered as the heart of the feed network. A phase shifter plays critical role in steering the beam toward a certain direction. There are sixteen phase shift states that can be achieved by this phase shifter. According to the digital input to the phase shifter from the digital lines, the phase shift corresponding to the input values is selected and applied to the incoming RF signal [38].

At each input from the decision making block (angles in Theta and Phi), the excitation phase calculation will be achieved. Then, the number of steps which is required to quantize the actual excitation phase will be converted to binary digits and will fed to the phase shifters as a binary stream. For example, for an excitation phase of 120^{o}, the digital phase shifter will represent this excitation phase as a 112.5^{o}. As the phase shifter deals only with steps of 22.5^{o} because it is a four bits phase shifter, 112.5^{o} corresponds to five steps of 22.5^{o} (least significant bit). Table 4.3 shows the truth table for the 4-bit phase shifter. In this table, the least significant bit is

Table 4.3: Truth table for the 4 bit digitally controlled phase shifter .

D6	D5	D4	D3	D2	D1	No Of Steps	Phase Shift
0	0	0	0	X	X	Initial	0
0	0	0	1	X	X	1	22.5^{o}
0	0	1	0	X	X	2	45^{o}
0	0	1	1	X	X	3	67.5^{o}
0	1	0	0	X	X	4	90^{o}
0	1	0	1	X	X	5	112.5^{o}
0	1	1	0	X	X	6	135^{o}
0	1	1	1	X	X	7	157.5^{o}
1	0	0	0	X	X	8	180^{o}
1	0	0	1	X	X	9	202.5^{o}
1	0	1	0	X	X	10	225^{o}
1	0	1	1	X	X	11	247.5^{o}
1	1	0	0	X	X	12	270^{o}
1	1	0	1	X	X	13	292.5^{o}
1	1	1	0	X	X	14	315^{o}
1	1	1	1	X	X	15	337.5^{o}

D6, while the most significant bit is D3. While D1 and D2 are do not care bits at the parallel mode. In Figure 4.7, the internal circuit for the digital phase shifter is shown. As we can see from this Figure, it is composed of four switches that are flipped between two delay lines. When the control signal is "1" then the switch will be flipped to the upper delay line. When the control signal is "0" then the switch will be flipped to the lower normal line. In Figure 4.8, the pin diagram for the phase shifter is shown .

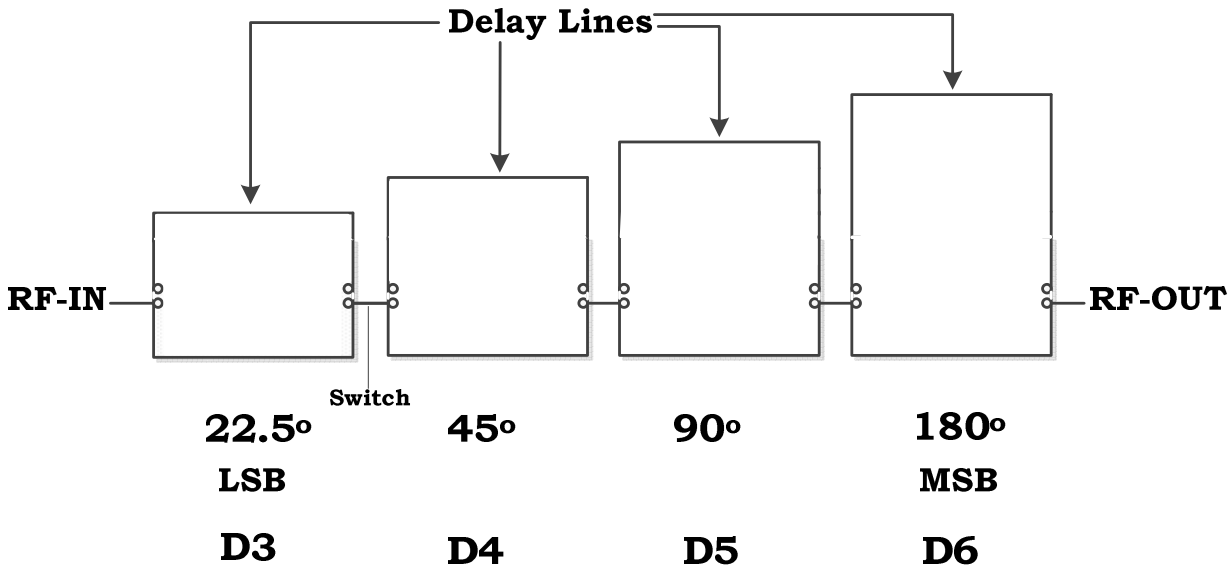

Figure 4.7: Phase Shifter Detail at the initial state(Reference Phase when phase shift=0)

In the diagram the pins 23 and 24 are connected to the ground plane as it is working in the parallel mode. For excitation phase of 112.5^{o} the phase shifter will receive the bits of 0101.

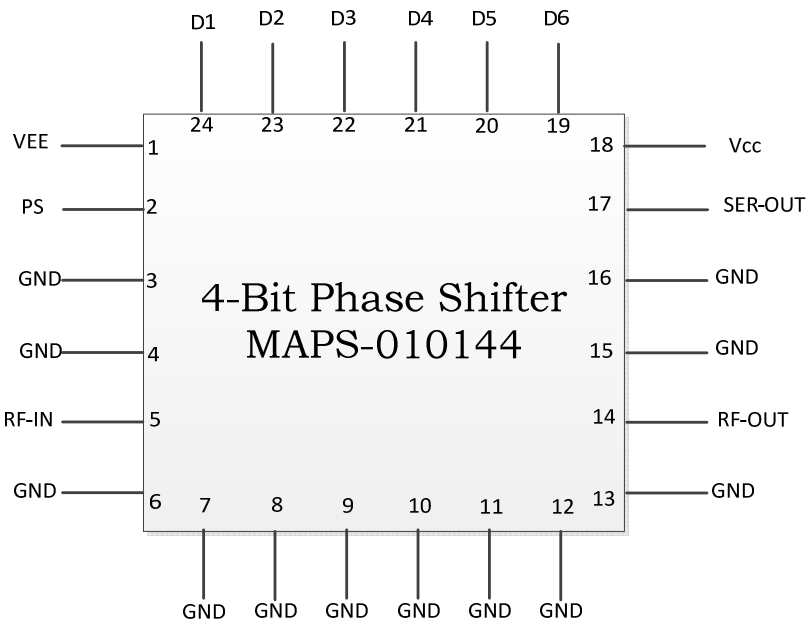

Figure 4.8:Pin diagram for the phase shifter

The phase shifter have the following specifications:

1. Frequency of operation 2.3 to 3.8 GHz
2. Insertion loss of 2.5dB

4.1.4 Microstrip Lines For The Feed Network

The width of the transmission line can be determined by using online calculators like emtalk, TXLINE and RFCALC. TXLINE is the physical dimension for the transmission line can be calculated based on the substrate permittivity, substrate height and the frequency of operation. For our problem, the substrate is Roger RO4350 with permittivity of 3.66, substrate height is

0.508mm, and frequency of operation is 2.45 GHz. As shown in Figure 4.9, the RF transmission line between the input port and any of the output ports should have the same length in order to maintain the same signal level that reach to the output ports as can be shown in Figure 4.3. When microstrip line makes a 90^{o} bend, this will create more radiation and more loss. This way of routing is not a recommended way because the 90^{o} bends adds capacitance which change the characteristic impedance of the transmission line.

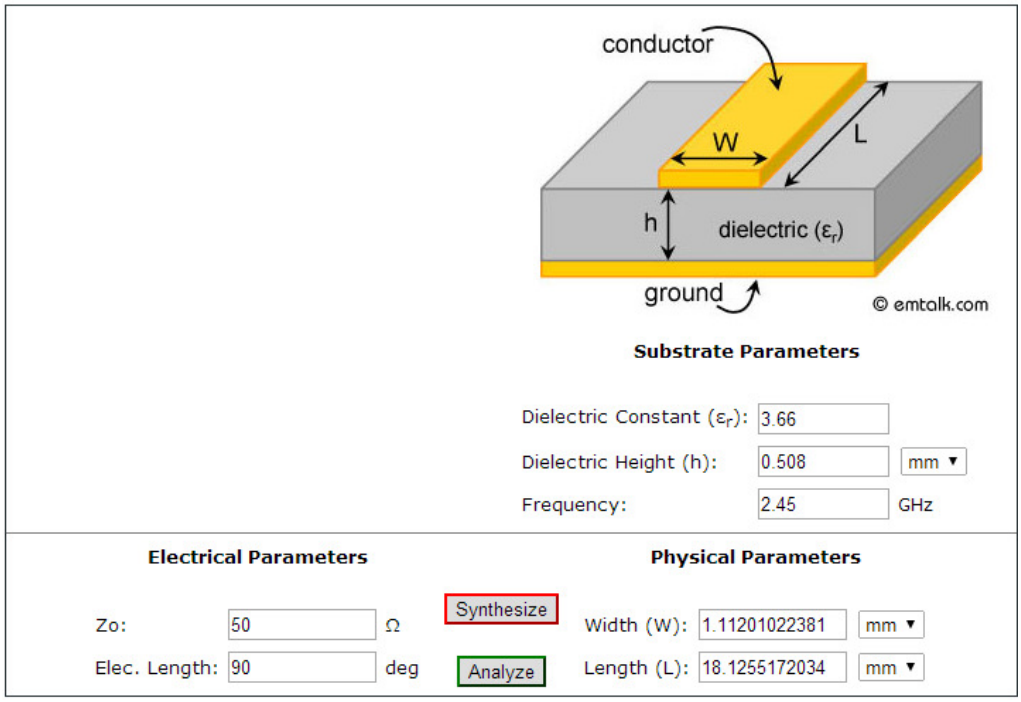

Figure 4.9: Microstrip Line Design Using EMTALK Software [39]

In our feed network, we used mitered lines. Mitering the bends will reduce the capacitance that is created by the bends which means that the transmission line characteristic impedance will be recovered to its initial value. The mitered equations are derived empirically. Figure 4.10 shows the dimensions of such a technique. The equations are related according to [40].

$$\mathbf{D} = \sqrt{\mathbf{W}} \tag{4.1}$$

$$\mathrm{X}=\mathrm{D}\times\left(\mathbf{0.52}+\mathbf{0.62}e^{\left(-\mathbf{1.35}\times\left(\frac{W}{H}\right)\right)}\right) \tag{4.2}$$

$$\mathrm{A}=\sqrt{\mathbf{X}-\frac{\boldsymbol{D}}{\mathbf{2}}} \tag{4.3}$$

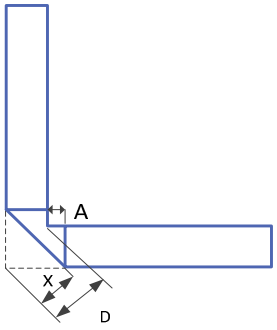

Figure 4.10: Proposed Mitered Bend.

4.2 Antenna Array Design

By using antenna arrays, beam scanning can be done to enhance the communication link between the UAV and the ground station. The array consists of 12 identical patch elements .The individual patch antenna which was operating at 2.45 GHz with a dimension of 40x31mm^2. An RO4350 material was used with ε_r=3.66. Figure 4.11 shows the dimension of a single patch. The feed location is also shown with coordinates of (9.5mm,20mm) as shown in Figure 4.11. The substrate thickness is 0.706mm.

The planar antenna design is performed using HFSS simulation software [41], where it is chosen the inter-space distance to be $\frac{\lambda}{2}$, thus it is 32mm in both directions x and y.

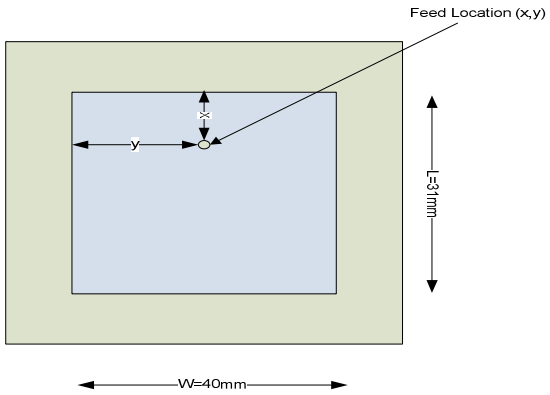

Figure 4.11 Single Patch Antenna

Figure 4.12 shows the simulated model. The dimension of the complete array was 459.06x161.9x1.27mm^3. The overall system level components and interconnections are shown in Figure 4.13

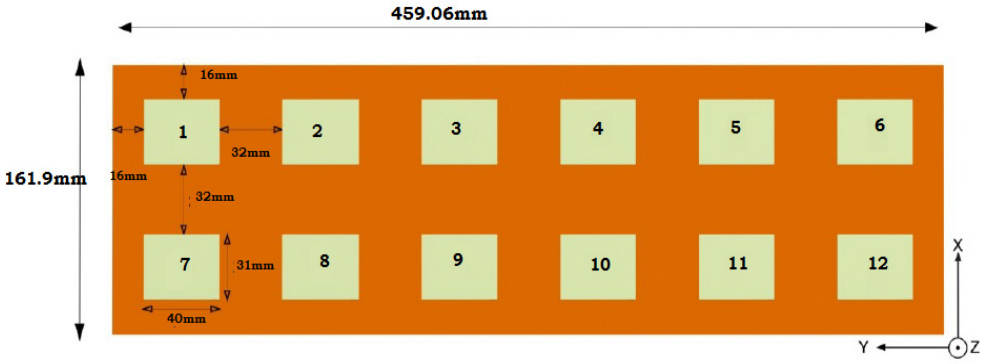

Figure 4.12: Simulated Antenna Array (HFSS model)[2].

The input angles (θ and φ) are calculated by the search algorithm, then the corresponding β_x and β_y are calculated using equations 2.28 and 2.29. After defining the corresponding βx and βy for a certain θ_o and φ_o, the desired excitation phase for each phase shifter is determined. The value of the excitation phase for each array element is shown in Table 4.4 as a function of β_x and β_y. In Figure 4.14, the proposed antenna array is loaded in the wing of the UAV.

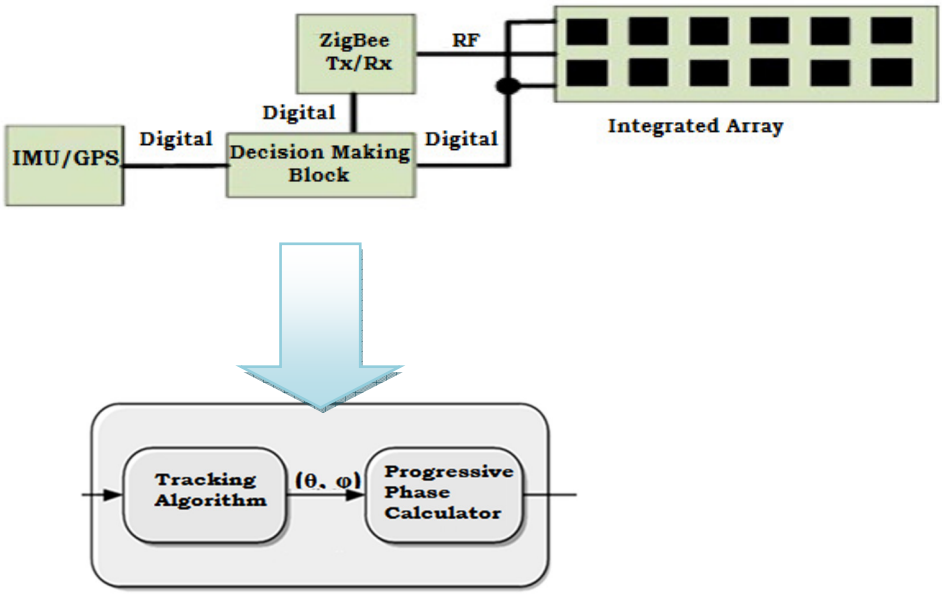

Figure 4.13: System level components and interconnections.

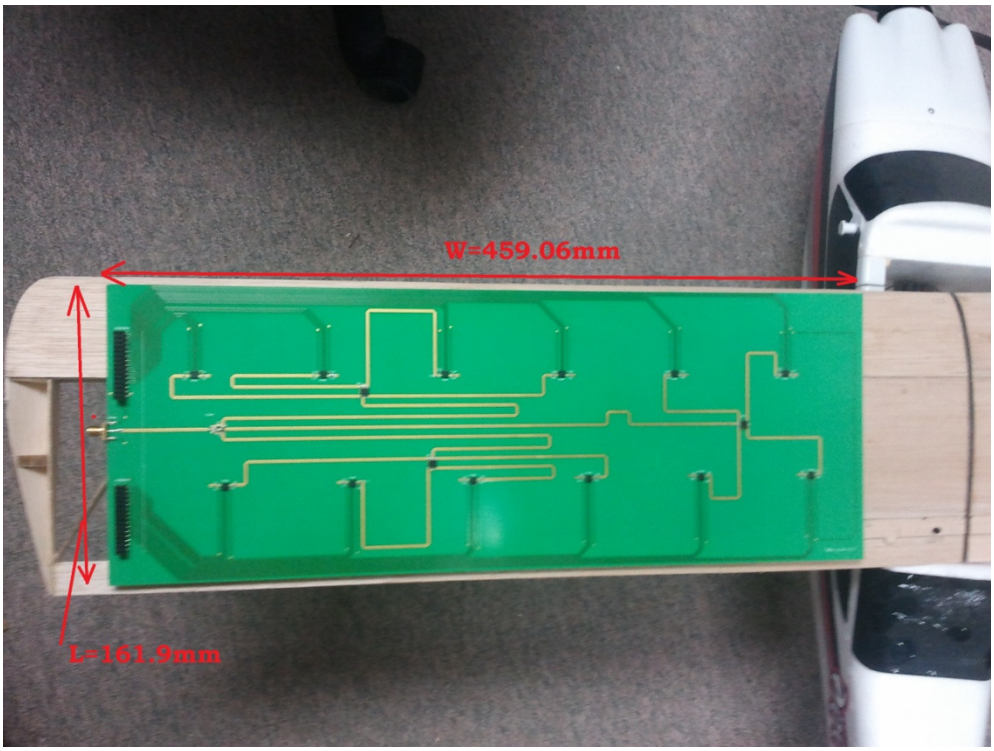

Figure 4.14 The fabricated antenna fixed on the wing of the UAV

Table 4.4:Corresponding excitation phase for each antenna element.

Antenna Element	Excitation Phase	Antenna Element	Excitation Phase
Ant-1	$\beta_1=\beta_y$	Ant-7	$\beta_7=\beta x+\beta y$
Ant-2	$\beta_2=2\beta_y$	Ant-8	$\beta_8=\beta x+2\beta y$
Ant-3	$\beta_3=3\beta_y$	Ant-9	$\beta_9=\beta x+3\beta y$
Ant-4	$\beta_4=4\beta_y$	Ant-10	$\beta_{10}=\beta x+4\beta y$
Ant-5	$\beta_5=5\beta_y$	Ant-11	$\beta_{11}=\beta x+5\beta y$
Ant-6	$\beta_6=6\beta_y$	Ant-12	$\beta_{12}=\beta x+6\beta y$

The phase shift state for the phase shifter is controlled by the 4-bit digital input. The decision making block will digitize the number of steps for each quantized excitation phase into binary. Then binary bits are transferred into the input of the phase shifter. As in our design, the phase shifter is operating in parallel mode which means that the input bits can reach the input of the phase shifters at the same time. Thus, faster performance than in serial mode is obtained. In Figure 4.15, the implemented block diagram in simulink [42] for progressive phase calculation is shown at the case of $\theta=30$ and $\varphi=225$. In Figure 4.15, the diagram is divided into five blocks. The first block is the block where the input parameters (θ_o,φ_o) are entered. Where in block 2, the MATLAB function that will be used to calculate the excitation phase corresponding to the value of Theta and Phi. This MATLAB function is presented as a flow chart which is shown in Figure 4.17. The third block is the display block which is showing the number of steps that are required to quantize the excitation phase into the nearest value to the actual excitation phase.

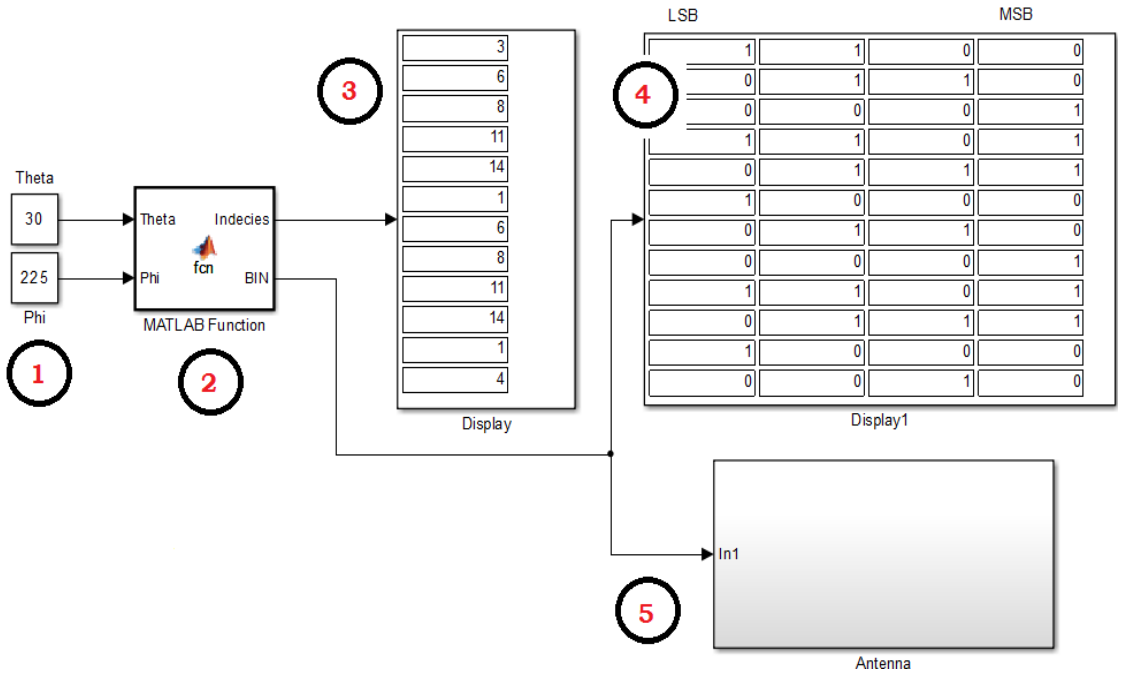

Figure 4.15: Simulink block diagram for progressive phase calculator [42]

After converting the number of steps into binary as shown in block 4, the digital bits to be transferred to the phase shifters to indicate for each phase shifter which phase shift state to be provided. While in block 5 the actual connection between the decision making block (Aurdino) and the headers in the integrated array is performed. The MATLAB function used for excitation phase calculation is presented in flow chart of Figure 4.17. In the flow chart, we can calculate β_x and β_y from the input parameters (θ_o,φ_o). For each antenna element, the excitation phase will be calculated as shown in Table 4.4. If any of the excitation phase is bigger than 360^o or less than -360^o, then we will subtract 360^o or add 360^o respectively. In the second loop, if any of the excitation phase is less than 0, then we will add to it 360. Finally we will divide the excitation phase for each element by 22.5 then we will convert the answer (which is the number of steps required to quantize the excitation phase) to binary.

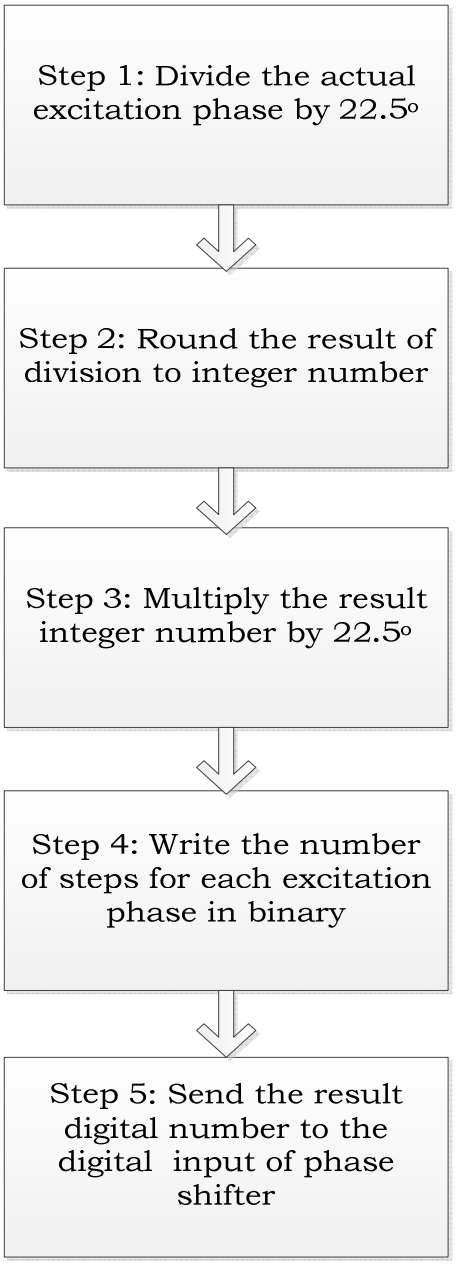

Figure 4.16: Procedure to map the actual excitation phase to the nearest quantization level of excitation phase

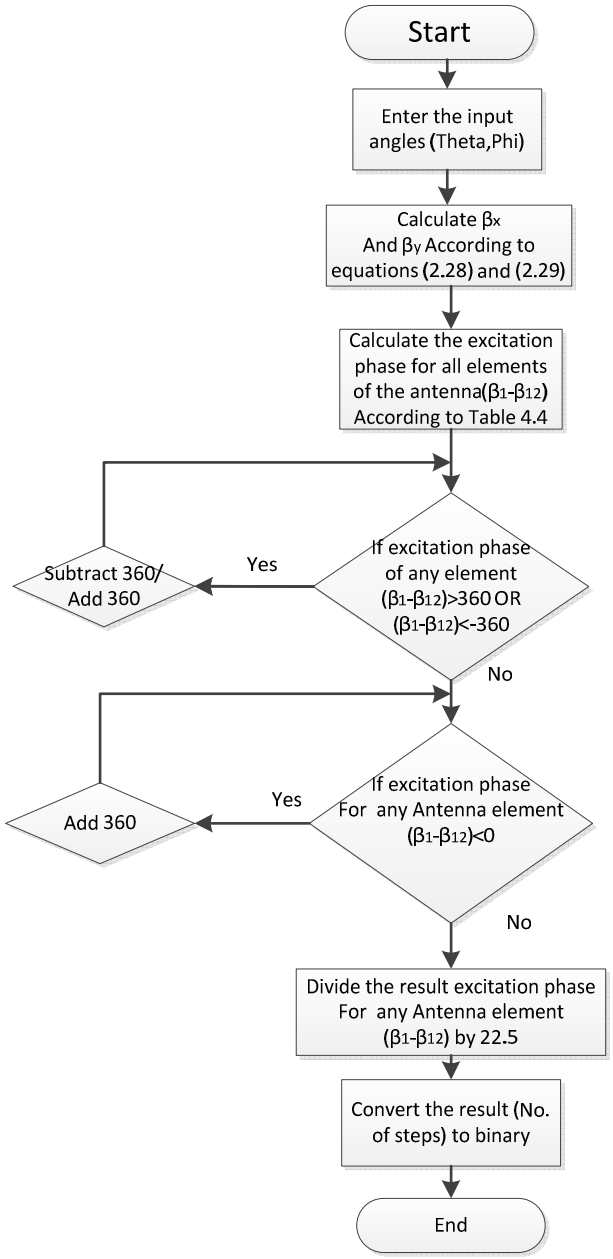

Figure 4.17 :Flow chart for the MATLAB function used for phase excitation calculation

4.3 Conclusions

The methodologies used for designing the feed network and the antenna array were introduced in this chapter. All the components used for implementing the feed network are described in details. The feed network consist of one three-way power combiner/splitter, three 4-way combiner/ splitter and twelve 4-bit digitally controlled phase shifters. The system level components were discussed in brief in order to come up with the full view of the implemented project. The decision making block was clarified and discussed in details as well.

CHAPTER 5

RESULTS

In this chapter, simulation and measurement results for the proposed antenna and feed network are discussed. The simulations for the 12 elements planar antenna array were done using high frequency structural simulator (HFSS) [41]. The Feed network was analyzed using Microwave office (MWO) [43]. Finally measurements were conducted for reflection coefficient, mutual coupling and the phase difference between the output ports and the input of the feed network. Figure 5.1 shows the two parts of the simulation results and measurement results conducted.

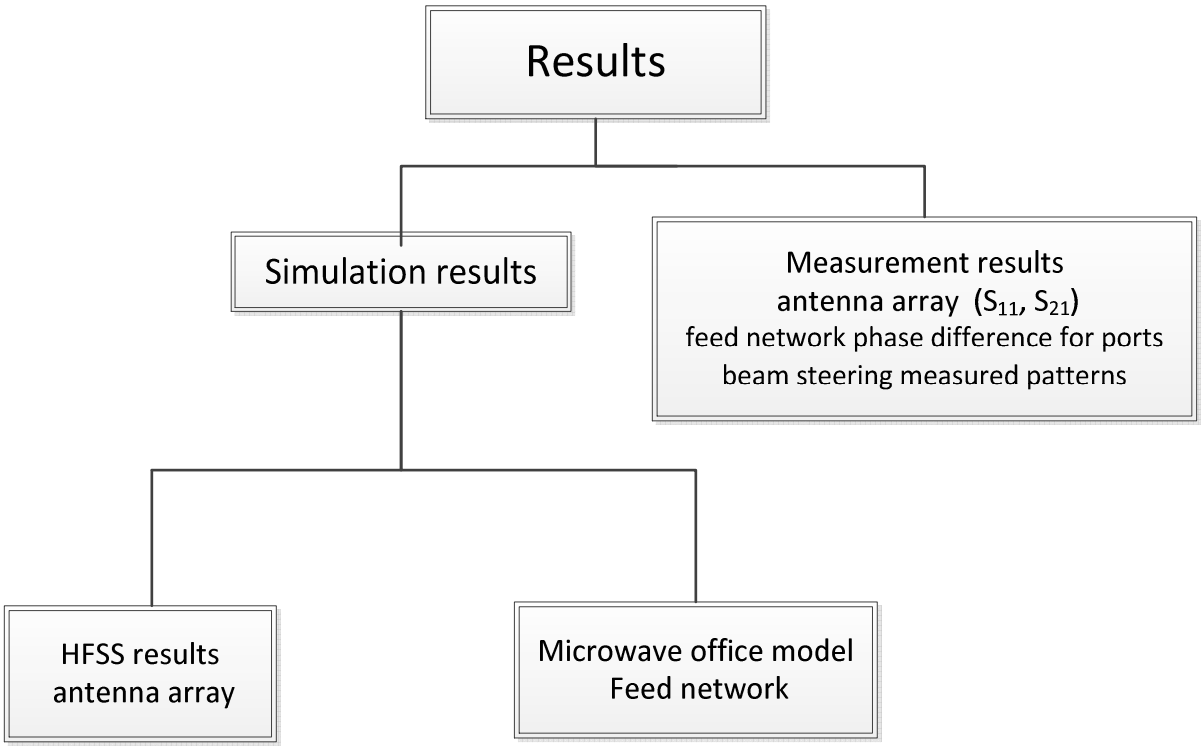

Figure 5.1: The final results tree

5.1 Simulation Results

5.1.1 Antenna Array Design

The HFSS model of the 12 element antenna array is shown in Figure 5.2. The antenna resonated at 2.45GHz with a Band Width of 24 MHz. The reflection coefficient curve for the 12 elements is shown in Figure 5.3. The worst case coupling value was -20dB.

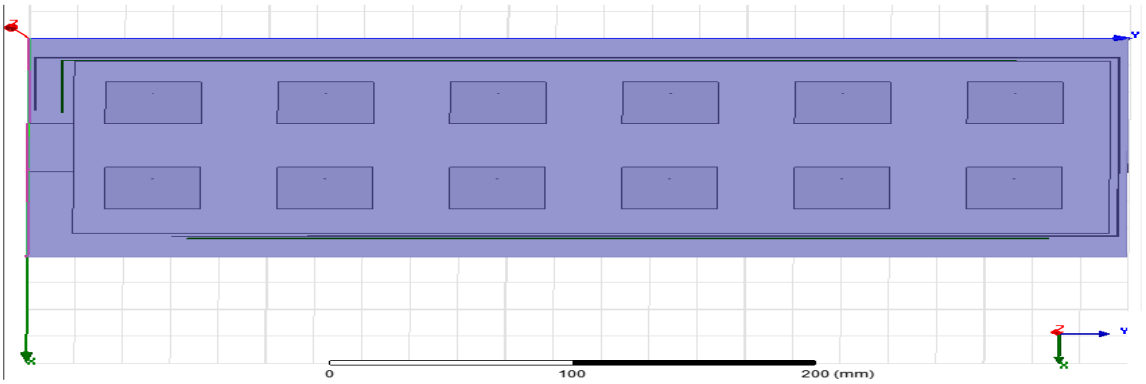

Figure 5.2 Antenna model Simulated in HFSS

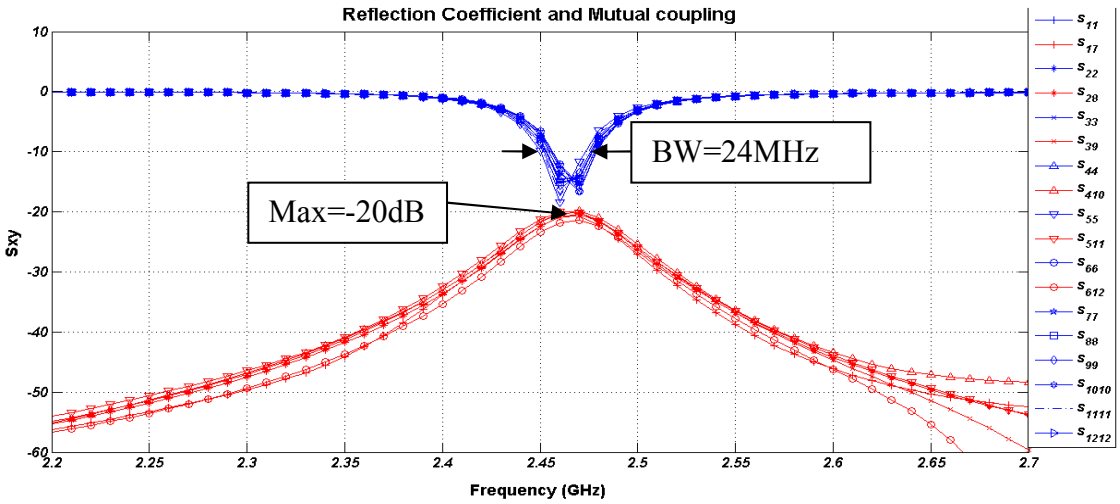

Figure 5.3 Simulated reflection coefficient and mutual coupling

In Figures 5.4-5.15 eleven cases for the beam steering process according to changing the values of θ_o and φ_o are presented. As the initial value of θ_o and φ_o change to certain value, the progressive phase in x and y are changed so this will change the beam direction and will be accordingly steered in each of the cases presented. A 3D contour plot of the gain pattern is shown along with 2D cuts for HPBW calculations.

In Figure 5.6, one example is shown where the beam is steered toward the angle $\theta=10^o$,$\varphi=300^o$. The maximum gain pattern to be located near to the centre of the contour plot towards the desired direction, while in Figure 5.10 ($\theta=40,\varphi=300$) the maximum antenna gain moved with respect to the first case. It is shown that an error due to approximation for determining the phase those are steering the beam to certain direction because of the 22.5 step angle for the 4-bit phase shifter. The maximum gain can be defined as 15.5 dBi at low values of theta, while the minimum 12 dBi at high theta (more than 70). In Figures 5.4 - 5.15 the beam is steered to the desired direction with error that can be clarified at Table 5.1. In Table 5.1 the gain, HPBW in theta and phi plane for 16 simulation cases are shown. The actual location of the beam has a good agreement with the desired location specially for elevation angles less than 50^o. It is desired to steer the beam toward $\theta_o=80^o$ and $\varphi_o=90^o$, but actually it is located at $\theta_o=50^o$. The main reason for this mismatch between the desired and the actual location is the ground plane that is reflecting any beam reaching near to it.

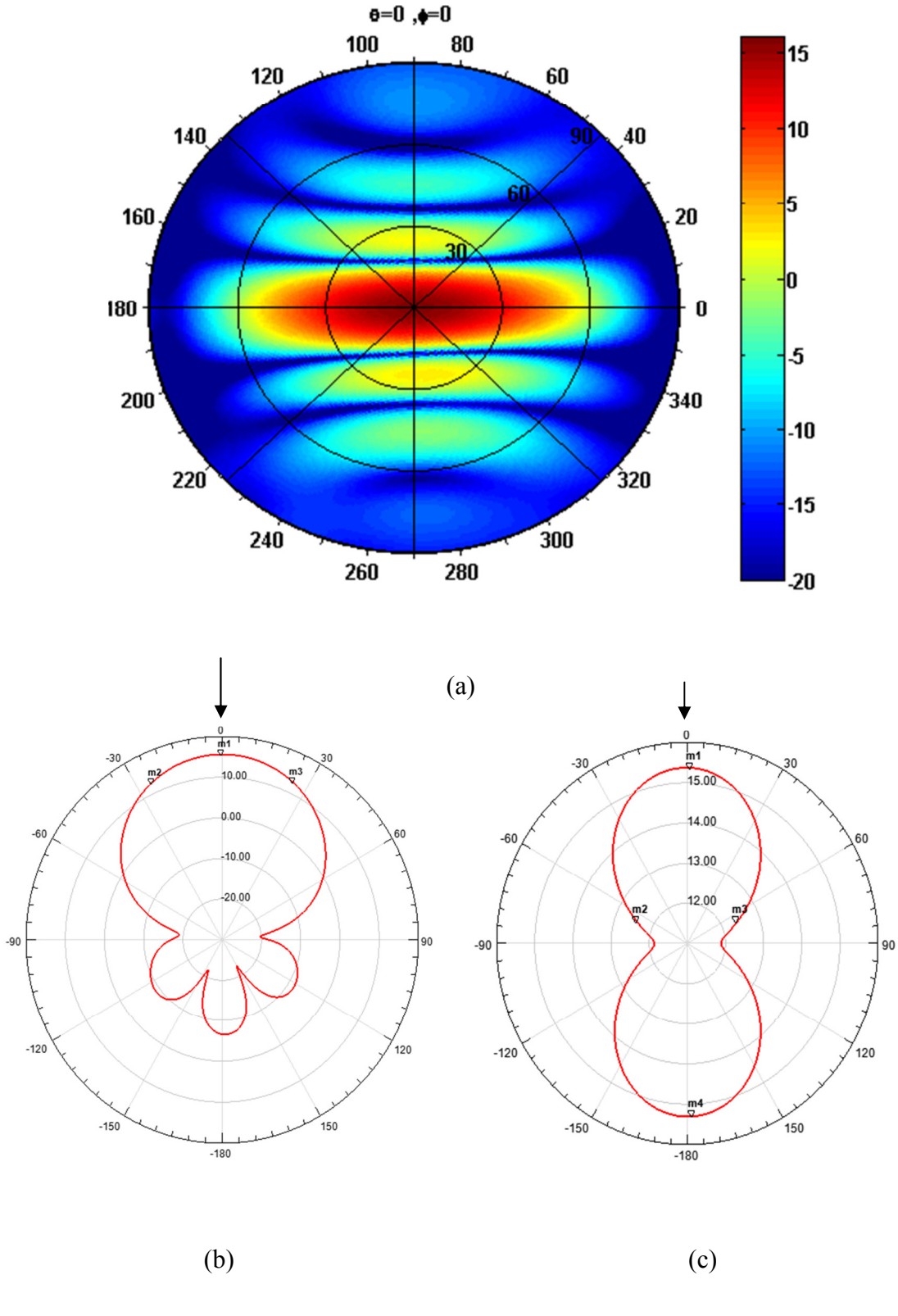

Figure 5.4: Beam steered toward θ=0,φ=0, (a) Contour plot for 3D Gain pattern,(b) Total Gain in Theta plane,(c) Total Gain in Phi Plane.

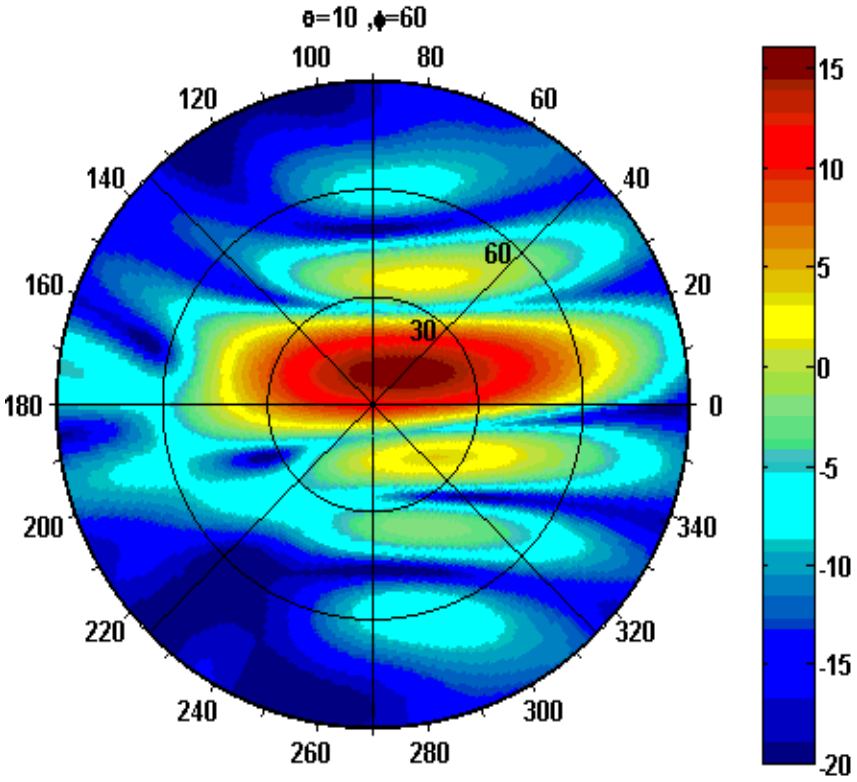

(a)

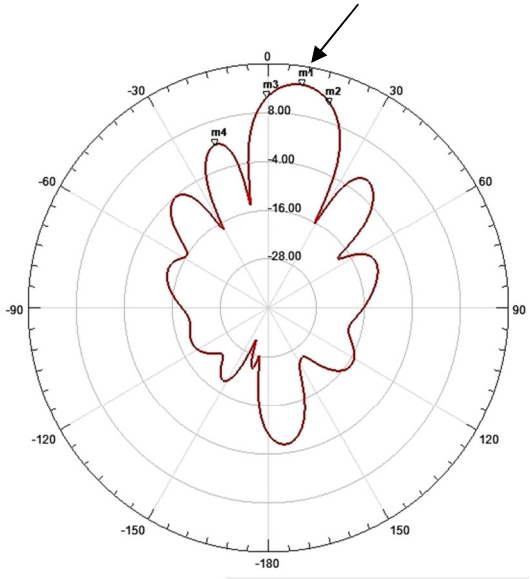

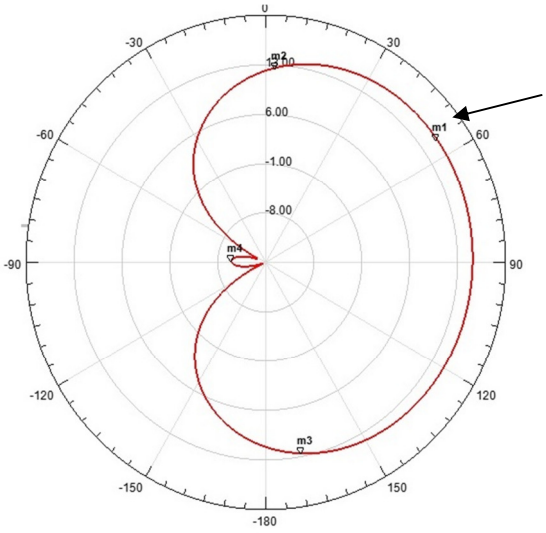

(b) (c)

Figure 5.5: Beam steered toward θ=10,φ=60,(a) Contour plot for 3D Gain pattern,(b) Total Gain in Theta plane,(c) Total Gain in Phi Plane.

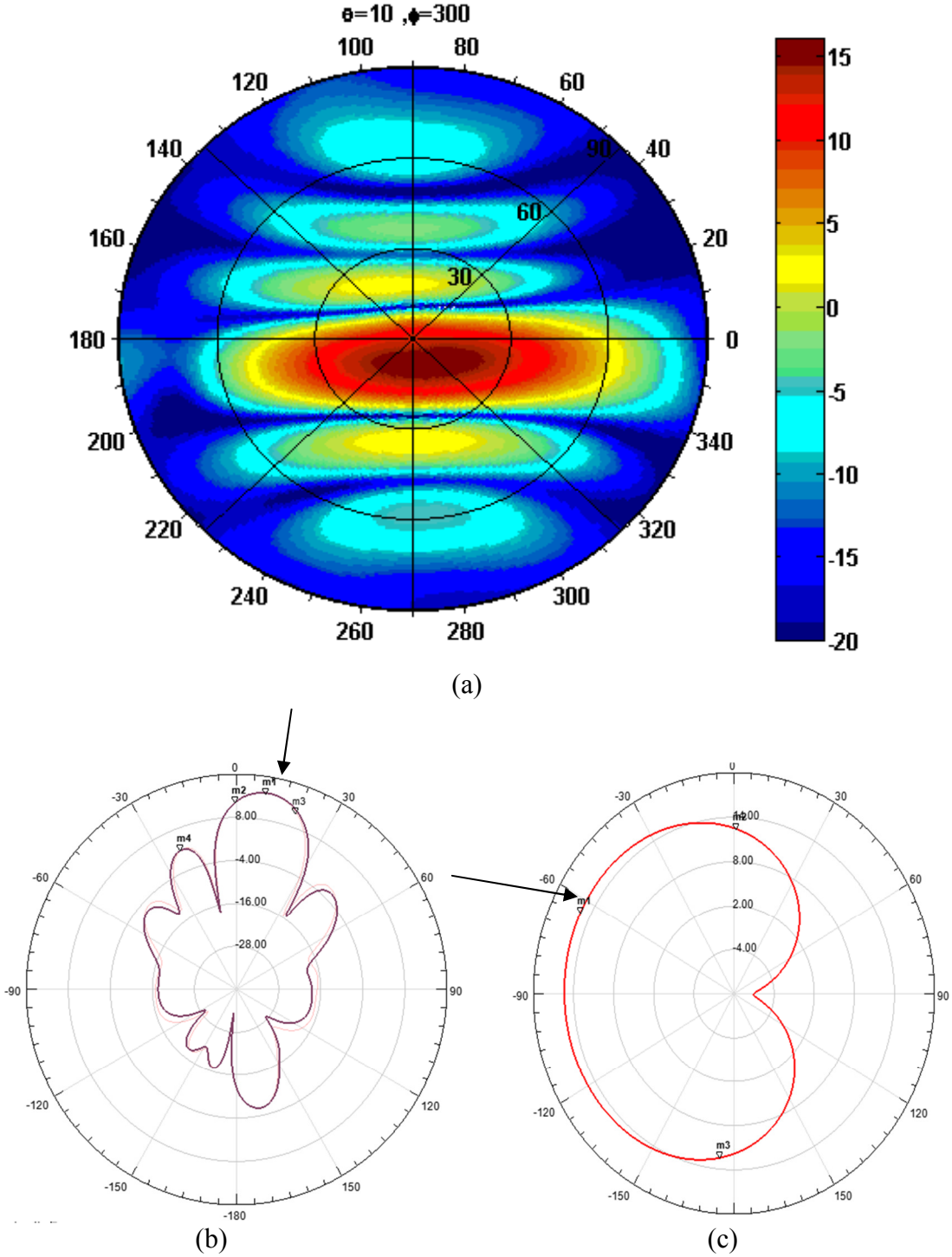

Figure 5.6: Beam steered toward θ=10,φ=300,(a) Contour plot for 3D Gain pattern,(b) Total Gain in Theta plane,(c) Total Gain in Phi Plane.

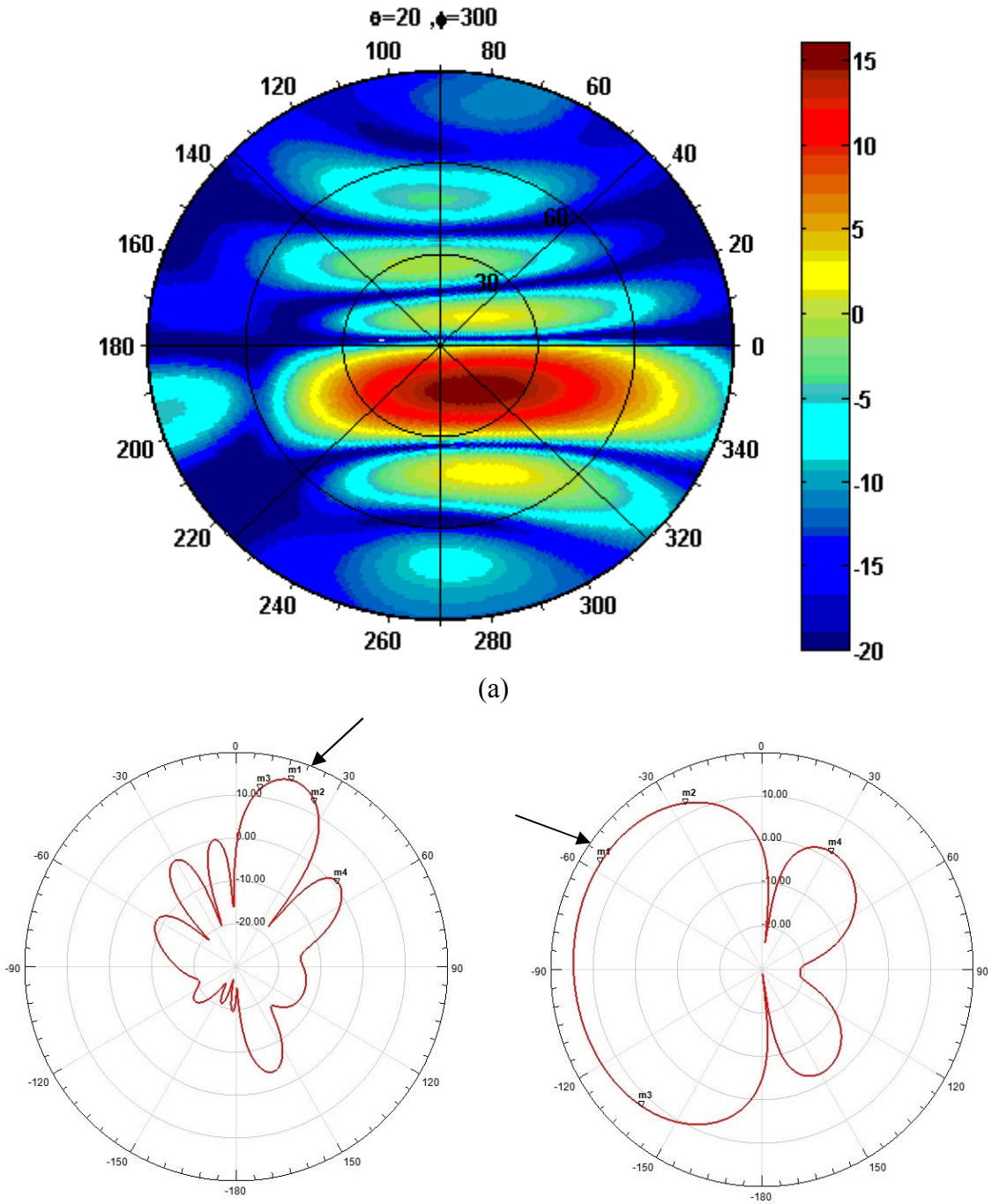

Figure 5.7: Beam steered toward θ=20,φ=300,(a) Contour plot for 3D Gain pattern,(b) Total Gain in Theta plane,(c) Total Gain in Phi Plane.

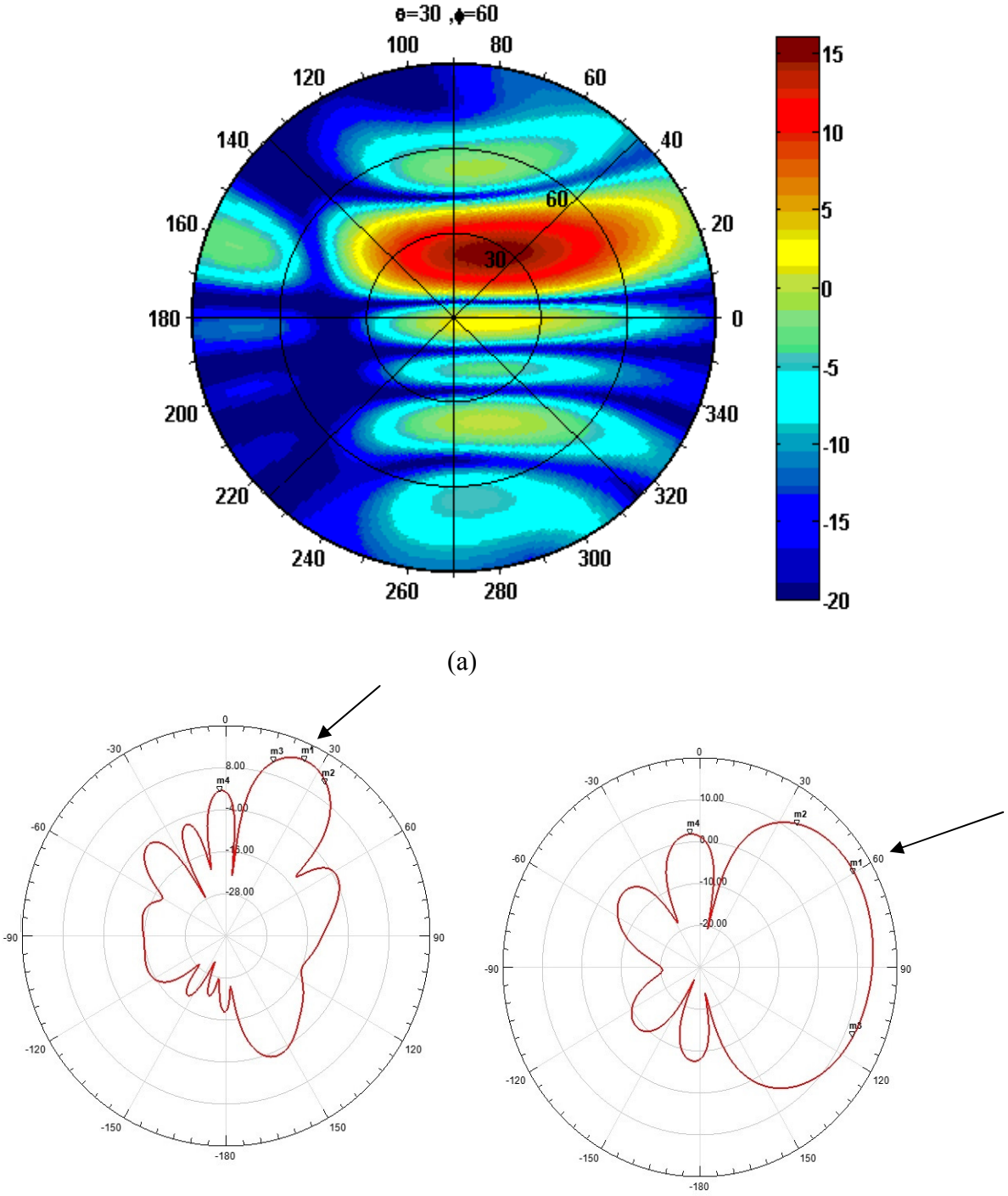

Figure 5.8: Beam steered toward θ=30,φ=60,(a) Contour plot for 3D Gain pattern,(b) Total Gain in Theta plane,(c) Total Gain in Phi Plane.

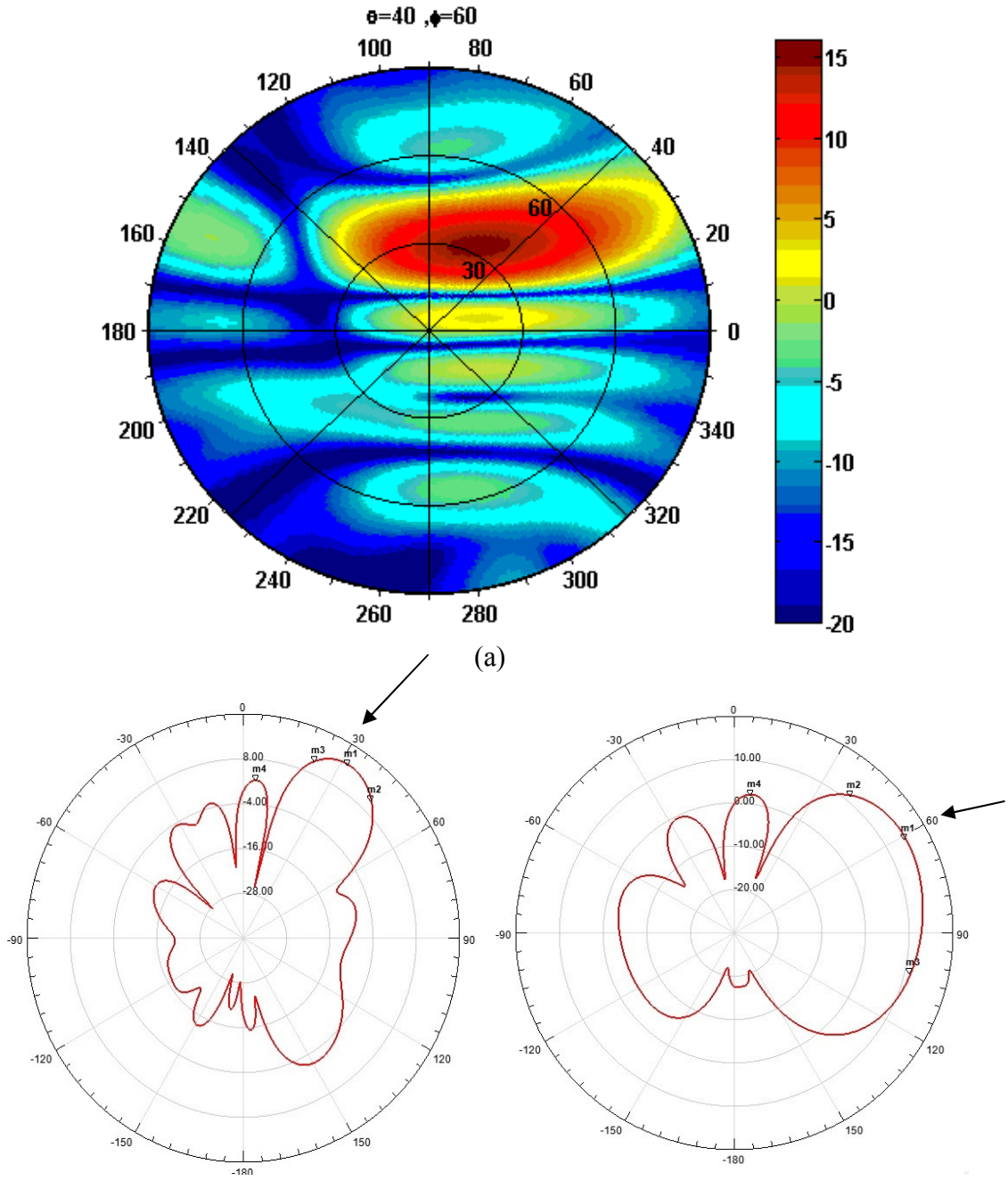

Figure 5.9: Beam steered toward θ=10,φ=300,(a) Contour plot for 3D Gain pattern,(b) Total Gain in Theta plane,(c) Total Gain in Phi Plane.

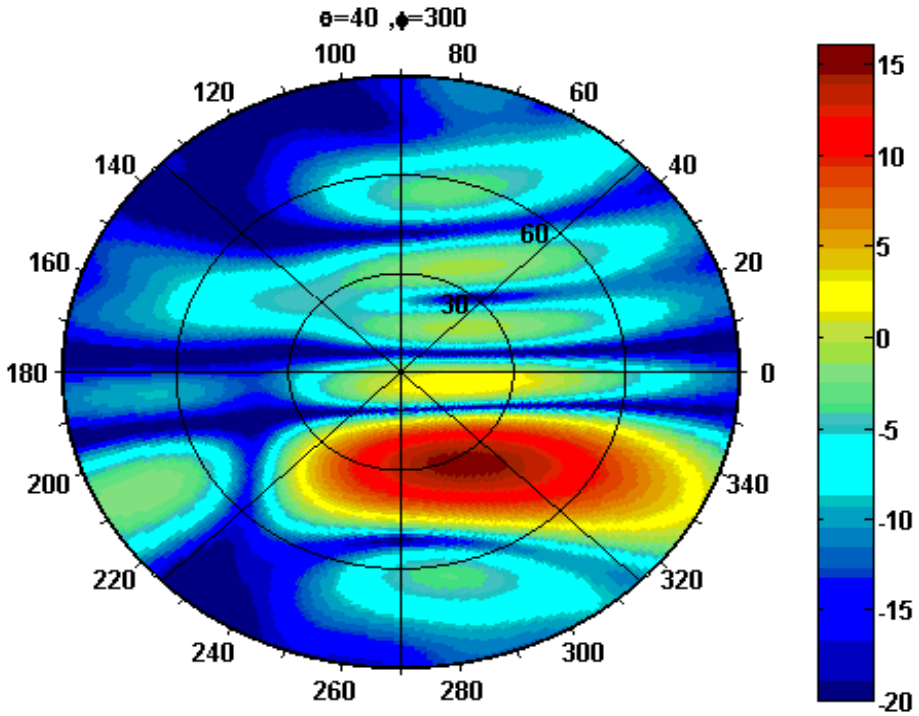

(a)

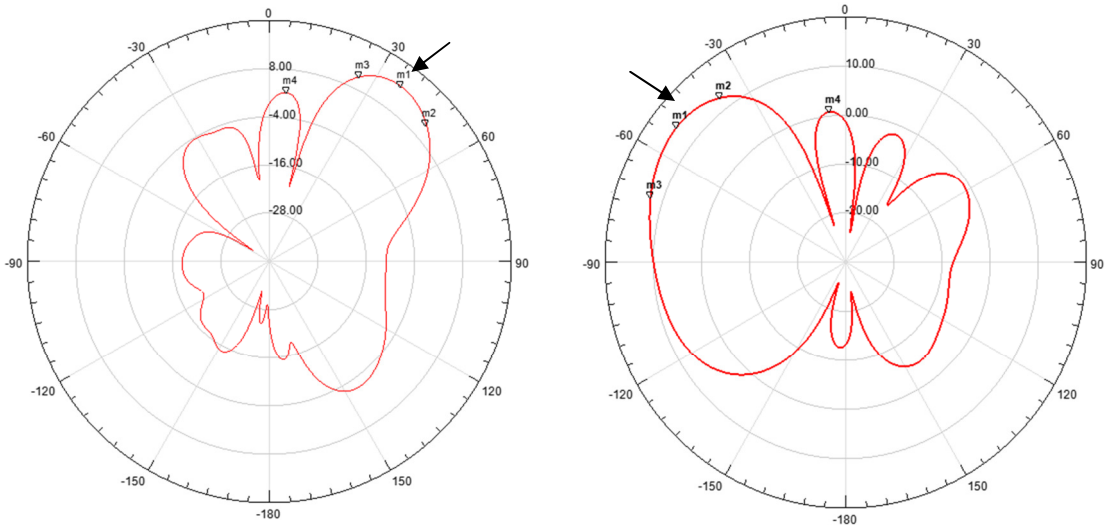

(b) (c)

Figure 5.10: Beam steered toward θ=40,φ=300,(a) Contour plot for 3D Gain pattern,(b) Total Gain in Theta plane,(c) Total Gain in Phi Plane.

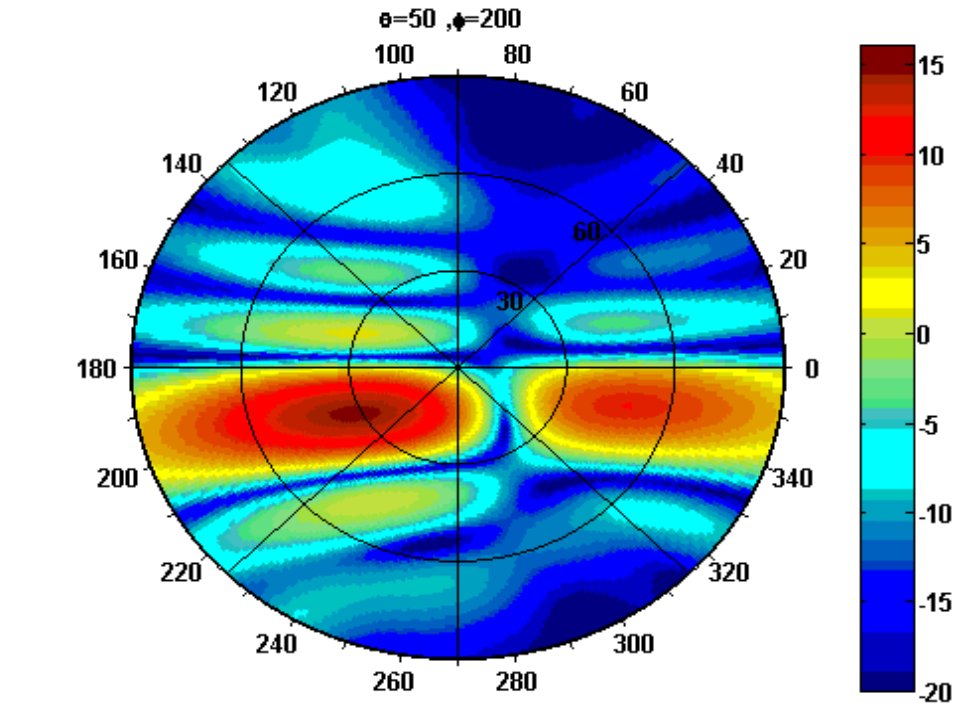

(a)

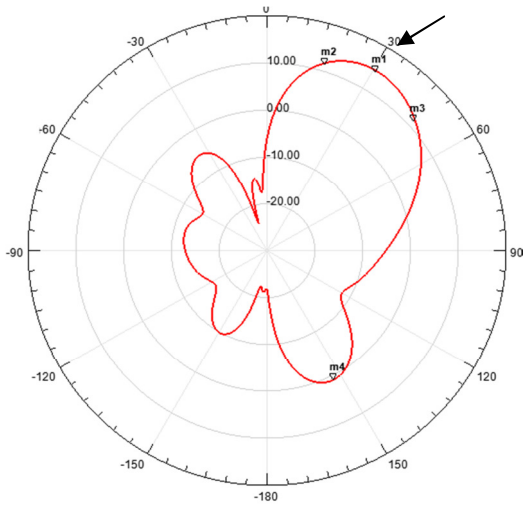

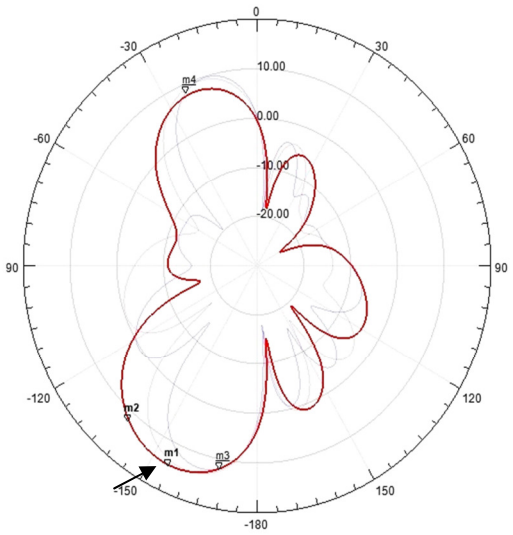

(b) (c)

Figure 5.11: Beam steered toward θ=50,φ=200,(a) Contour plot for 3D Gain pattern,(b) Total Gain in Theta plane,(c) Total Gain in Phi Plane.

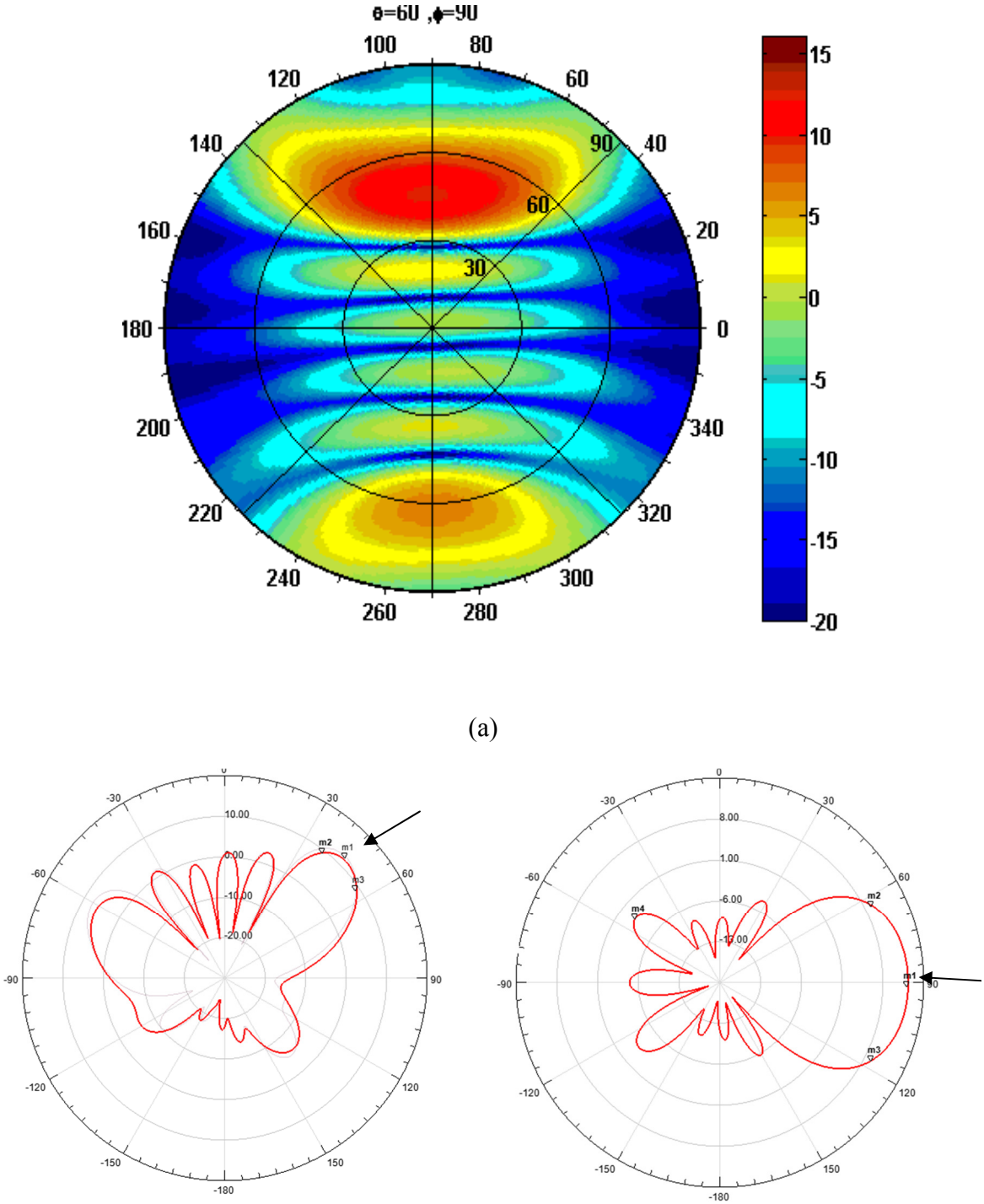

Figure 5.12: Beam steered toward θ=60,φ=90,(a) Contour plot for 3D Gain pattern,(b) Total Gain in Theta plane,(c) Total Gain in Phi Plane.

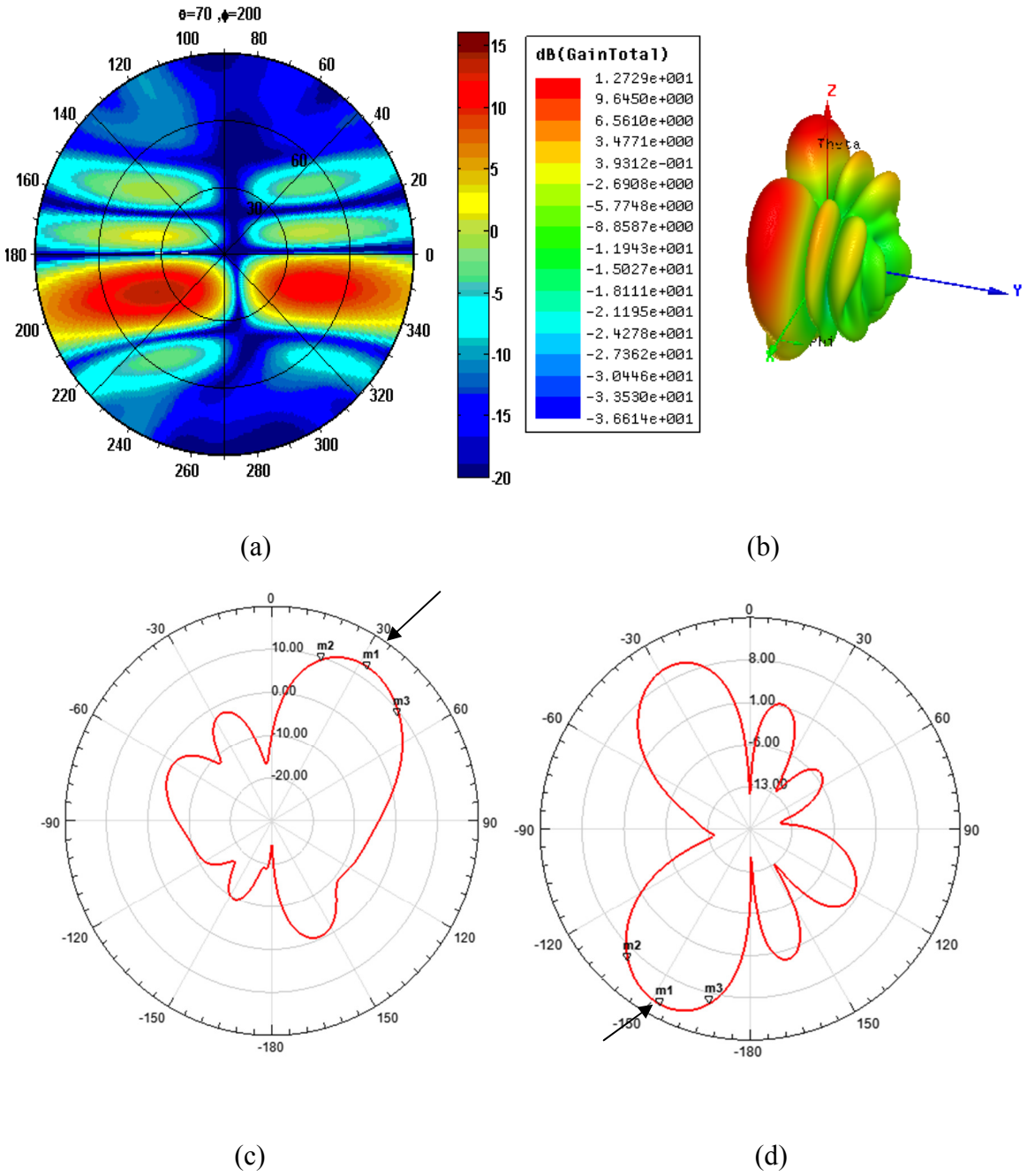

(a) (b)

(c) (d)

Figure 5.13: Beam steered toward θ=70,φ=200,(a) Contour plot for 3D Gain pattern,(b) 3D radiation pattern, (c) Total Gain in Theta plane,(d) Total Gain in Phi Plane.

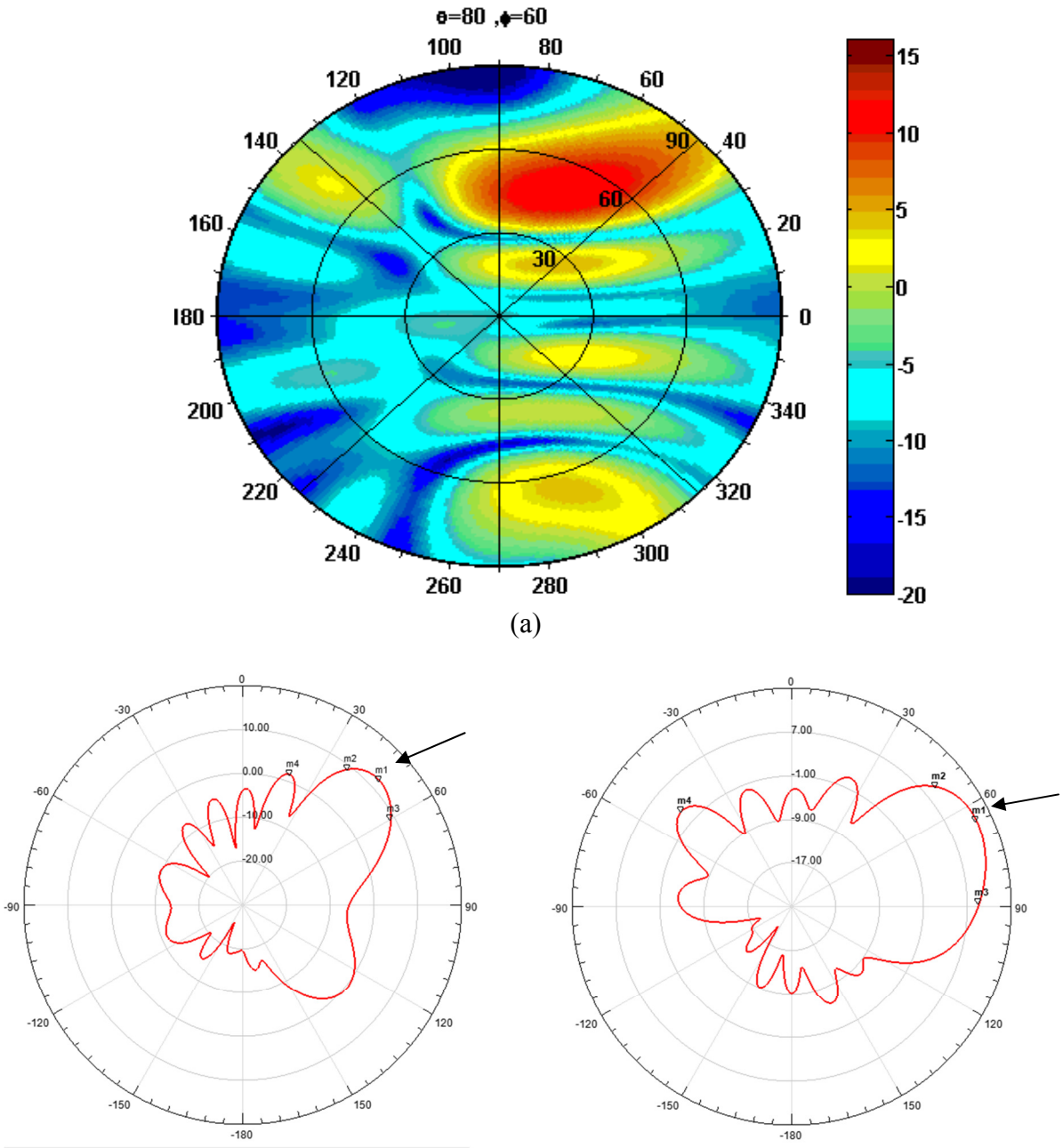

Figure 5.14: Beam steered toward θ=80,φ=60,(a) Contour plot for 3D Gain pattern,(b) Total Gain in Theta plane,(c) Total Gain in Phi Plane.

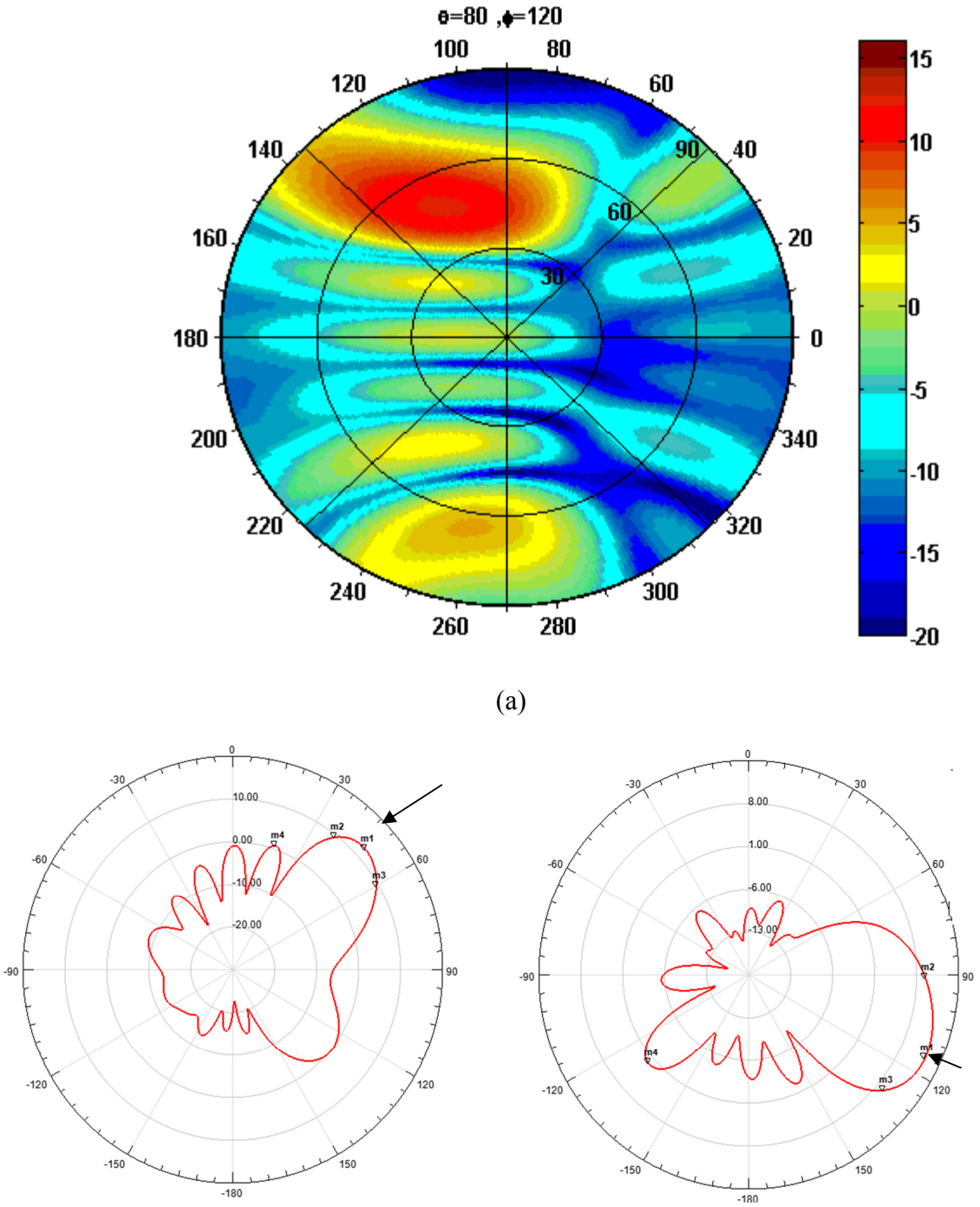

Figure 5.15: Beam steered toward θ=80,φ=120,(a) Contour plot for 3D Gain pattern,(b) Total Gain in Theta plane,(c) Total Gain in Phi Plane.

Table 5.1: Gain, Half power beam for 16 cases of beam steering.

Desired		Actual							
Theta	Phi	Theta	Phi	Error in location (Theta)%	Error in location (Phi)%	Max Gain Theta	Max Gain Phi	HPBW Theta	HPBW Phi
0	0	1	1	0.2	0.2	51	136	15.6	15.6
10	300	8	313	20	4.3	19	184	15.4	15.5
10	60	9	55	10	8.3	19	166	15.47	15.48
20	120	17	122	15	1.6	17	114	15.4	15.4
20	300	17	303	15	1	18	113	15.43	15.43
30	60	25	60	16.7	0	18	77	15.18	15.18
30	225	24	217	20	3.5	25	54	15.2	15.4
40	60	32	61	20	1.6	21	63	14.18	14.18
40	300	37	312	7.5	4	23	34	14.8	14.6
50	0	30	360	40	0.2	48	30	14.6	14.6
50	200	31	205	38	2.5	31	30	14.59	14.59
60	0	33	0	45	0	48	27	13.9	13.9
60	90	45	115	25	27.7	18	54	12.3	12.3
70	200	36	205	48.6	2.5	34	27	13.7	13.7
80	60	48	66	40	10	22	39	12.2	12.2
80	120	48	115	40	4.1	22	39	12.4	12.4

In Table 5.1, the Antenna gain, half power beam width (HPBW) are found for the 16 cases of steering angles. In Table 5.1 for the sixteen cases, the HPBW in theta plane, show relatively small variations, while HPBW in phi plane have large variation at small values of theta. In general for maximum gain in the elevation plane, the maximum gain decays as the elevation angle increases. For small values of elevation angles, the array factor achieves the maximum gain, as the elevation angle gets bigger and bigger, the array factor gain gets lower values. The shape of the antenna pattern mainly can be controlled by the pattern shape of the array factor, since the pattern of individual elements has the same response for different values of

elevation and azimuth angles. The error in location equal to the desired location (θ,φ) minus Actual location, divided by the actual location.

5.1.2 Feed Network Design

The first version (V1) design for the microwave feed network in the top layer of the phased array antenna, the amplitudes between the input port (SMA connector) and the antenna feeds, have maximum deviation of 1.1dB. This deviation can be interpreted because of amplitude imbalance of the combiners and some small differences in path length between input and the different output terminals. The manufacturer claimed that the combiner creates maximum of 1dB amplitude imbalance. Figure 5.16, shows the feed network layout of the first version. The wiring diagram was shown to clarify connections between various components in the feed network. In Figure 5.17, The curves for insertion loss for the initial design are shown where the values for all traces were between -14.5dB and -15.5dB. The difference in amplitude between input and output ports (as shown in Figure 5.17) will not affect the beam steering process. In Figure 5.18, the phase difference between the feeds of the antennas have maximum deviation of -25^{o}, this is due to the combiner phase imbalance and some differences in the path length for the different output terminals for V2. While the insertion loss between the input port and output port 1 feed of the antenna in six different phase states (0^{o},22.5^{o},45^{o},90^{o},180^{o} and 360^{o}) is shown in Figure 5.19.

The design was updated to have exactly the same path length between the input and the antenna feed terminals. In this third version (V3) of the design, the maximum deviation in amplitude was 0.5dB while the maximum phase difference between antenna feed paths was 7^{o} as shown in Figures 5.20 and 5.21. The insertion loss between the input port and the first output port at six different phase shift states (0, 22.5, 45, 90, 180 and 337.5) for the final design as shown in Figure 5.22

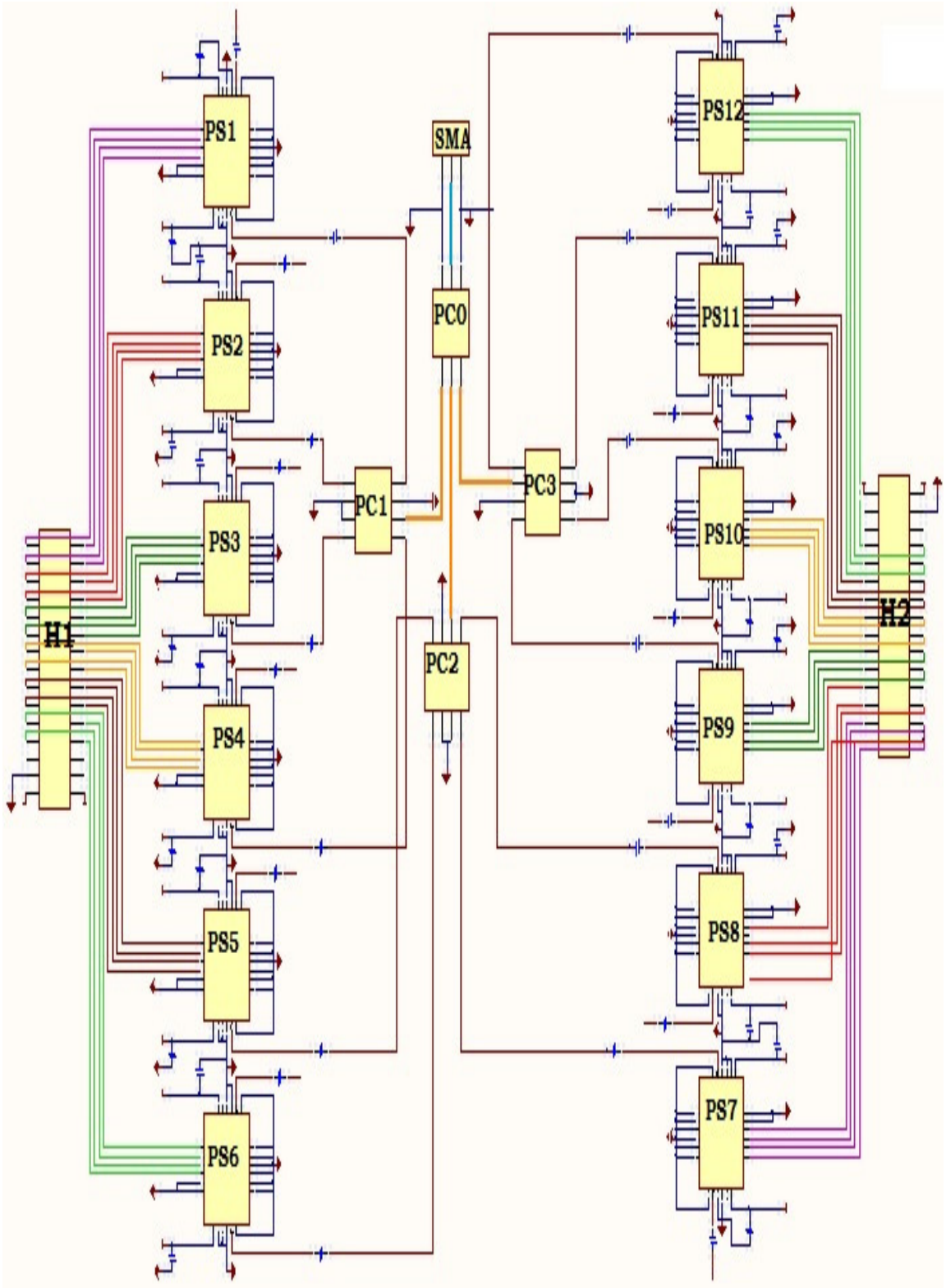

Figure 5.16:Schematic diagram for the feed network(V1).

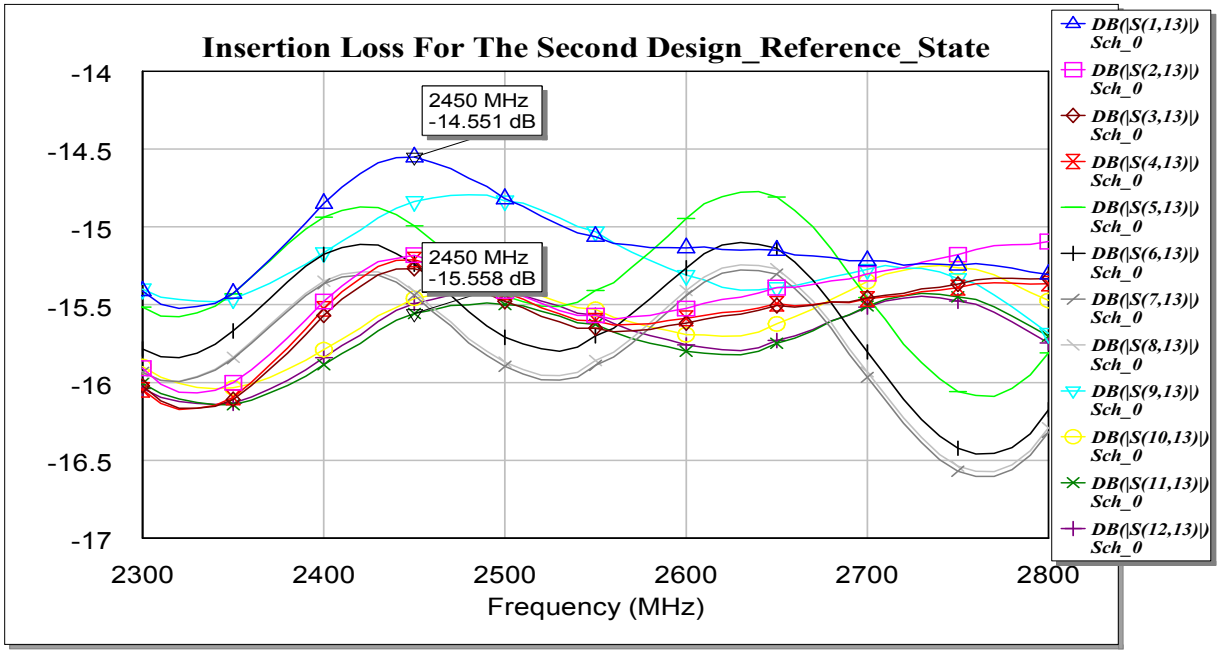

Figure 5.17 The Insertion Loss For The Model At Reference State (V2)

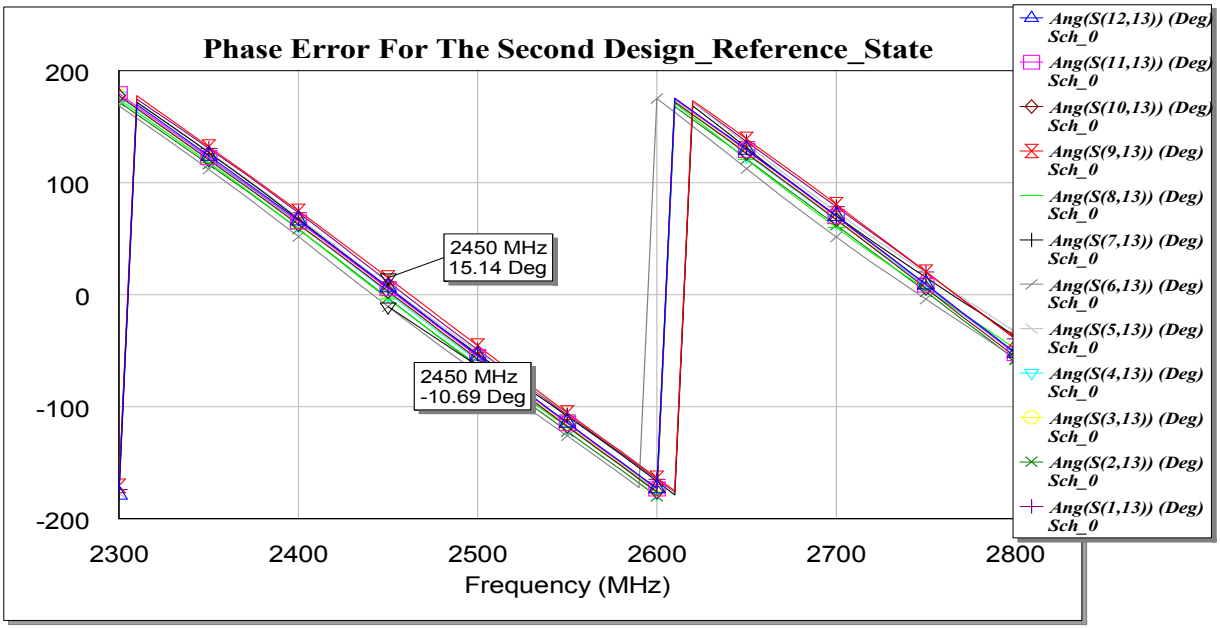

Figure 5.18: Phase Error For The Model At Reference State (V2)

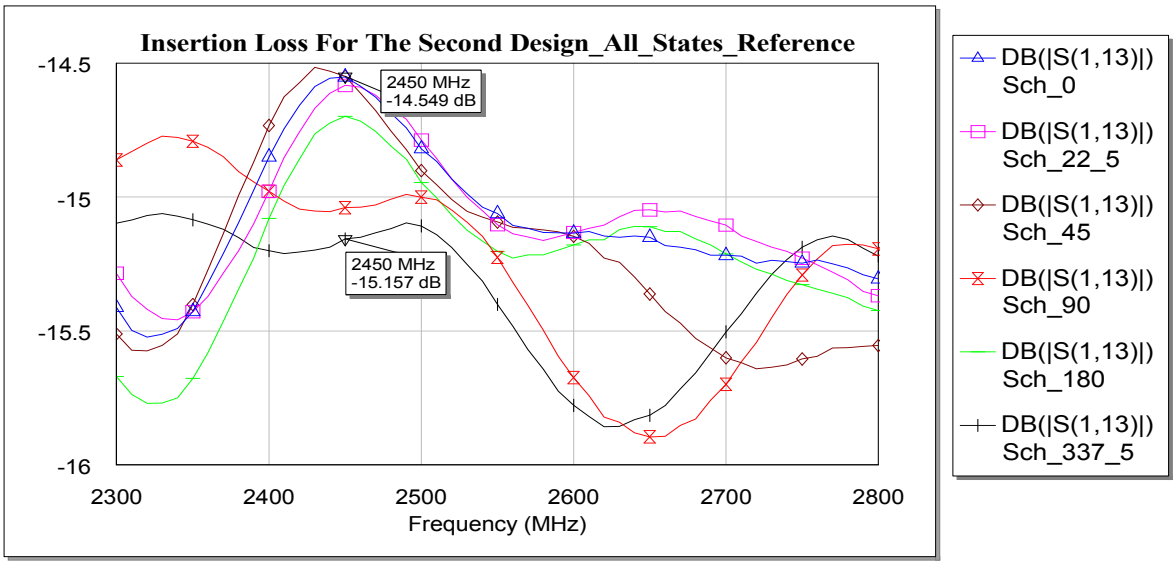

Figure 5.19: The Insertion Loss For The Model Between Input Port and First Output Port For All Phase Shift States (V2)

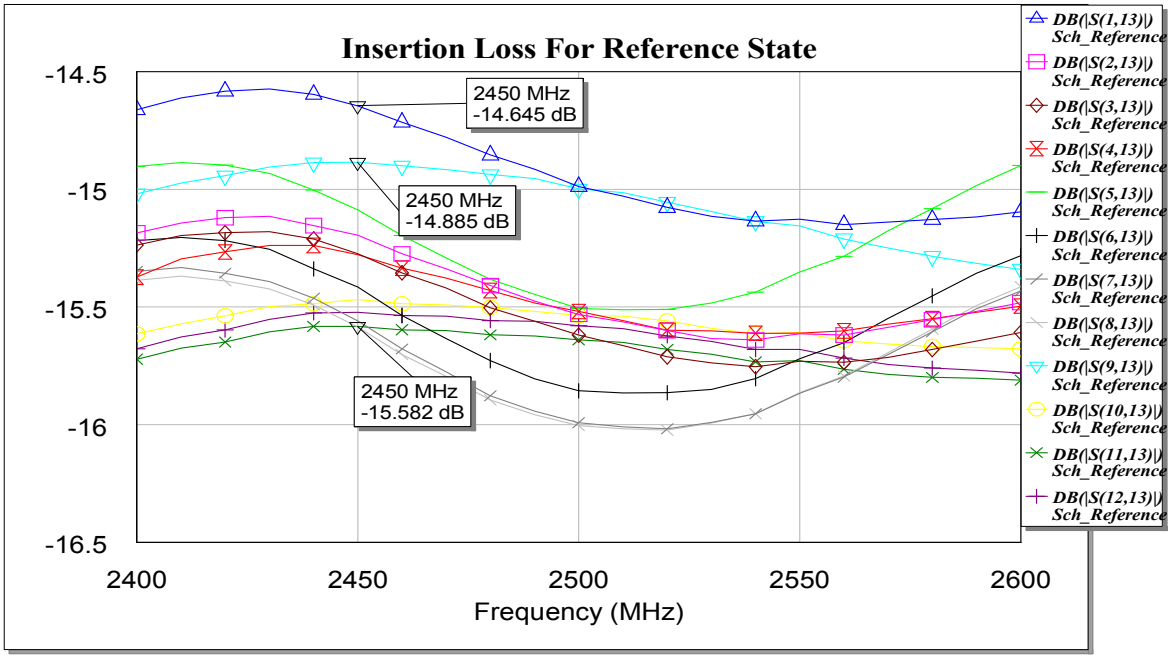

Figure 5.20 The Insertion Loss For The Model At Reference State (V3)

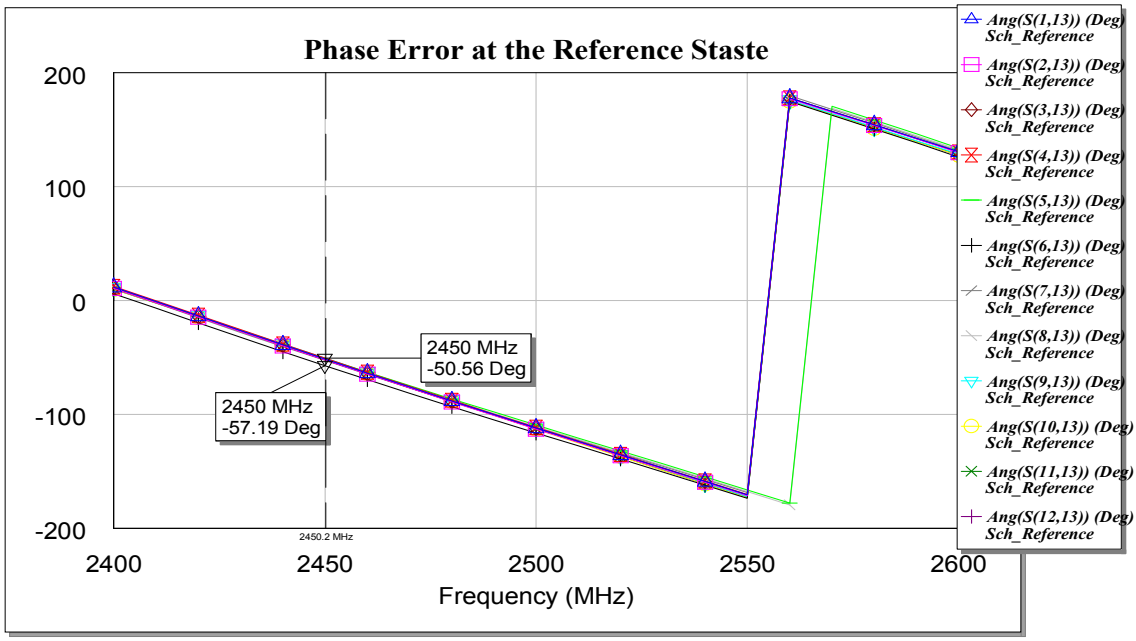

Figure 5.21: Phase Error For The Model At Reference State (V3)

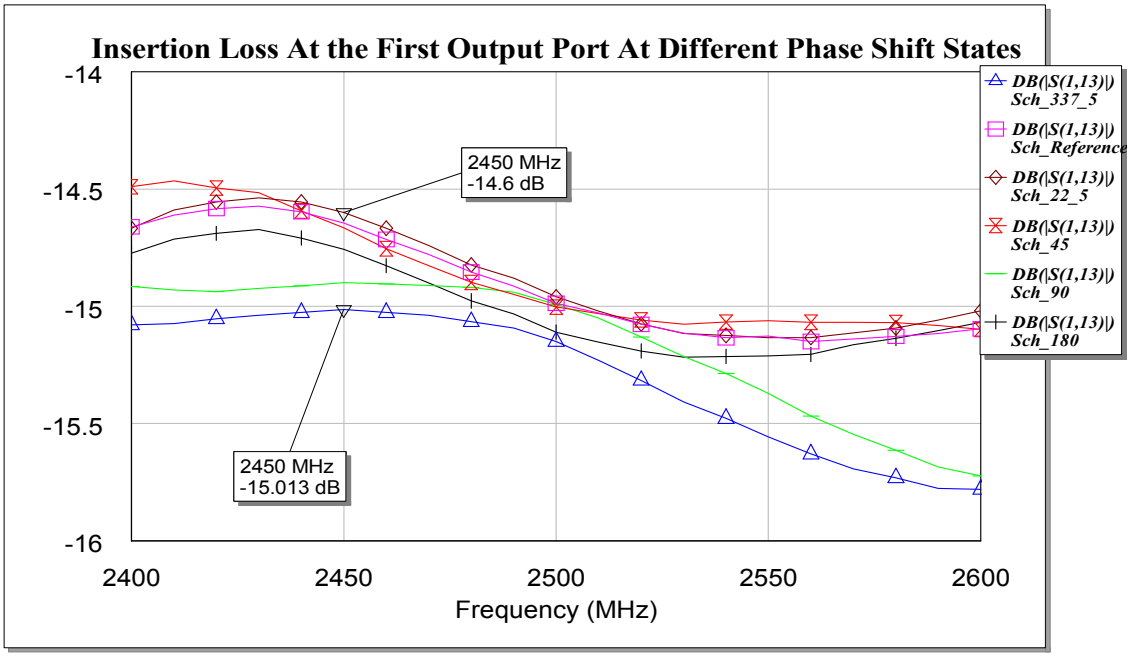

Figure 5.22: The Insertion Loss For The Model Between Input Port and First Output Port For All Phase Shift States (V3)

5.2 Measurement Results

In this section, the reflection coefficient and the mutual coupling of the proposed antenna are measured. Moreover, the phase and the amplitude difference between the input port of the array (connected to the SMA connector) and output terminals for the arrays are measured as well. The measurements were conducted in the Antennas and Microwave Structure design lab (AMSDL) at KFUPM using an Agilent N9918A vector network analyzer (VNA). These measurements were done by connecting the measuring device at antenna feed port through coaxial cables as shown in Figure 5.23. Figure 5.24 shows the reflection coefficient curves for the different radiating elements. A maximum mutual coupling of -20dB can be seen in Figure 5.25. The measured phase difference between output ports is presented in Figure 5.26. This Figure shows significant difference in phase 32^{o}. Figure 5.27 shows 1.75dB difference in amplitude. The differences are due to amplitude and phase imbalance in the combiners and the difference in path length between the input port and the output terminals.

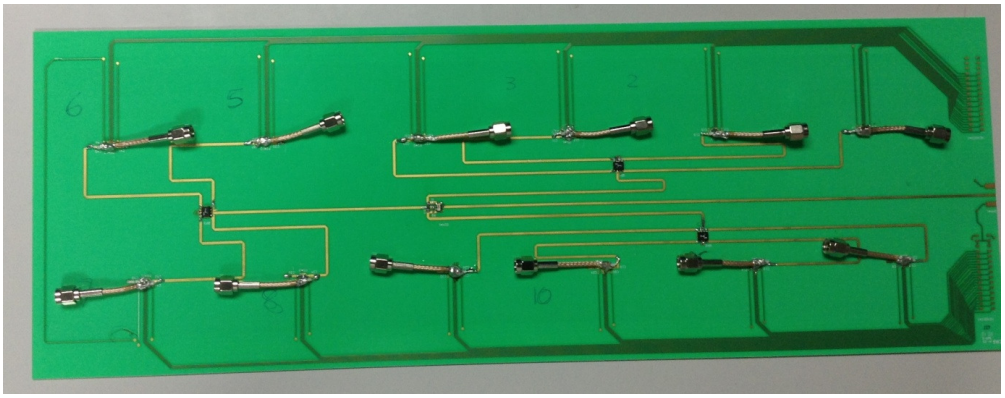

Figure 5.23: Fabricated (V1) feed network

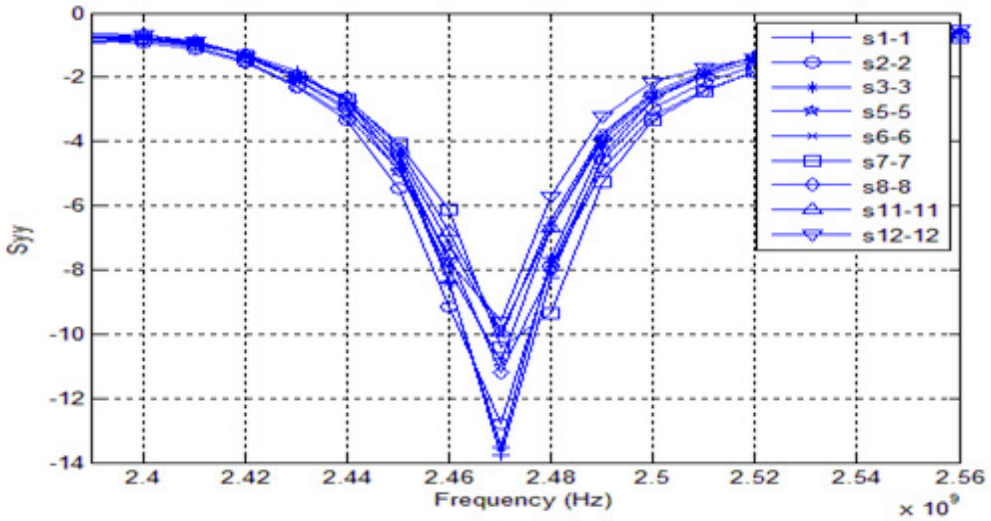

Figure 5.24: Reflection coefficient for different antenna elements (V1)

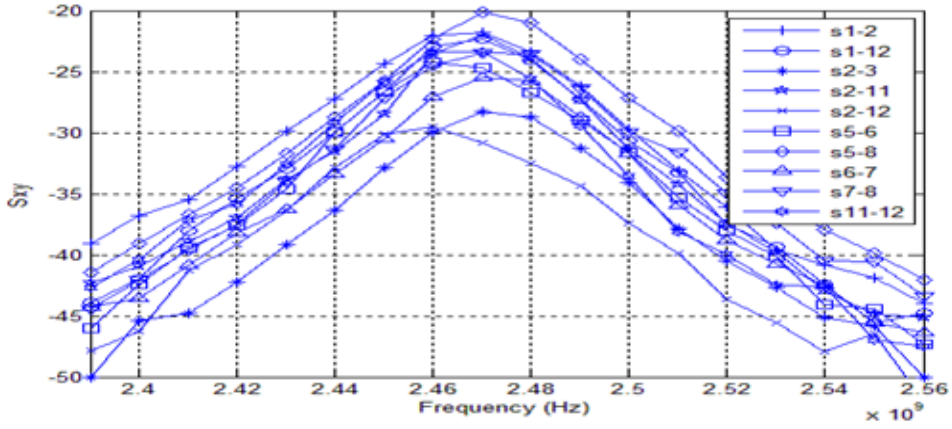

Figure 5.25: Mutual coupling for different antenna elements (V1)

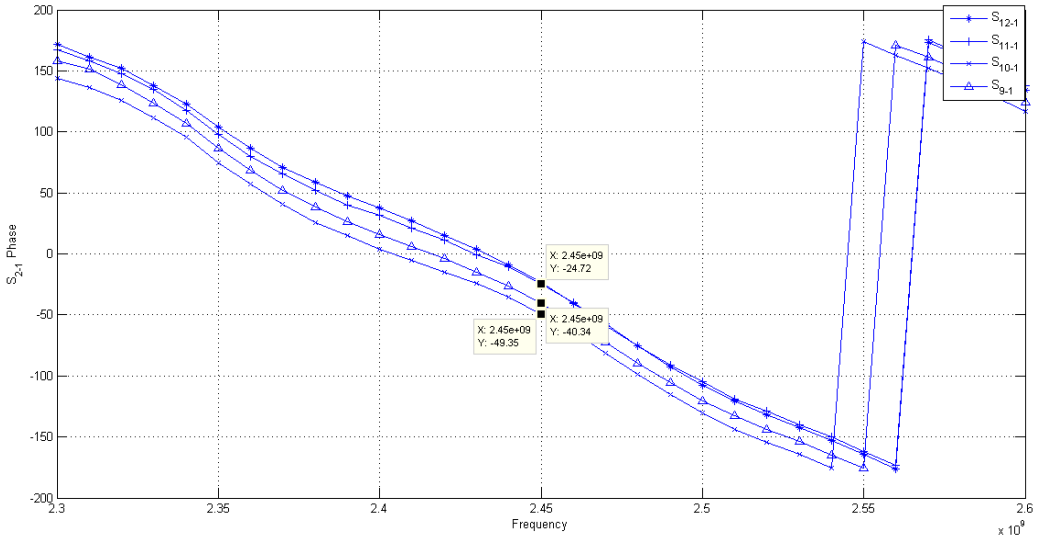

Figure 5.26: Measured phases at different output terminals (V1)

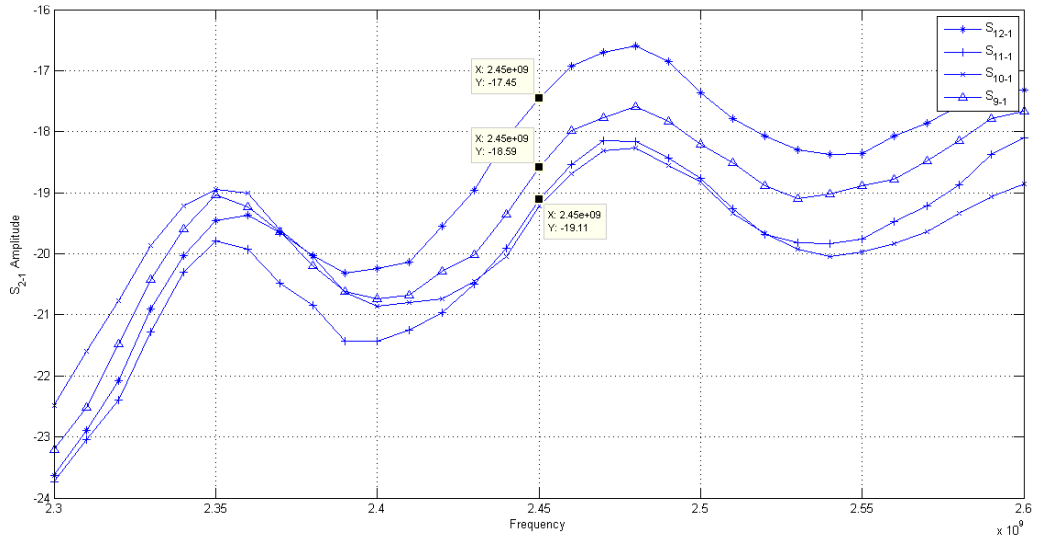

Figure 5.27: Measured Amplitudes at different output terminals (V1)

5.3 Conclusion

A 12-element planar antenna array with patch elements operating at 2.47 GHz along with its integrated feed network is presented. The array has beam steering capabilities via the use of digitally controlled radio frequency (RF) phase shifters. The array and its feed network were fabricated on a 3-layer PCB of RO4035 material with total dimensions of 460 x161.9x 1.27mm^3. To total array weight was 229 gm. The array is to be integrated within the wing structure of a small to medium size UAV. Simulated and measured results are presented for the array performance metrics.

CHAPTER 6

Minimum Number of phase Shifters For A Phased Array Design

In this chapter, four methods are investigated to reduce the number of phase shifters to reduce the design complexity and investigate its effect on the beam scanning capability. The four methods are applied on the previously described planar 12-element array. In the First method, we use one phase shifters for each row feeding two patch elements simultaneously. The phase difference between two adjacent patch elements in the same row is β_x which means that at each θ two values at φ 90^o and 270^o was considered. In the second method, the patch elements in each column require a single phase shifter. This yields at phi 0^o and 180^o. The third method is the combination of the first and second methods which means that at each θ four φ angles 0^o,90^o,180^o and 270^o can be provided. In this design, six phase shifters, can be used along with three 4x2 switched matrix IC (HMC276QS24 / 276QS24E, or HMC276LP4 / HMC276LP4E) RF switch. In the fourth method, six two-way 90^o hybrid coupler are used to provide full coverage under the wing structure. Also six transfer switch is used as well to switch the polarity between the two columns.

6.1 First Method

In this method the beam scanning is provided for limited values of phi. The beam scanning can be performed at all values of θ at two values of φ at 90^o and 270^o. In this design, the following components are required.

1. One SMA connecter
2. Two three-way splitter/combiner
3. Six phase shifters
4. Seven two-way power combiner

The number of phase shifters is reduced to less than 50% of that used in the original design with 12 phase shifters. The power loss in the traces is also reduced according to the components reduction. The proposed design is shown in Figure 6.1. In Figure 6.2, the proposed integrated antenna array diagram for the first method is shown with new routing methodology in the top layer.

Figure 6.3 shows the 3-D gain pattern for $\theta=50^{o}$ and $\varphi=90^{o}$. Figure 6.4 shows 2-D gain pattern at theta plane, while Figure 6.5 shows 2-D gain pattern at phi plane. In Table 6.1, all theta and phi combinations that can be covered by this design are presented .

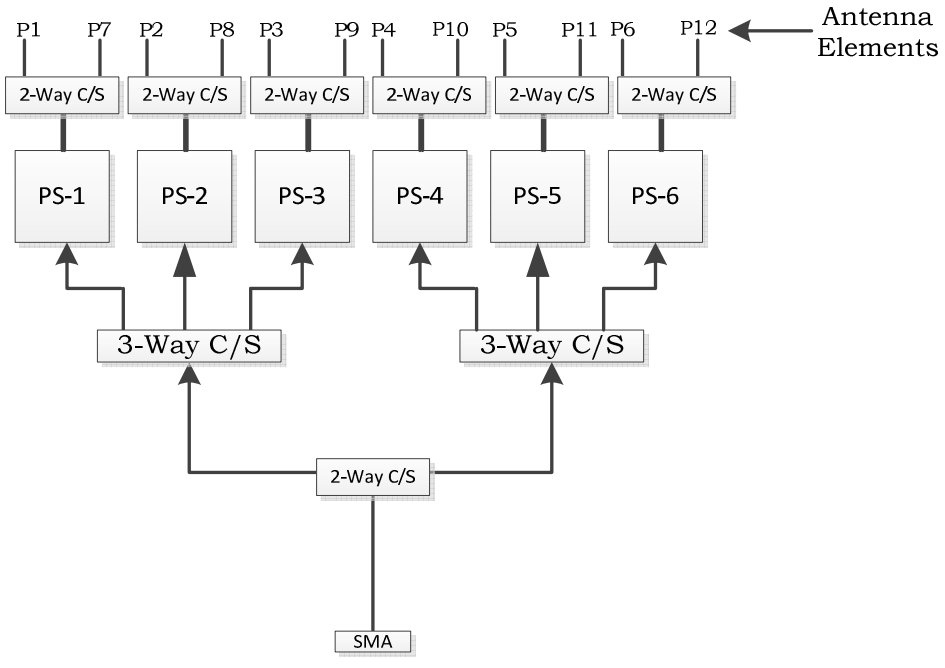

Figure 6.1: The schematic of the first design

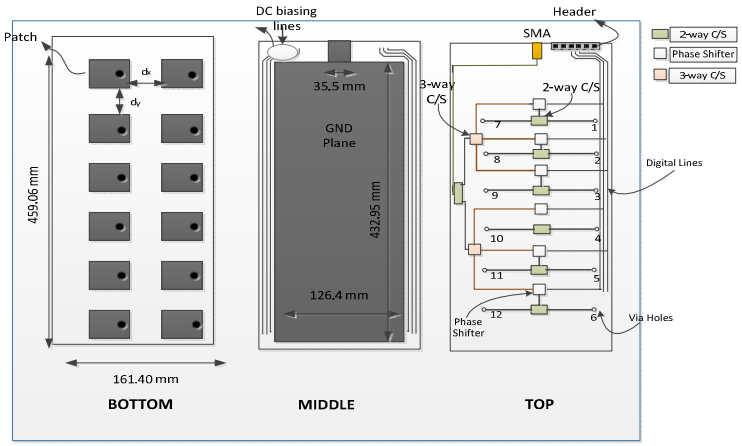

Figure 6. 2: Proposed integrated antenna array diagram,

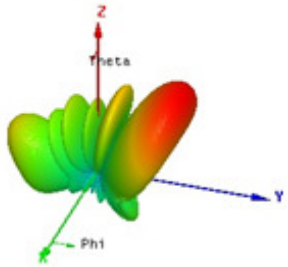

Figure 6.3: Radiation pattern for the total gain at θ=50, φ=90

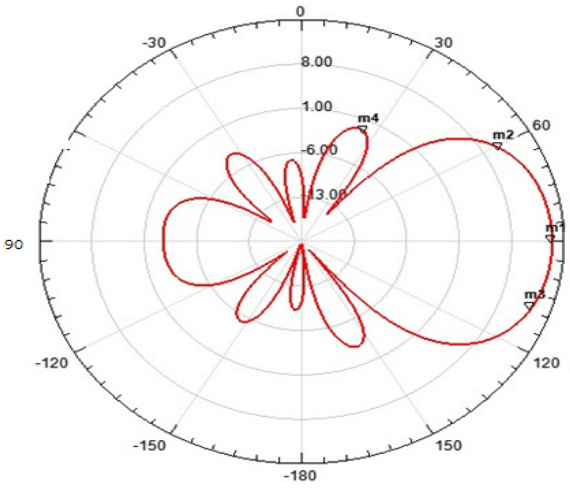

Figure 6.4: Total gain in Theta plane at φ=90

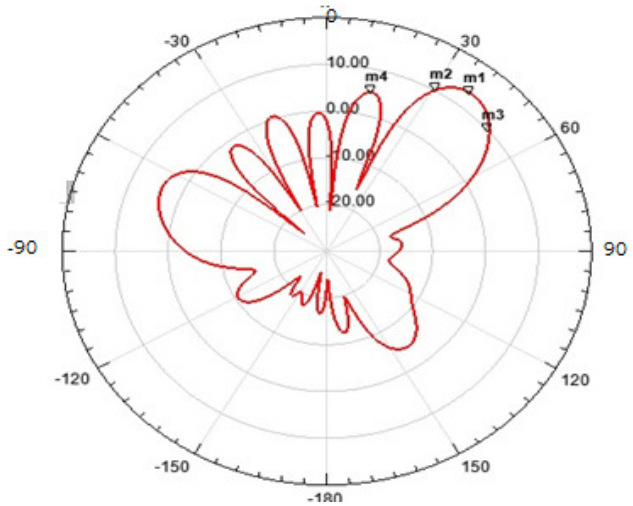

Figure 6.5: Total gain in Phi plane at θ=50

Table 6.1: Simulation results for the first design

Desired		Actual							
Theta	Phi	Theta	Phi	Location error (Theta)%	Location error (Phi)%	Max Gain Theta	Max Gain Phi	HPBW Theta	HPBW Phi
10	90	9	77	10	14.4	15.044	15.044	14	154
10	270	9	281	10	4.1	15.019	15.019	14	156
20	90	17	76	15	15.6	15.127	15.127	15	105
20	270	16	272	20	0.7	15.374	15.374	15	105
30	90	24	90	20	0	14.961	14.961	16	79
30	270	25	271	16.7	0.37	15.016	15.016	16	82
40	90	33	90	17.5	0	14.364	14.364	17	66
40	270	33	271	17.5	0.37	14.442	14.442	17	67
50	90	39	90	22	0	13.428	13.428	19	57
50	270	39	271	22	0.37	13.519	13.519	19	60
60	90	45	91	25	1.11	12.34	12.34	20	53
60	270	45	270	25	0	12.489	12.489	20	53
70	90	48	91	31.4	1.11	11.408	11.408	21	50
70	270	48	270	31.4	0	11.66	11.66	21	52
80	90	50	91	37.5	1.11	10.758	10.758	22	47
80	270	51	272	36.25	0.74	10.648	10.648	21	48

In Table 6.1, the average HPBW at θ plane is 18 and at Phi plane is 77. In Figure 6.6 the schematic diagram for the MWO model is shown. In Figures 6.7, and 6.8 the insertion loss and

phase error curves between the input port and the output ports are shown respectively Note that the insertion loss was less than 0.5dB and the phase imbalance was 8 degrees. In Figure 6.16, the total coverage of the first design where, θ=20 and φ=90,270, θ=40 and φ=90,270, θ=80 and φ=90,270, θ=0, φ=0 are shown. Some spots are not covered by the beam produced by the first method while most of the space is covered as shown in the figure 6.16. Table 6.2 is showing the excitation phase for Theta=40 and Phi=90, while in Table 6.3 the excitation phase at θ=40 and φ=270. The excitation phases for adjacent elements in the same row have the same value. Because the difference between each adjacent elements in the same row is β_x and β_x equal to zero at φ=90 and φ=270 where β_x is given by equation (2.29). Figures 6.9 to 6.15 show the coverage of each angle in a separate 3-D gain contour plot. While Figures 6.16 and 6.17 shows the total coverage of all angles superimposed in single plot.

Table 6.2: Excitation phase at θ =40, φ =90

Antenna Elements	No of Steps	Excitation Phase	Antenna Elements	No of Steps	Excitation Phase
Ant-1	5	-112.5	Ant-7	5	-112.5
Ant-2	10	-225	Ant-8	10	-225
Ant-3	15	-337.5	Ant-9	15	-337.5
Ant-4	5	-112.5	Ant-10	5	-112.5
Ant-5	10	-225	Ant-11	10	-225
Ant-6	15	-337.5	Ant-12	15	-337.5

Table 6.3: Excitation phase at θ =40, φ =270

Antenna Elements	No of Steps	Excitation Phase	Antenna Elements	No of Steps	Excitation Phase
Ant-1	5	112.5	Ant-7	5	112.5
Ant-2	10	225	Ant-8	10	225
Ant-3	15	337.5	Ant-9	15	337.5
Ant-4	21	112.5	Ant-10	21	112.5
Ant-5	26	225	Ant-11	26	225
Ant-6	31	337.5	Ant-12	31	337.5

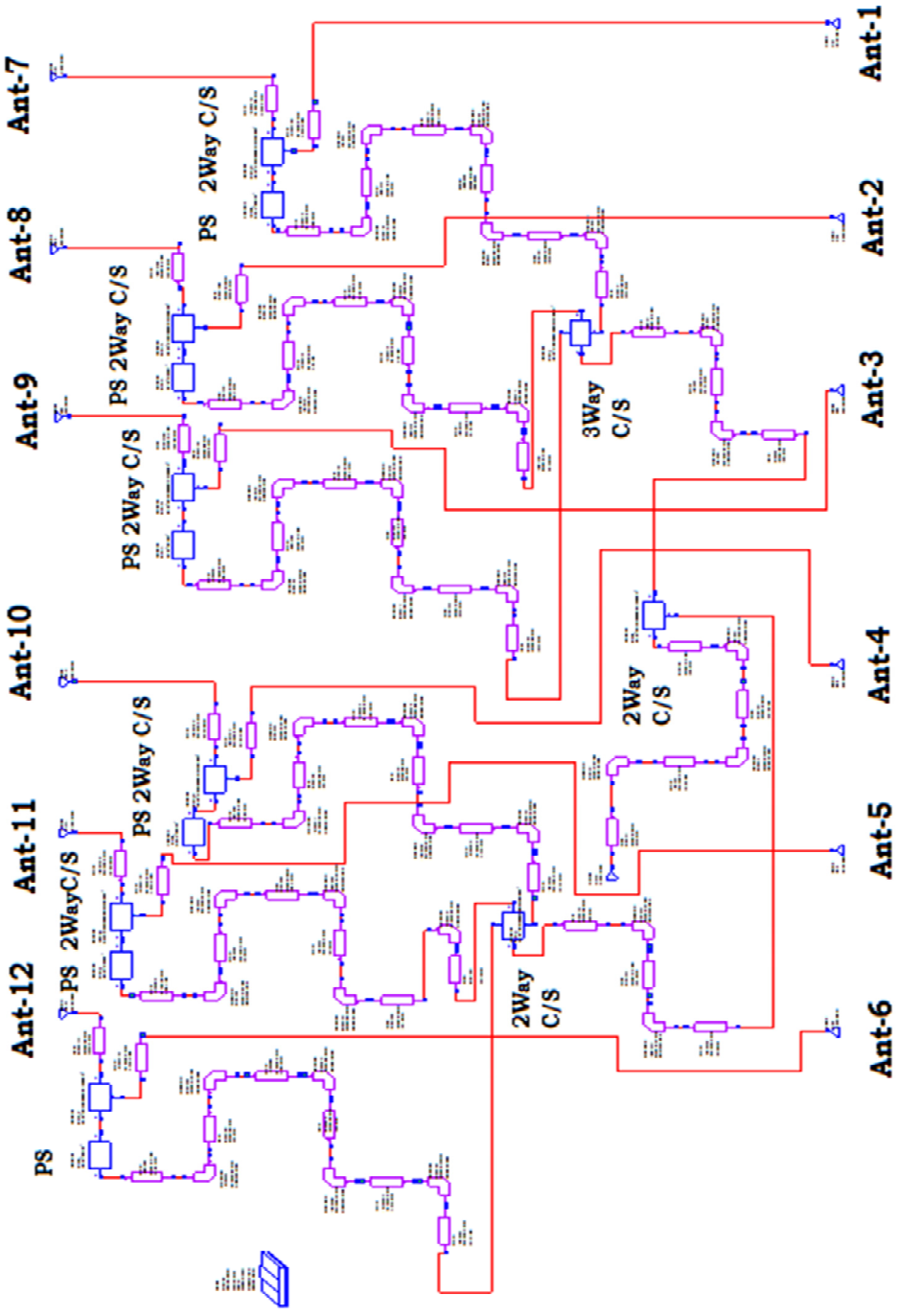

Figure 6.6: Schematic Diagram For The MWO Model For The First Method

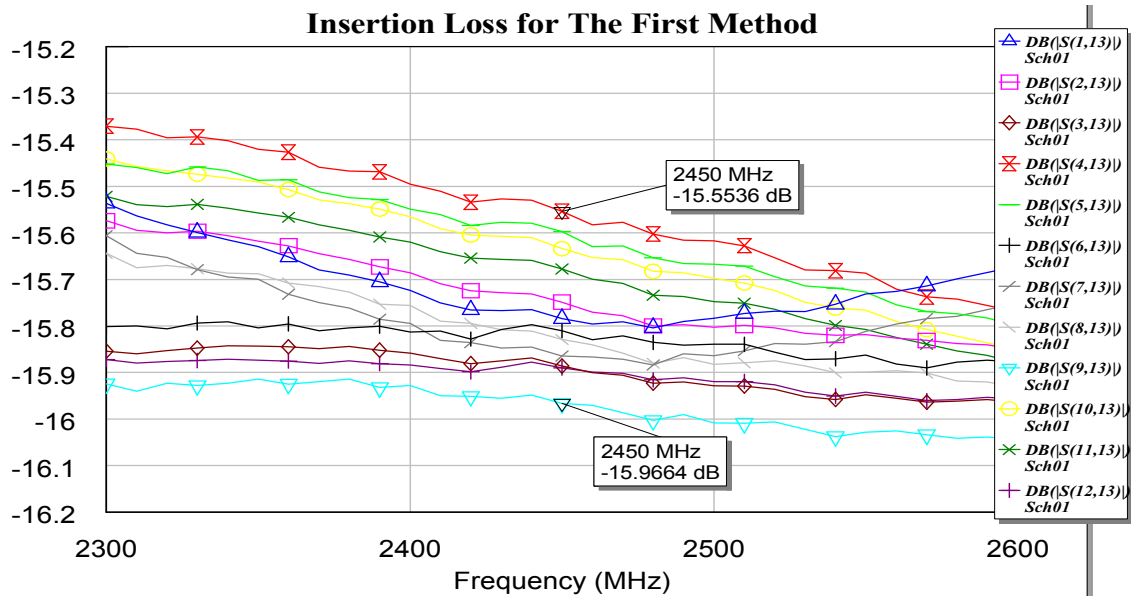

Figure 6.7: Insertion loss for the first method

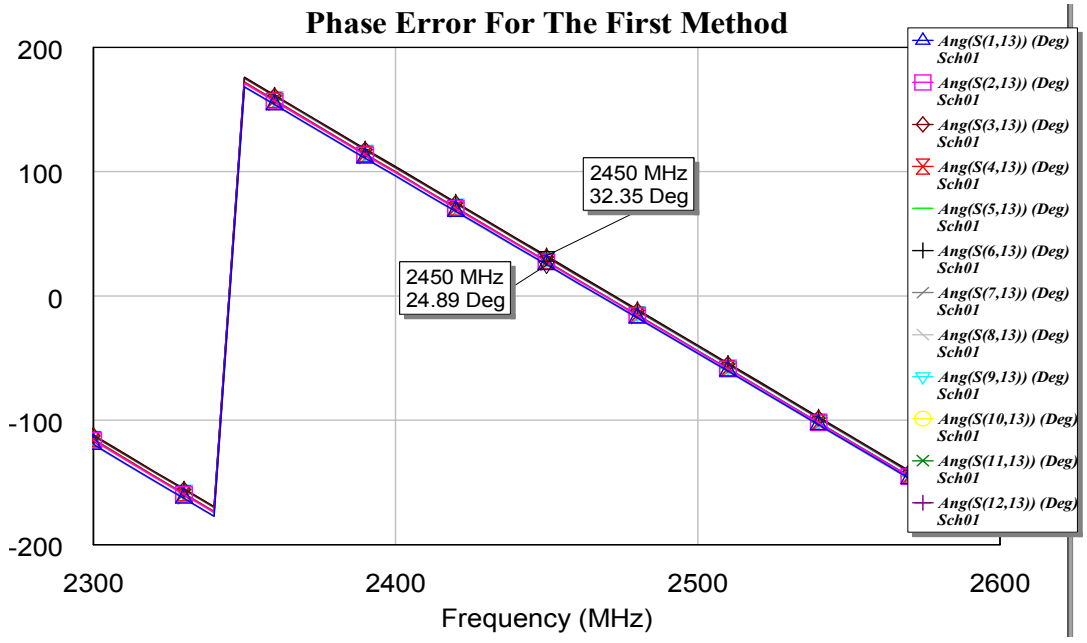

Figure 6.8: The phase difference between the input and the output ports

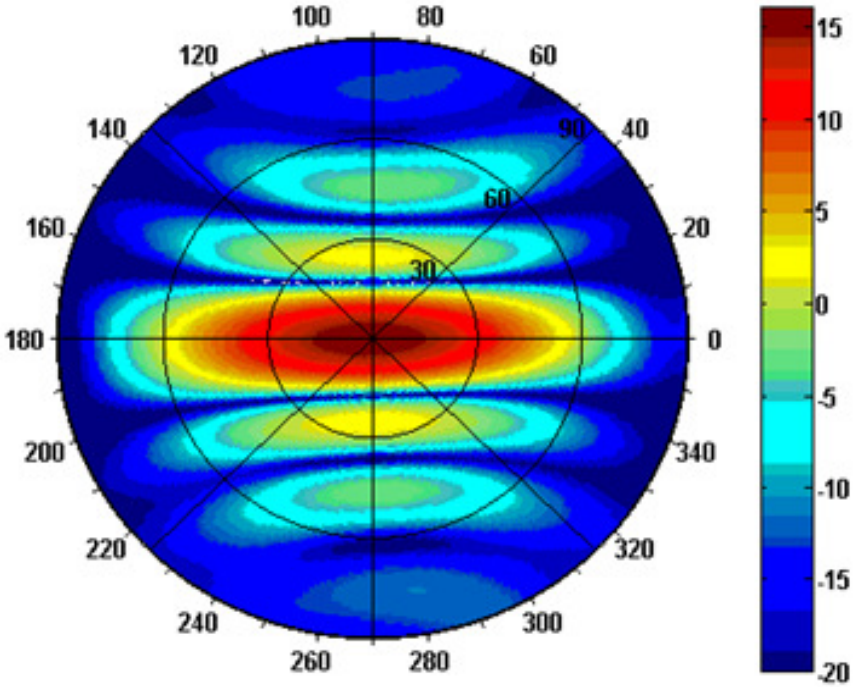

Figure 6.9: Simulated 3D pattern at θ=0,φ=0

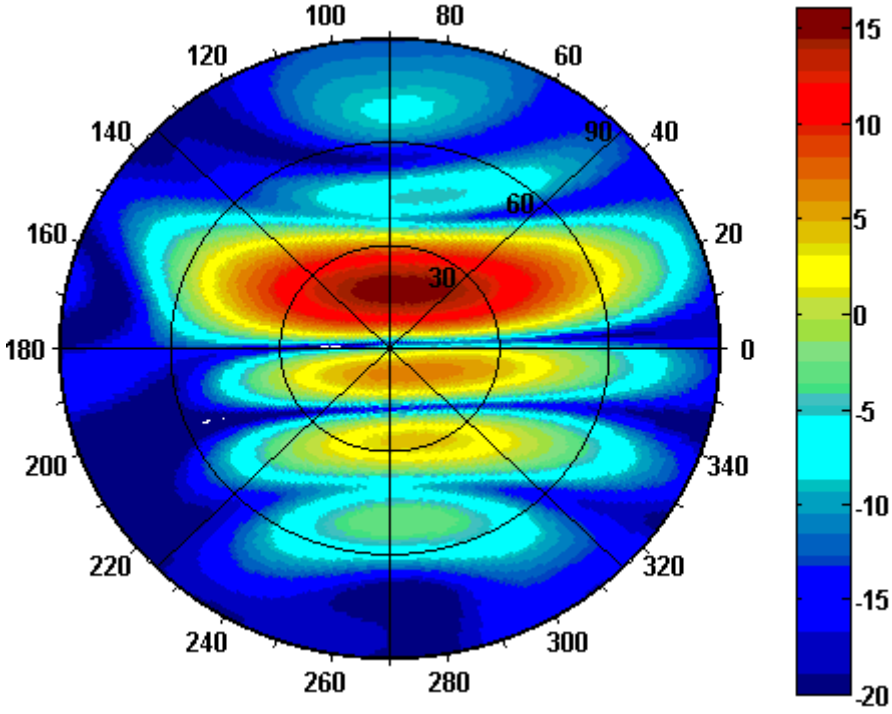

Figure 6.10: Simulated 3D pattern at θ=20,φ=90

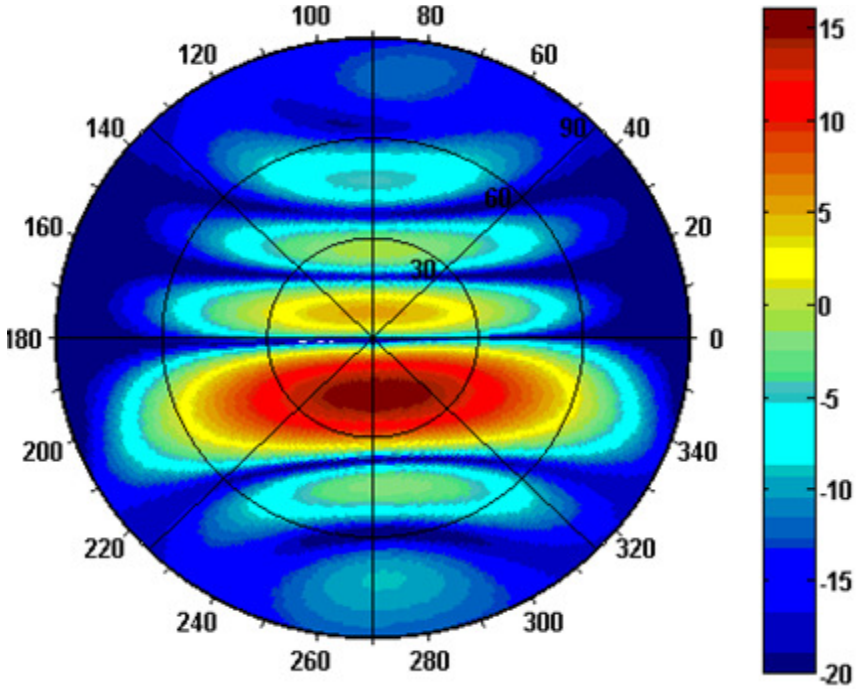

Figure 6.11: Simulated 3D pattern at θ=20,φ=270

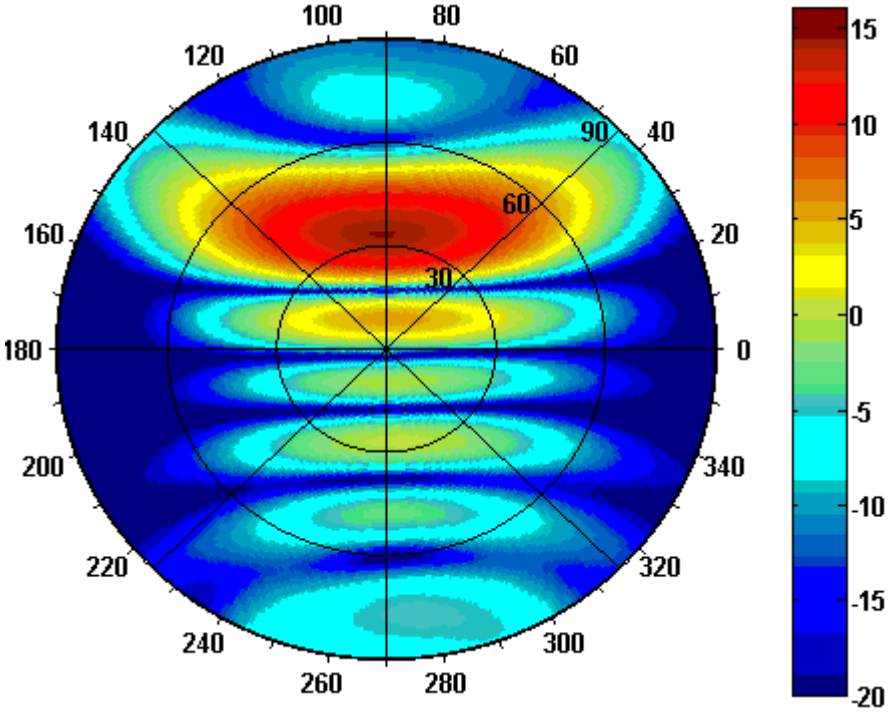

Figure 6.12: Simulated 3D pattern at θ=40,φ=90

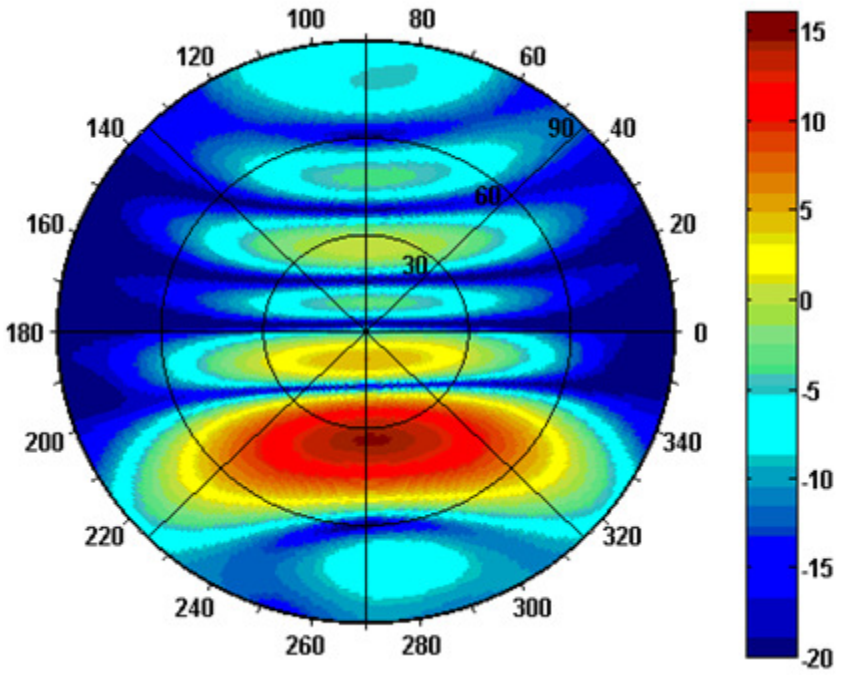

Figure 6.13: Simulated 3D pattern at θ=40,φ=270

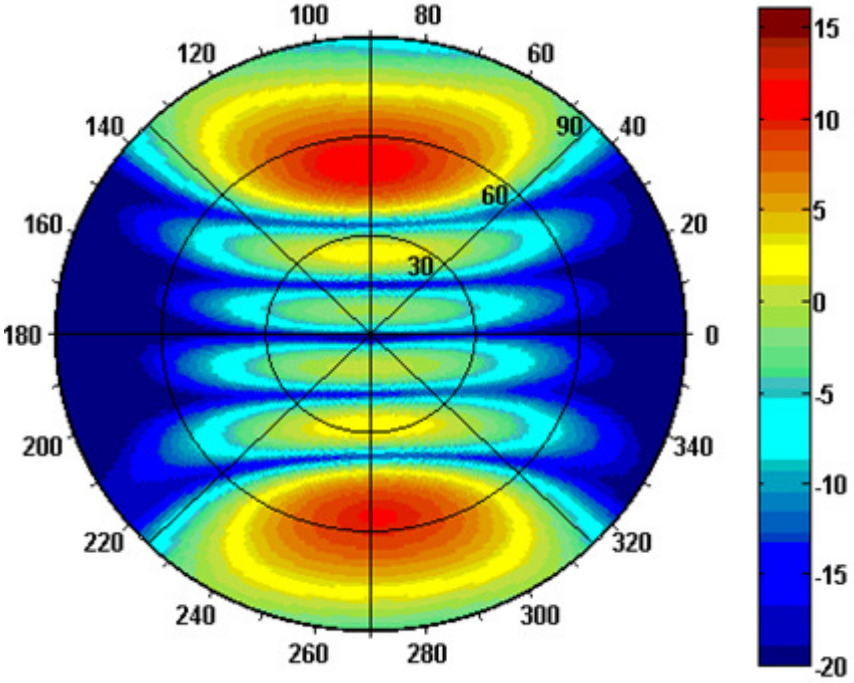

Figure 6.14: Simulated 3D pattern at θ=80,φ=90

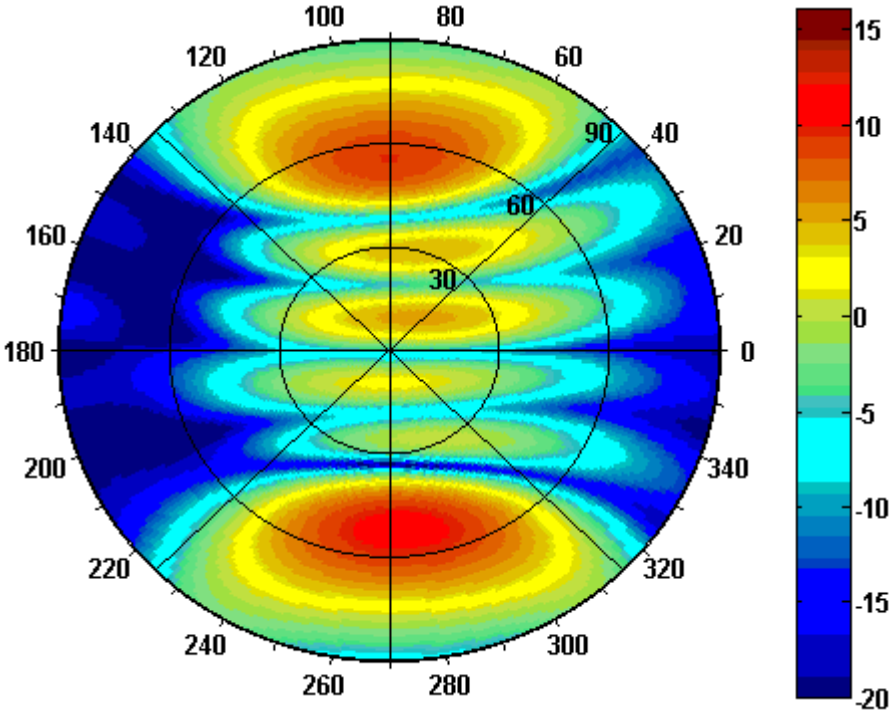

Figure 6.15: Simulated 3D pattern at θ=80,φ=270

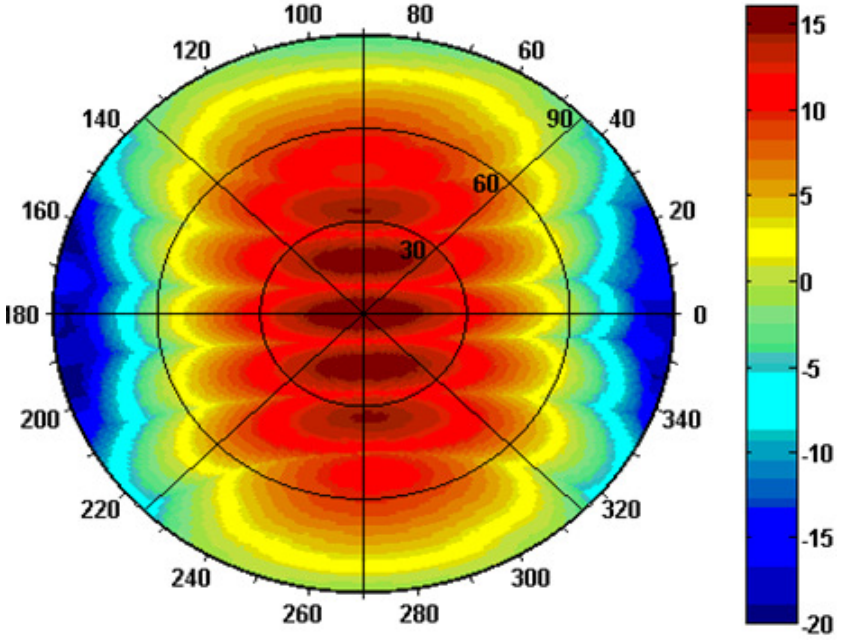

Figure 6.16: Total coverage for simulated 3D pattern using first method

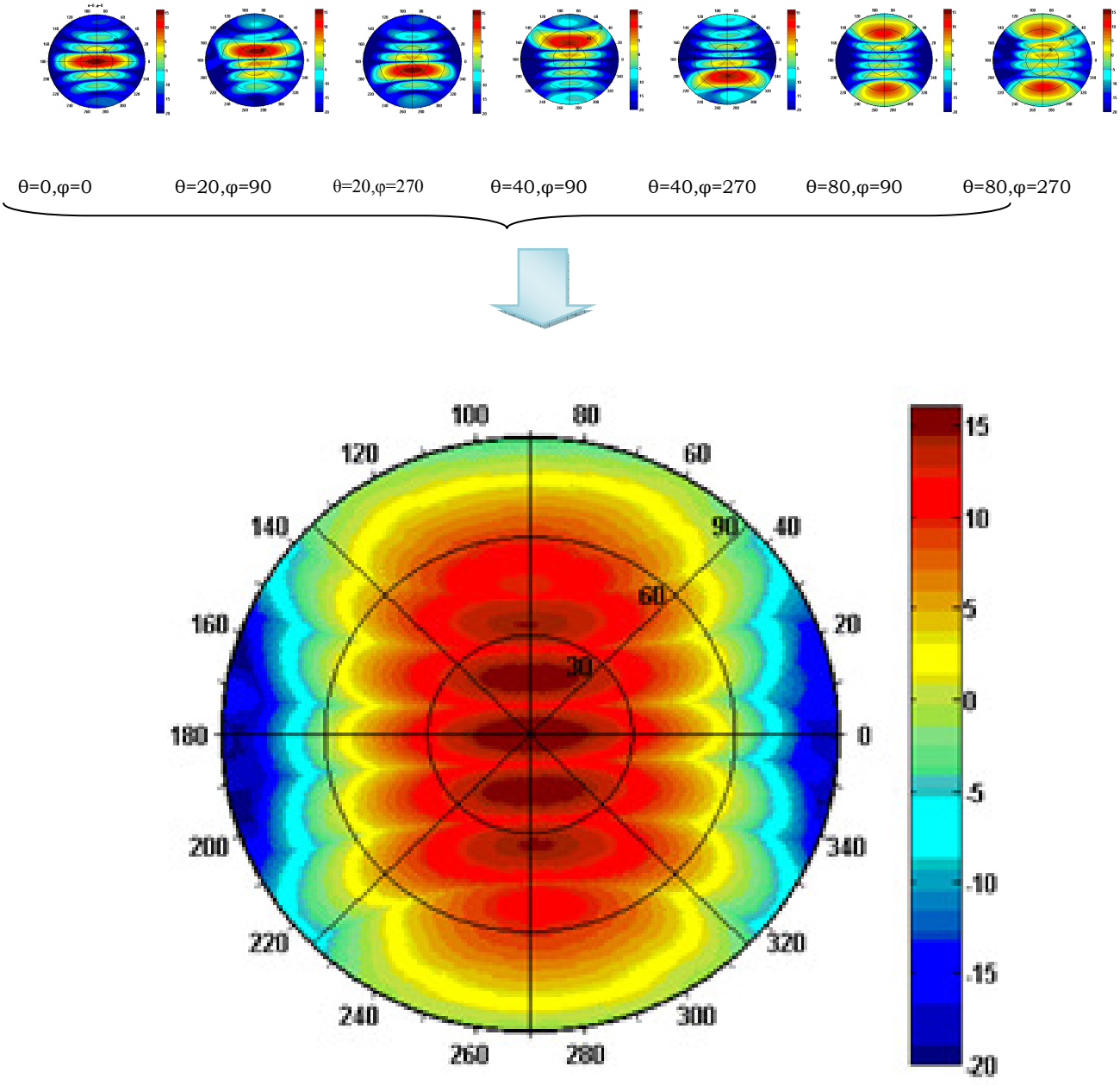

Figure 6.17 :Total coverage for the first method

6.2 Second Method

In this method, the beam scanning is provided for limited values in φ as well. The beam scanning can be performed at all values of θ_o along two φ angles at 0^o and 180^o. In this design, the following components are required:

1. One SMA connecter
2. Two phase shifters
3. Four three-way splitters/combiners
4. Three two-way splitters/combiners

In this simple design, the beam scanning is performed for all values of θo along φ at 0^o and 180^o.The insertion loss due to components will be less than the original design. In Figure 6.18, the schematic of the second method is proposed. Phase excitation at φ equal to 0^o and 180^o has only two values, one value for each column. For this reason, only two phase shifters are required to perform the phase shift at these values. The 3D radiation pattern for this design is shown in Figure 6.20. Phi plane and theta plane at theta 40^o and phi 0^o are shown in Figures 6.21 and 6.22 respectively. In Table 6.4 the HPBW for θ and φ planes is given with the maximum gain values. In Figure 6.23, the schematic diagram for the second method is shown. In Figures 6.24 and 6.25, the insertion loss (with deviation of 0.3dB) and the phase error between output ports are shown (with deviation of 1 degree). In Figure 6.32, the total coverage of the second method is shown. In Figures 6.26 to 6.32, the 3D gain patterns for the array gain at the following angles are shown: θ=0,φ=0; θ=40,φ=0; θ=40,φ=180; θ=80,φ=0; θ=80,φ=180. The radiation pattern for the merged angles in one graph is shown in Figure 6.31 and 6.32.

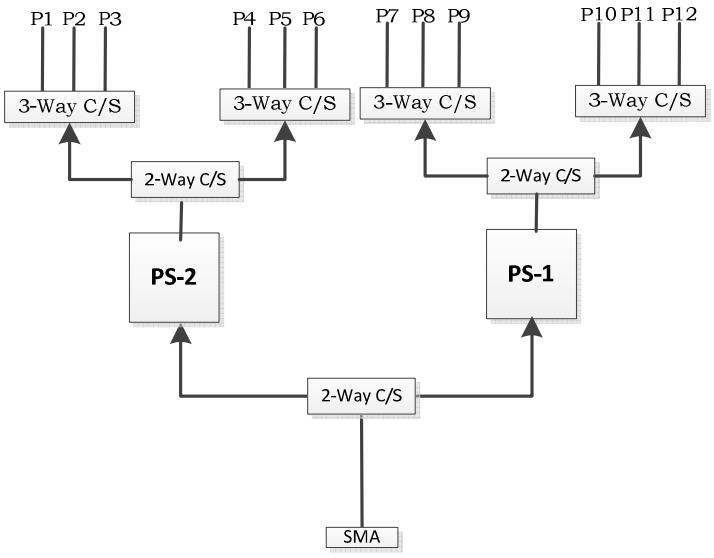

Figure 6.18: The schematic of the second method

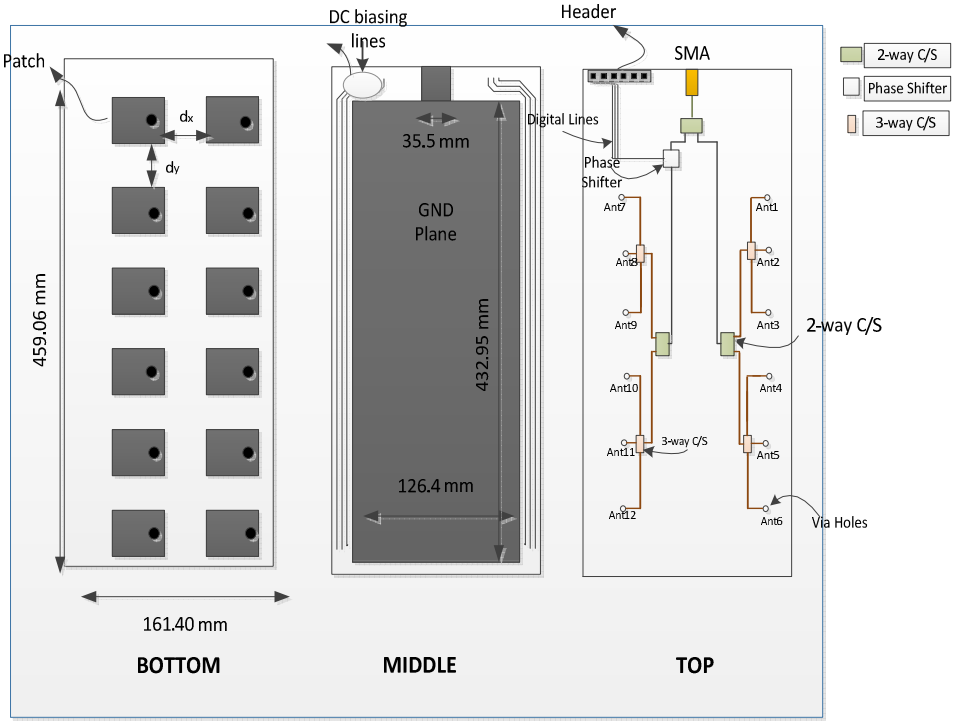

Figure 6.19: Proposed phased array antenna for the second design

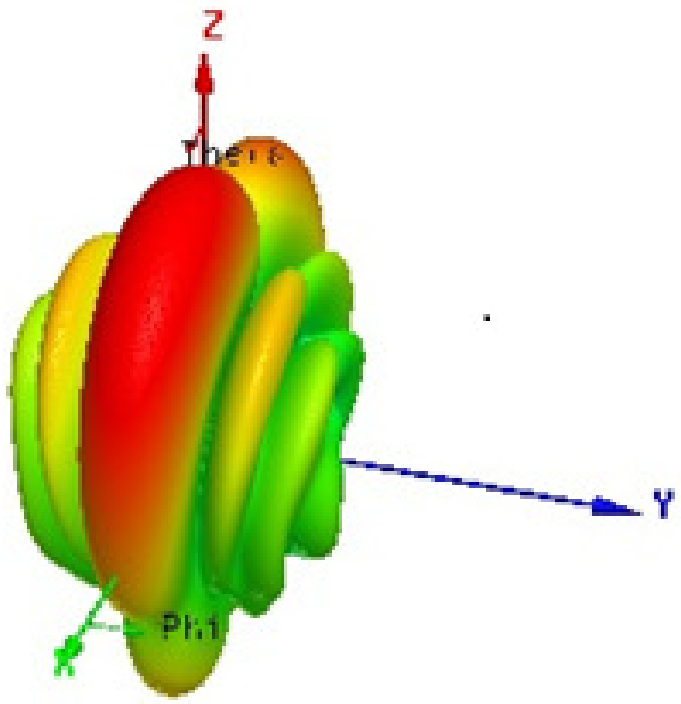

Figure 6.20: 3D Radiation pattern for Total gain at theta 40 Phi0

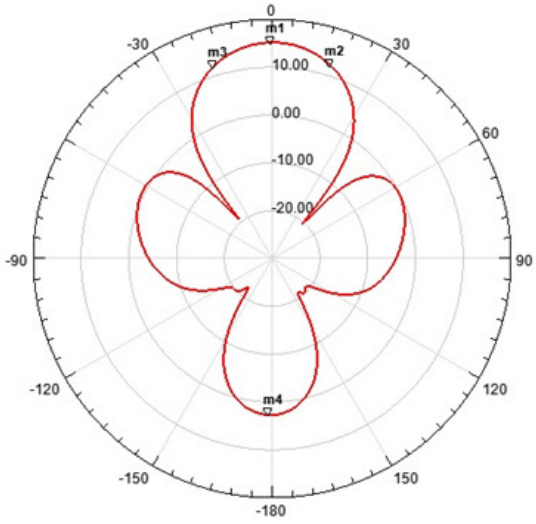

Figure 6.21: Total gain in φ plane at θ=26

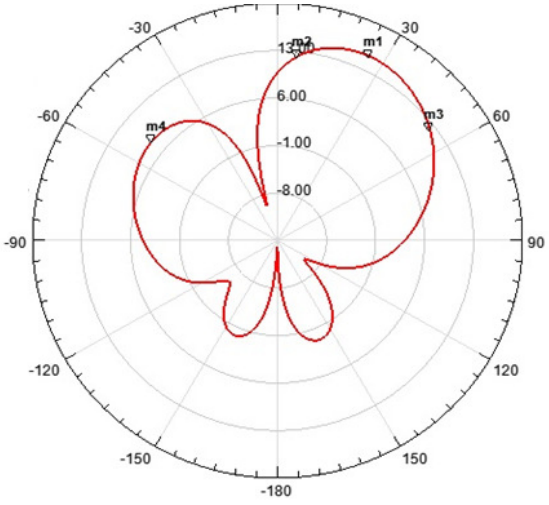

Figure 6.22: Total gain in θ plane at φ=0

Table 6.4: The simulation results for the second design

Desired		Actual							
Theta	Phi	Theta	Phi	Location error (Theta)%	Location error (Phi)%	Max Gain Theta	Max Gain Phi	HPBW Theta	HPBW Phi
10	0	7	0	0	0	15.615	15.615	50	167
10	180	6	180	40	0	15.642	15.642	50	170
20	0	18	0	10	0	15.607	15.607	32	48
20	180	17	180	15	0	15.627	15.627	48	52
30	0	22	0	27	0	15.45	15.45	48	40
30	180	21	180	30	0	15.439	15.439	48	41
40	0	26	0	35	0	15.136	15.136	20	34
40	180	24	180	40	0	15.135	15.135	47	36
50	0	31	2	38	1	14.358	14.358	47	29
50	180	29	181	42	1	14.252	14.252	48	31
60	0	31	355	48	1.39	13.307	13.307	45	30
60	180	29	175	52	2.8	13.231	13.231	45	31
70	0	34	178	51	50.5	13.045	13.045	47	26
70	180	35	358	50	33.7	13.241	13.241	48	26
80	0	34	178	58	50.5	13.045	13.045	47	26
80	180	35	358	56	33.7	13.241	13.241	48	26

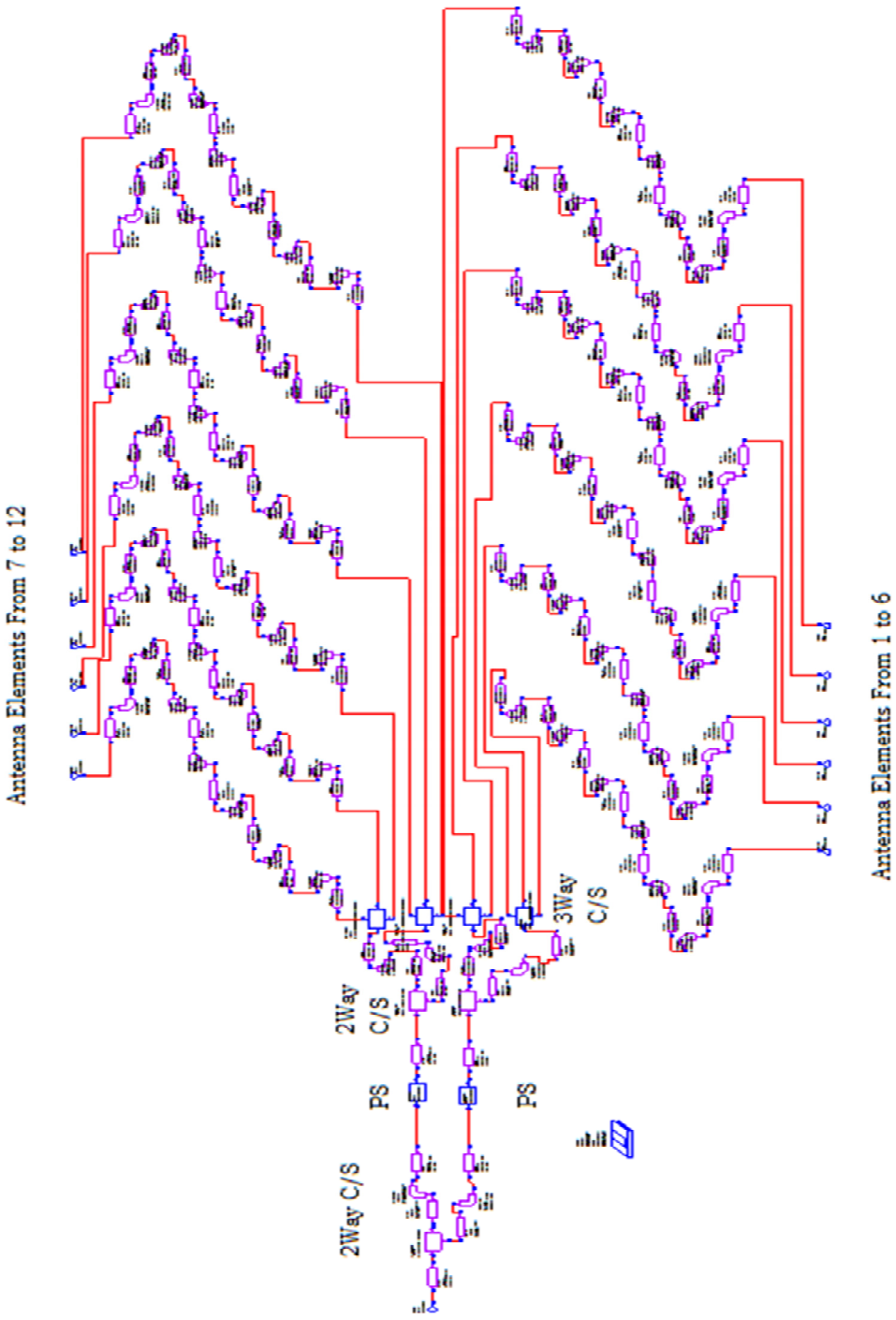

Figure 6.23 Schematic diagram for the MWO model by using the second method

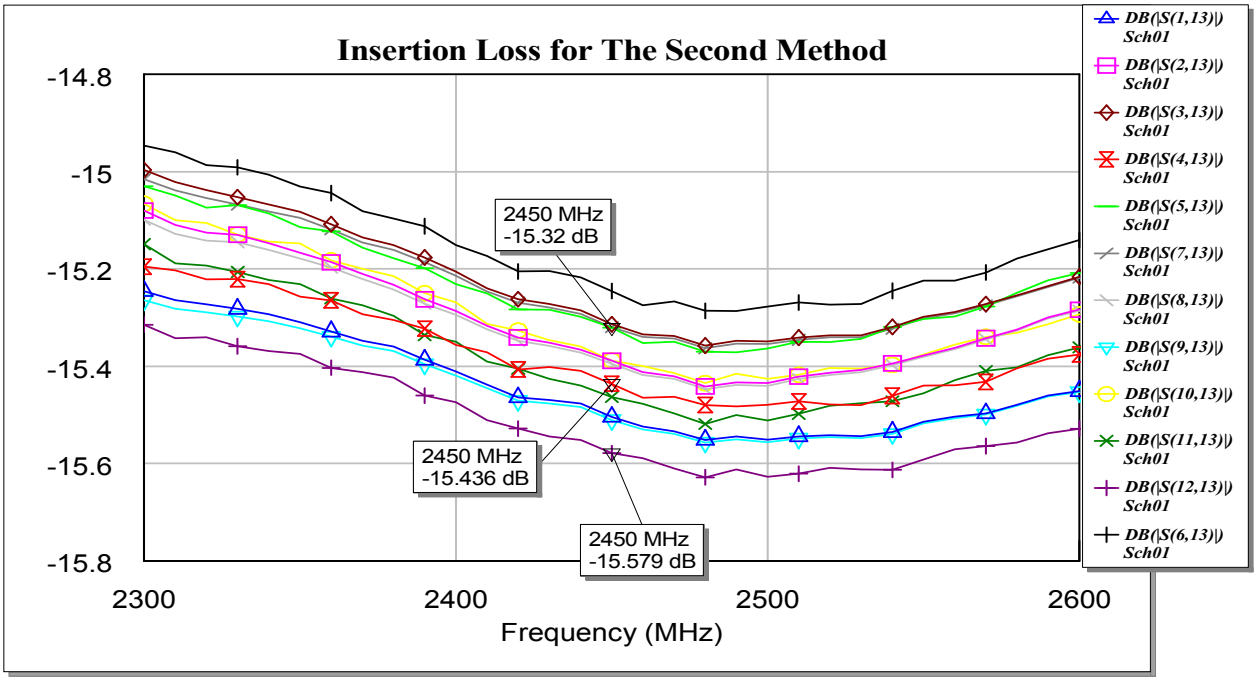

Figure 6.24 The Insertion loss for the second method

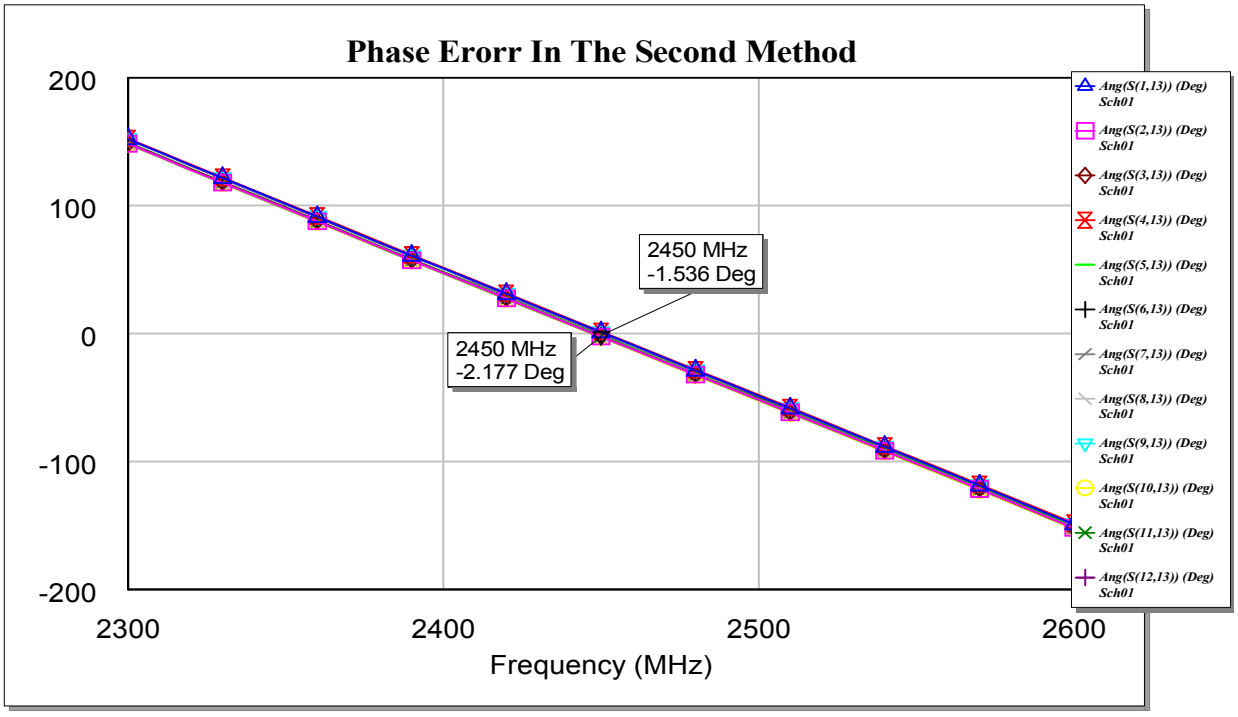

Figure 6.25 The phase error for different output ports

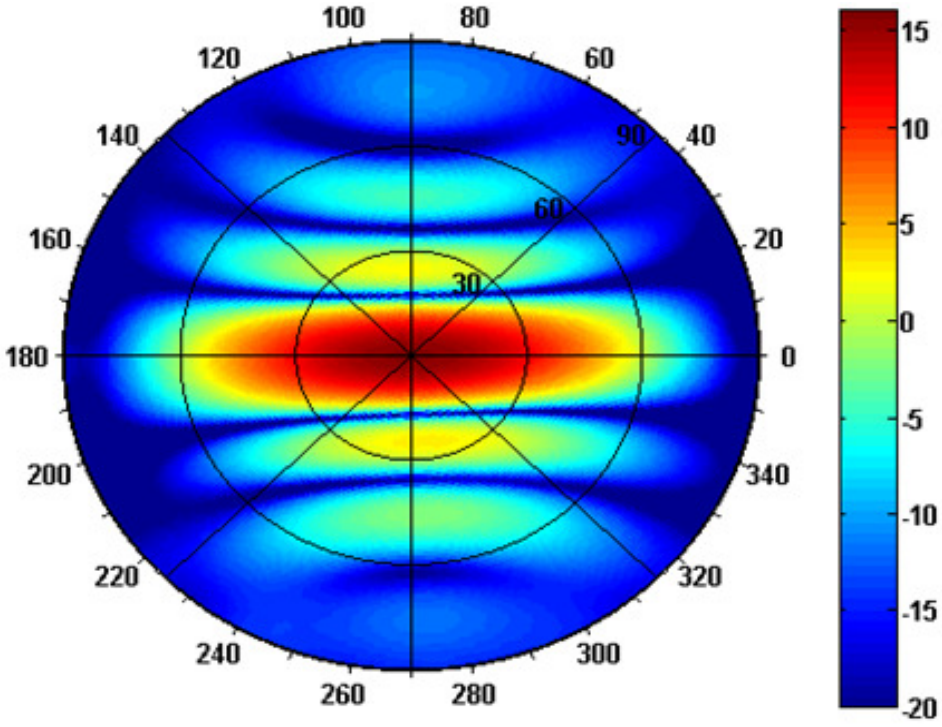

Figure 6.26: Simulated 3D gain pattern at θ=0,φ=0

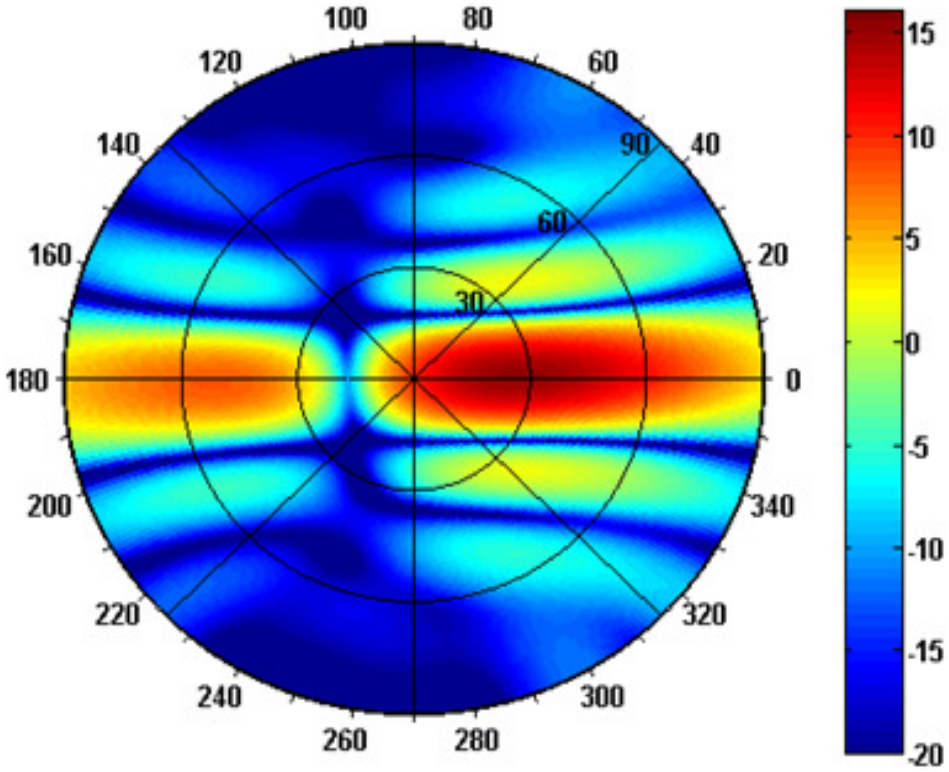

Figure 6.27: Simulated 3D gain pattern at θ=40,φ=0

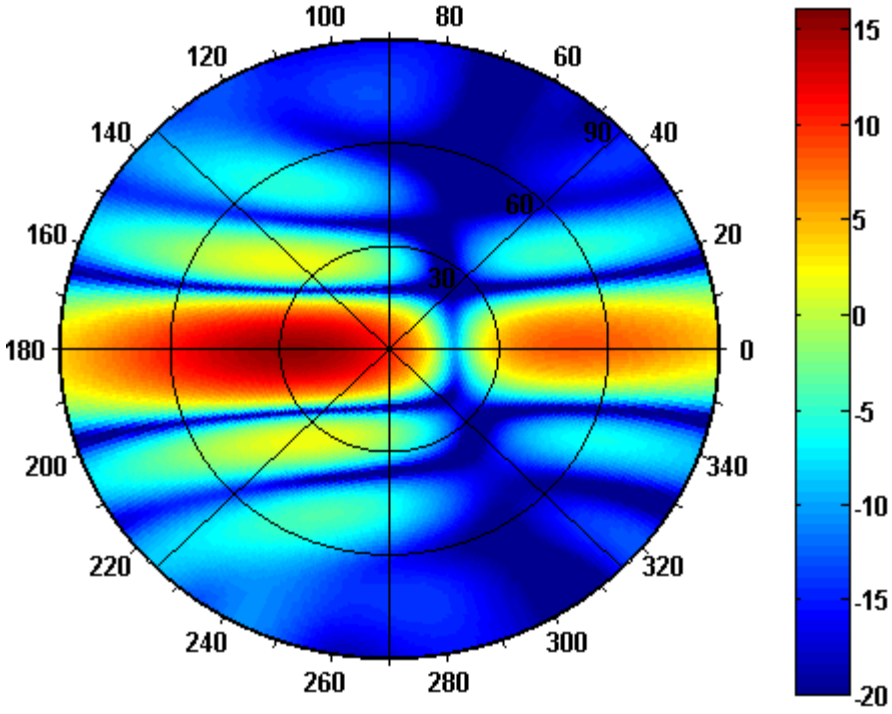

Figure 6.28: Simulated 3D gain pattern at θ=40,φ=180

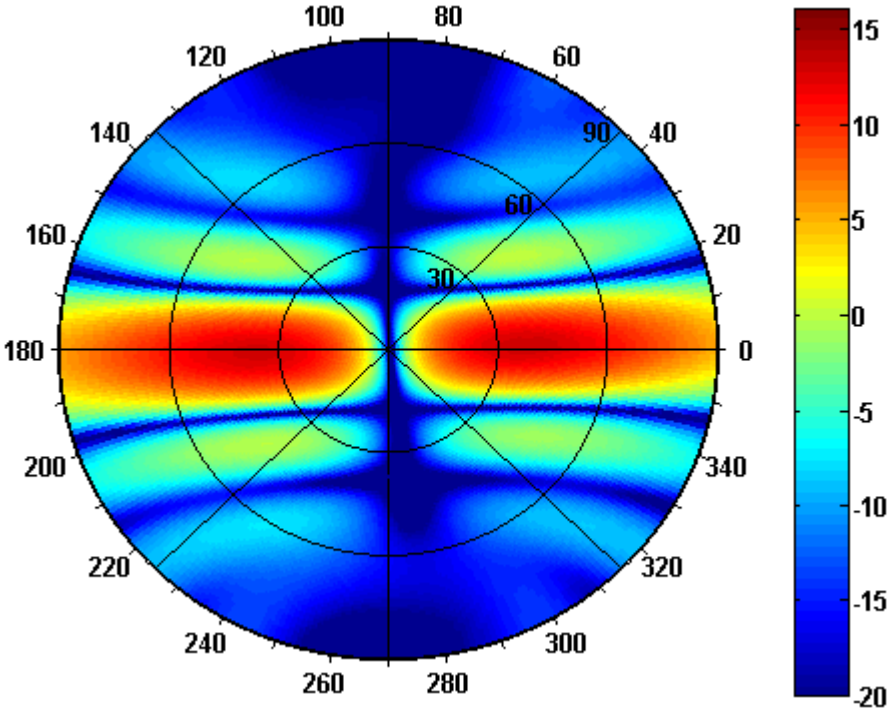

Figure 6.29: Simulated 3D gain pattern at θ=80,φ=0

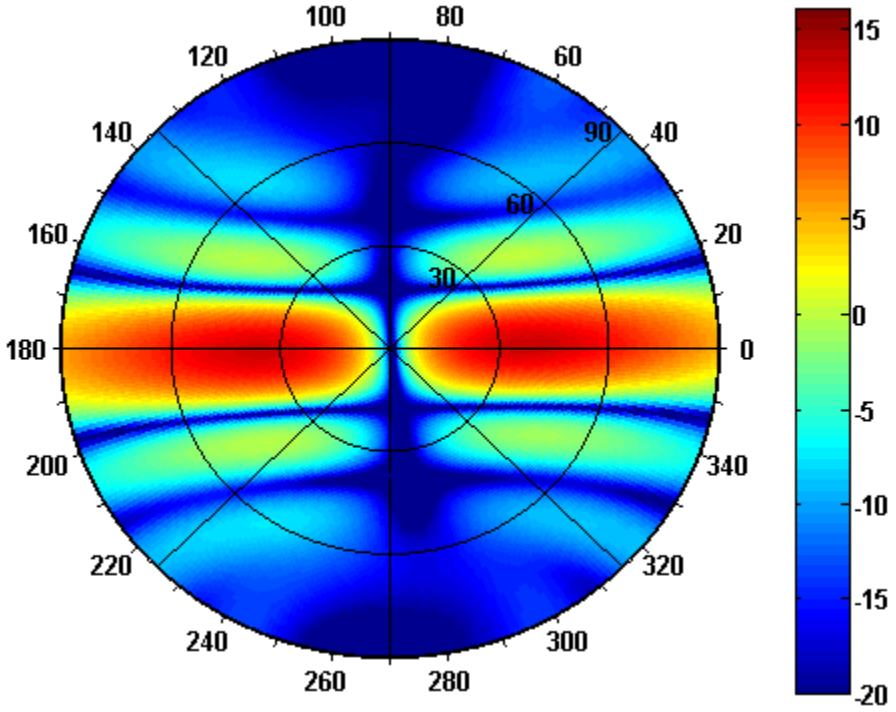

Figure 6.30: Simulated 3D gain pattern at θ=80,φ=180

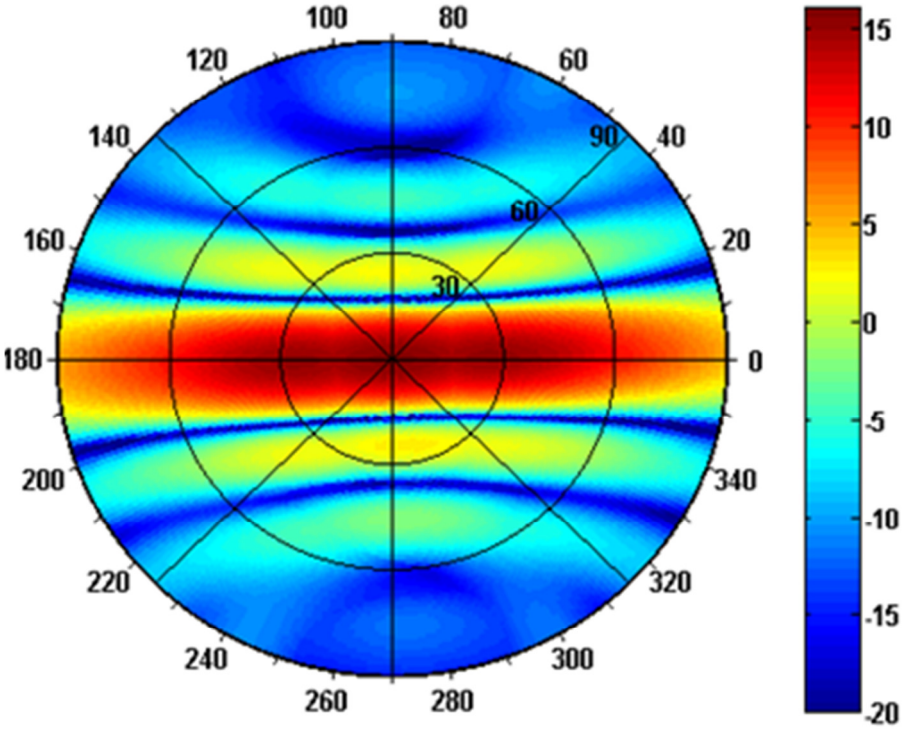

Figure 6.31: Total coverage for simulated 3D gain pattern for the second method

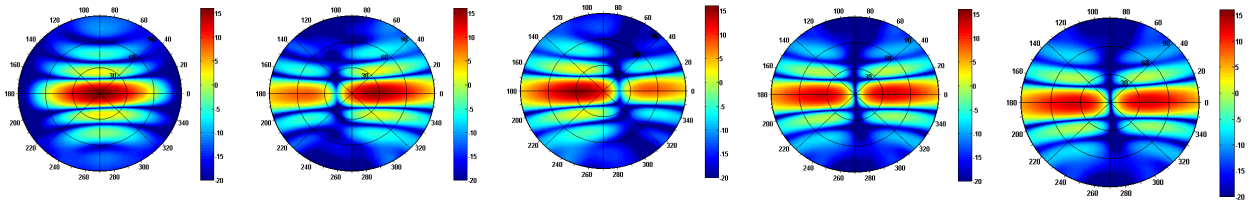

θ=0,φ=0 θ=40,φ=0 θ=40,φ=180 θ=80,φ=0 θ=80,φ=180

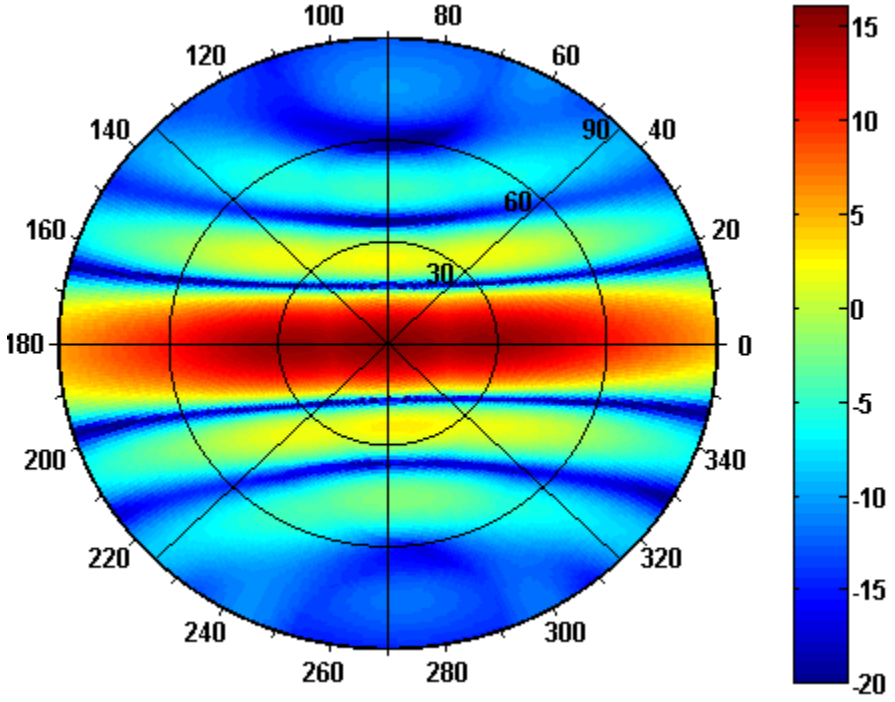

Figure 6.32: Total coverage of the meraged angles pattern For The Second Method.

From Figure 6.31 and 6.32, it is clear that this method is very poor in terms of beam coverage. Tables 6.5 and 6.6, are showing the excitation phases at theta=40,Phi=0,180. Each column has single value, and always the column contains the elements 1,2,3,4,5 and 6 have excitation phase equal to zero due to equation (2.29)

At φ=0 and 180 ,β_y will become 0, then the column which contains elements 7,8,9,10,11 and 12 will be with only one value which is βx as shown in Table 6.5 and Table 6.6

Table 6.5: Excitation phase at θ =40, φ=0

Antenna Elements	No of Steps	Excitation Phase	Antenna Elements	No of Steps	Excitation Phase
Ant-1	0	0	Ant-7	-5	-112.5
Ant-2	0	0	Ant-8	-5	-112.5
Ant-3	0	0	Ant-9	-5	-112.5
Ant-4	0	0	Ant-10	-5	-112.5
Ant-5	0	0	Ant-11	-5	-112.5
Ant-6	0	0	Ant-12	-5	-112.5

Table 6.6: Excitation phase at θ =40, φ =180

Antenna Elements	No of Steps	Excitation Phase	Antenna Elements	No of Steps	Excitation Phase
Ant-1	0	0	Ant-7	5	112.5
Ant-2	0	0	Ant-8	5	112.5
Ant-3	0	0	Ant-9	5	112.5
Ant-4	0	0	Ant-10	5	112.5
Ant-5	0	0	Ant-11	5	112.5
Ant-6	0	0	Ant-12	5	112.5

6.3 Third Method

This method has beam scanning capability that can cover all values of theta while phi is at four different angles 0^o, 90^o, 180^o and 270^o. The first method and the second method are merged into a single design which is the third method. This technique has better beam coverage than the first and second methods but also it contains many components and the insertion loss is even more than the original design by 3 dB but it saves 6 phase shifters. The components required are:

1. Four 3-Way power combiners
2. Two 2-Way power combiners
3. One SMA connectors
4. Six phase shifters
5. Three 4x2 Switch matrix (HMC276LP4 / HMC276LP4E)

In this method, the output of the phase shifters is divided into two branches. One transmission line which is connected to the 4x2 switched matrix and the other is connected directly to antenna element (6, 7, 8, 9, 10, 11 and 12) .The output of the switch is connected directly to antenna elements (6, 7, 8, 9, 10, 11 and 12), The input of the matrix switch can be switched between the first output of phase shifter and the transmission line which is not connected to any phase shifter as shown in Figure 6.33. It is observed that the output of the switch suffers from power loss due the IC insertion loss which means that phase and amplitude compensation should be done for transmission lines connected to antenna elements 7, 8, 9, 10, 11 and 12.

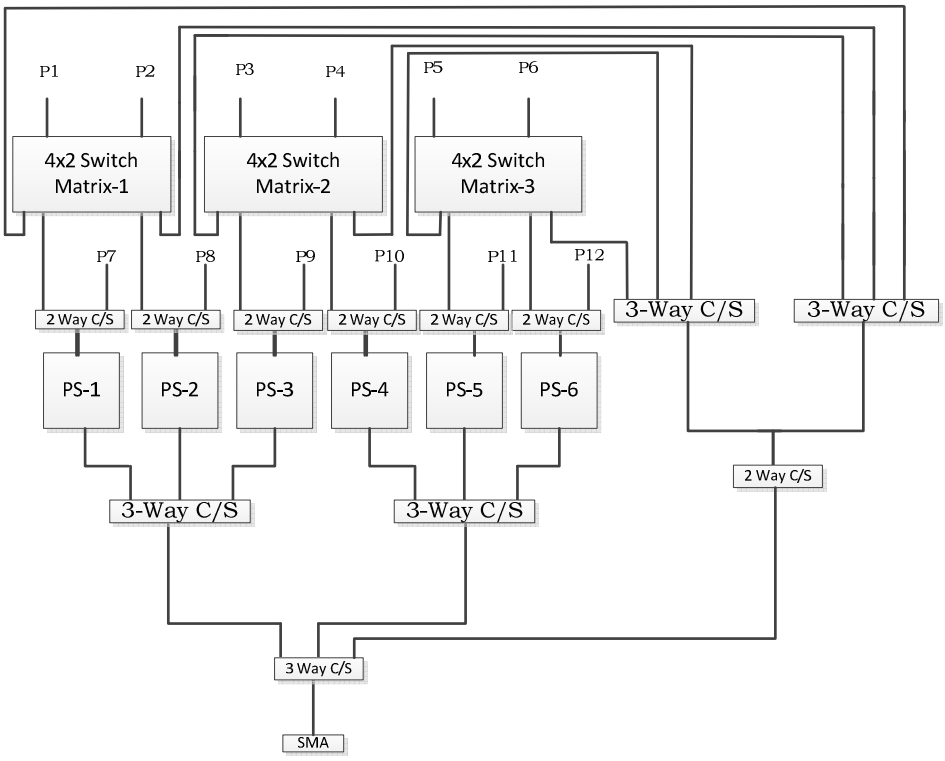

Figure 6.33: Schematic diagram for the third method

The 4x2 switch matrix change the output according to the desired φ_o. At φ_o 0^o and 180^o the switch matrix will be connected to the transmission line which is not connected with any phase shifter. But at φ_o equal to 90^o and 270^o the switch matrix will be flipped to the output of the phase shifter, which means that adjacent elements in the same row should have the same phase. The output of the switch matrix is controlled by four control inputs (HV1,HV2,Tone1 and Tone2). The proposed layout for this design is shown in Figure 6.34. The values of insertion loss are found to be between -18.8dB to -20dB. Figure 6.35 is the schematic diagram for the third method.

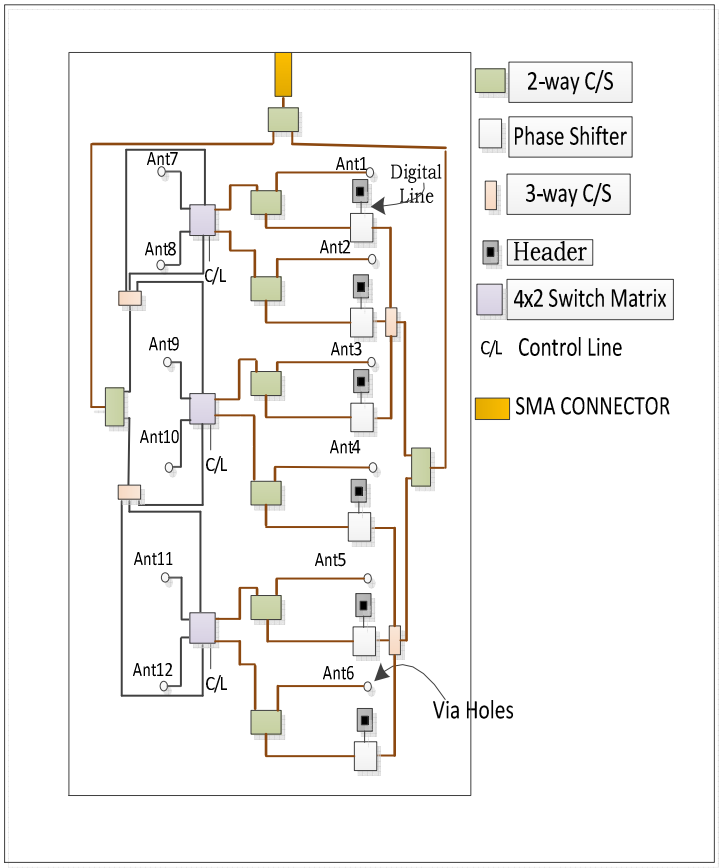

Figure 6.34: Compact layout for the phased array antenna for the third design

In Figure 3.36, the insertion loss has maximum deviation of 1.2dB. Where in Figure 6.37 the pin diagram for switch matrix, while the switch matrix is controlled by the control bits as shown in Figure 6.37. The output of the switch matrix is varied between two states, state 3 and state 8. For φ equal to 0^o and 180^o, the switch output will take the feed from input HL and VL and the third state of operation is considered. The eighth state of operation will be considered for the case where φ equal to 90^o and 270^o as can be shown in Table 6.7. In this design, the coverage capability in φ plane is 63 degree on average at each θo as shown in Figure 6.38. It is shown in Figure 6.38 that most of the critical areas to be covered in the communication between the UAV and earth station is covered with very small gaps.

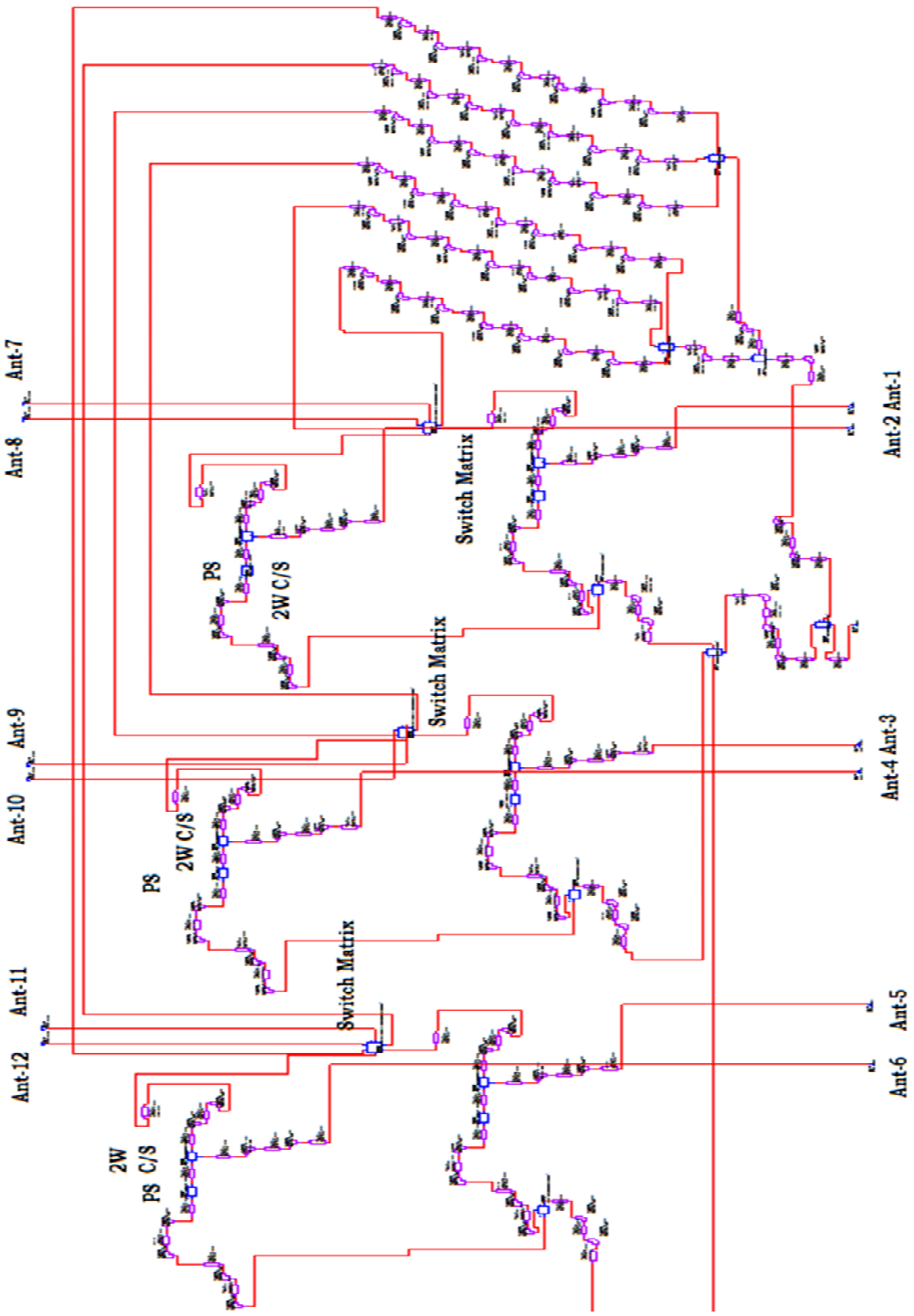

Figure 6.35 Schematic diagram for the MWO model by using the third method

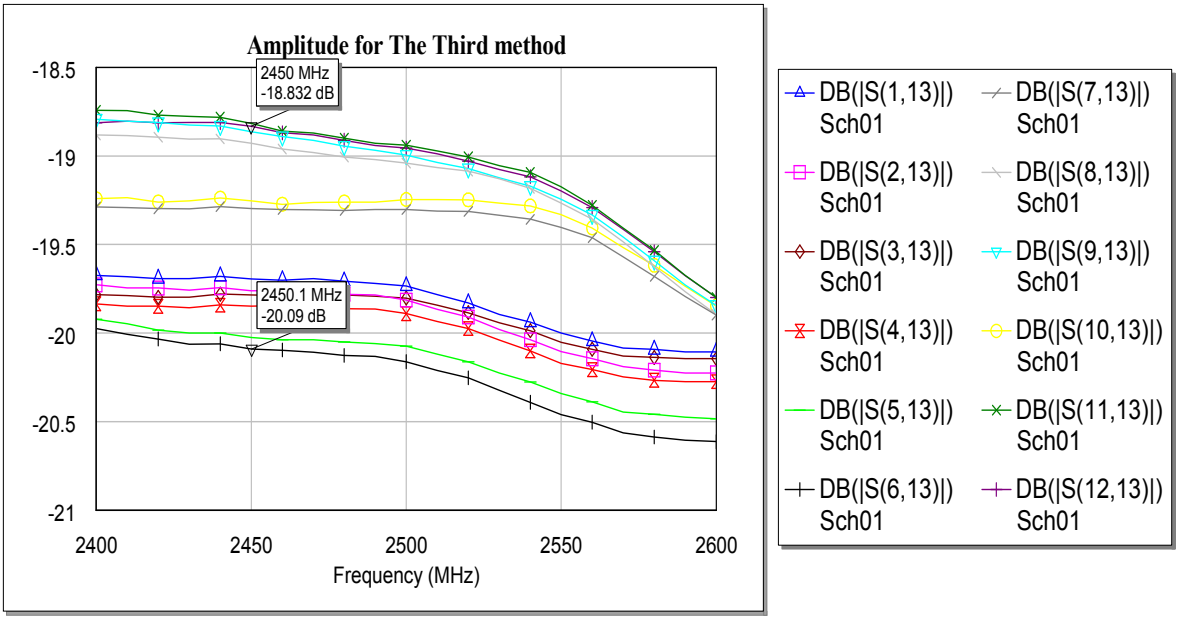

Figure 6.36 :Insertion loss for the third method

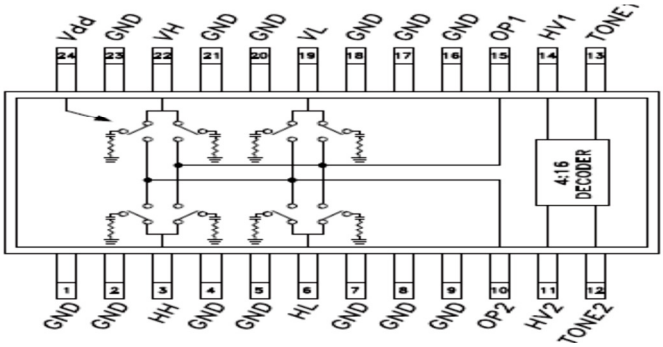

Figure 6.37 Pin Diagram For The Switch Matrix [44]

Table 6.7 The Different States of operation For Switch Matrix [44]

	Control Input				Output to Input State		RF Path State							
State	HV 1	Tone 1	HV 2	Tone 2	OP1	OP2	VL to OP1	HL to OP1	VH to OP1	HH to OP1	VL to OP2	HL to OP2	VH to OP2	HH to OP2
1	0	0	0	0	VL	VL	LOSS	ISOL	ISOL	ISOL	LOSS	ISOL	ISOL	ISOL
2	0	0	0	1	VL	VH	LOSS	ISOL	ISOL	ISOL	ISOL	ISOL	LOSS	ISOL
3	0	0	1	0	VL	HL	LOSS	ISOL	ISOL	ISOL	ISOL	LOSS	ISOL	ISOL
4	0	0	1	1	VL	HH	LOSS	ISOL	ISOL	ISOL	ISOL	ISOL	ISOL	LOSS
5	0	1	0	0	VH	VL	ISOL	ISOL	LOSS	ISOL	LOSS	ISOL	ISOL	ISOL
6	0	1	0	1	VH	VH	ISOL	ISOL	LOSS	ISOL	ISOL	ISOL	LOSS	ISOL
7	0	1	1	0	VH	HL	ISOL	ISOL	LOSS	ISOL	ISOL	LOSS	ISOL	ISOL
8	0	1	1	1	VH	HH	ISOL	ISOL	LOSS	ISOL	ISOL	ISOL	ISOL	LOSS
9	1	0	0	0	HL	VL	ISOL	LOSS	ISOL	ISOL	LOSS	ISOL	ISOL	ISOL
10	1	0	0	1	HL	VH	ISOL	LOSS	ISOL	ISOL	ISOL	ISOL	LOSS	ISOL
11	1	0	1	0	HL	HL	ISOL	LOSS	ISOL	ISOL	ISOL	LOSS	ISOL	ISOL
12	1	0	1	1	HL	HH	ISOL	LOSS	ISOL	ISOL	ISOL	ISOL	ISOL	LOSS
13	1	1	0	0	HH	VL	ISOL	ISOL	ISOL	LOSS	LOSS	ISOL	ISOL	ISOL
14	1	1	0	1	HH	VH	ISOL	ISOL	ISOL	LOSS	ISOL	ISOL	LOSS	ISOL
15	1	1	1	0	HH	HL	ISOL	ISOL	ISOL	LOSS	ISOL	LOSS	ISOL	ISOL
16	1	1	1	1	HH	HH	ISOL	ISOL	ISOL	LOSS	ISOL	ISOL	ISOL	LOSS

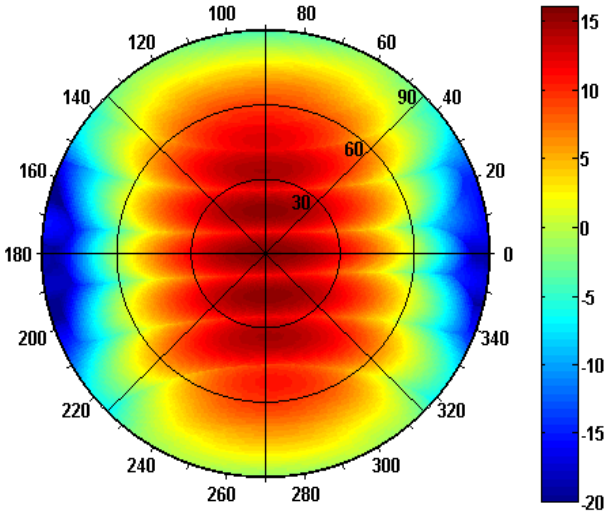

Total coverage for simulated 3D pattern for the first method

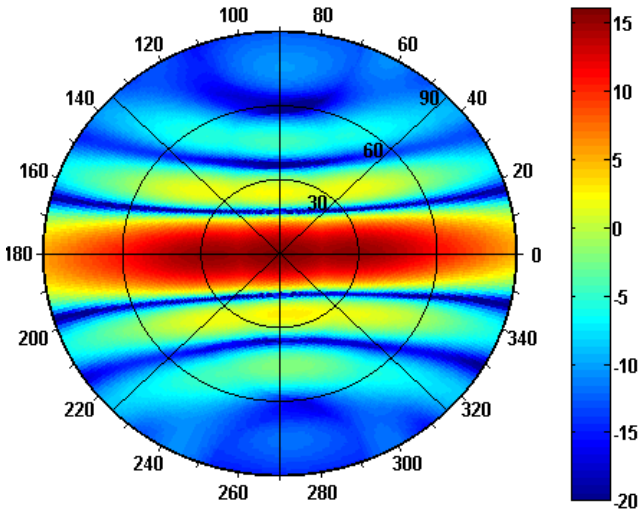

Total coverage for simulated 3D pattern for the second

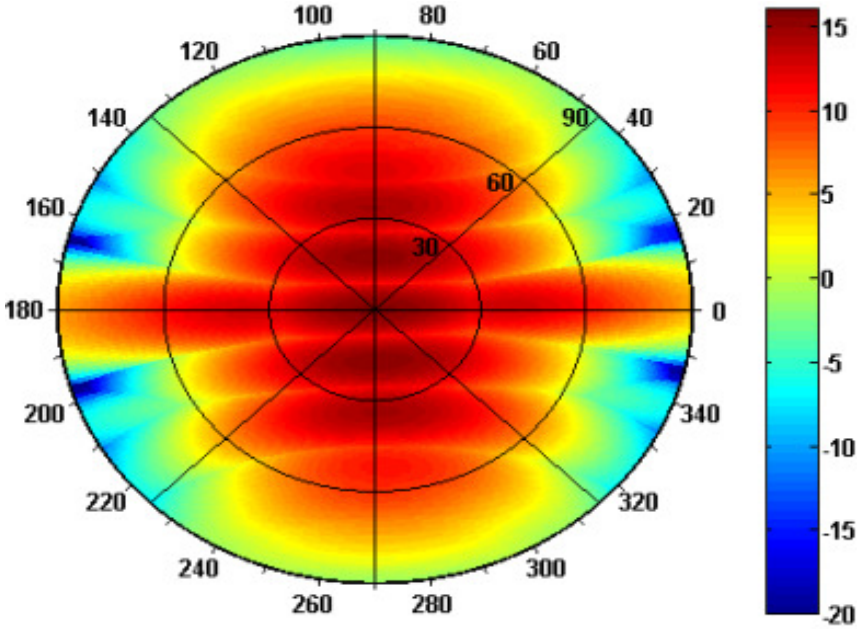

Figure 6.38: Total coverage for simulated 3D pattern for the third method

6.4 Fourth Method

In this method, two-way 90^{o} hybrid couplers/splitters are utilized to perform the best coverage capability among the previous methodologies. In this method, the following components are used:

1. One SMA connecter
2. Two three-way splitter/combiner
3. Six phase shifters
4. One two-way power combiner
5. Six two-way 90^{o} hybrid power combiner
6. Six transfer switches (HMC427LP3/427LP3E)

The schematic diagram for this method is shown in Figure 6.39 where a transfer switch is used to perform the required coverage. This comes at the expense of more components other than the phase shifters.

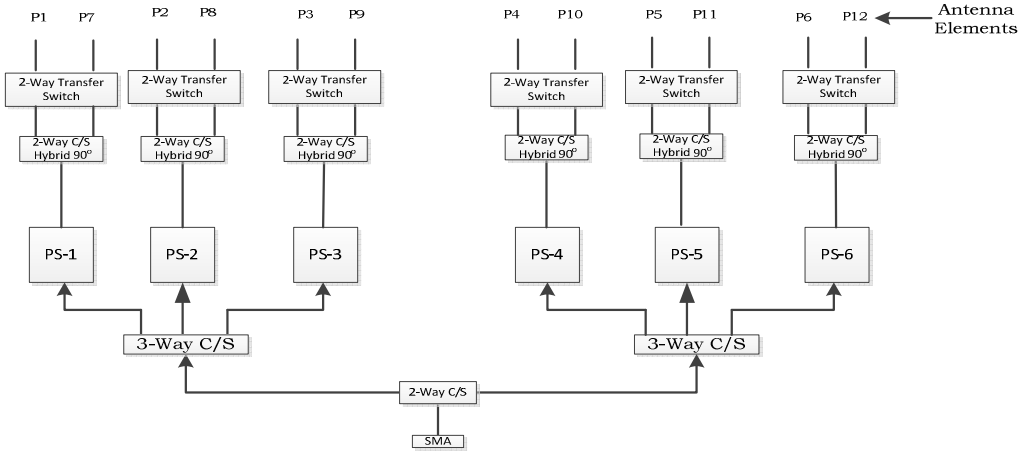

Figure 6.39: The Schematic diagram For The Fourth Method

- **Case-1: Combiner Terminal With Leading Phase Connected to the First Column of Antenna Array**

By using the 90^o hybrid splitter/combiner, where the first column of the array (antenna elements 1, 2, 3, 4, 5 and 6) are connected to the splitter/combiner output with leading phase of 90^o. Since one phase shifter is hired for the same row, this means that each adjacent elements in the same row can be fed by one phase shifter (for example antenna elements 1 and 7 both have excitation phase of β_1), Then the excitation phase for the antenna array elements will be as follow:

Table 6.8: The Progressive Phase For Antenna Elements in Case-1 of method four.

Antenna Element	Excitation Phase	Antenna Element	Excitation Phase
Ant-1	β_1+90^o	Ant-7	β_1
Ant-2	β_2+90^o	Ant-8	β_2
Ant-3	β_3+90^o	Ant-9	β_3
Ant-4	β_4+90^o	Ant-10	β_4
Ant-5	β_5+90^o	Ant-11	β_5
Ant-6	β_6+90^o	Ant-12	β_6

The schematic of the model is shown in Figure 6.40. In Figures 6.41 and 6.42 the insertion loss and the phase error difference between the input port and output ports are shown where the maximum deviation is for insertion loss was 0.5dB, while for phase error the maximum deviation was 9 degree. Figure 6.42 shows that two different groups of phase for the antenna elements. Antenna elements in the first column of the array should have different phase than that in the second column of the array. Because the antenna elements connected to the leading terminal of the 90^o hybrid two-way power combiner/splitter always will lead in phase the antenna elements connected to the other terminal. The 3D gain contour plots for case-1 are shown in Figures 6.43 to 6.50 while Figure 6.50 shows the total Coverage for case-1.

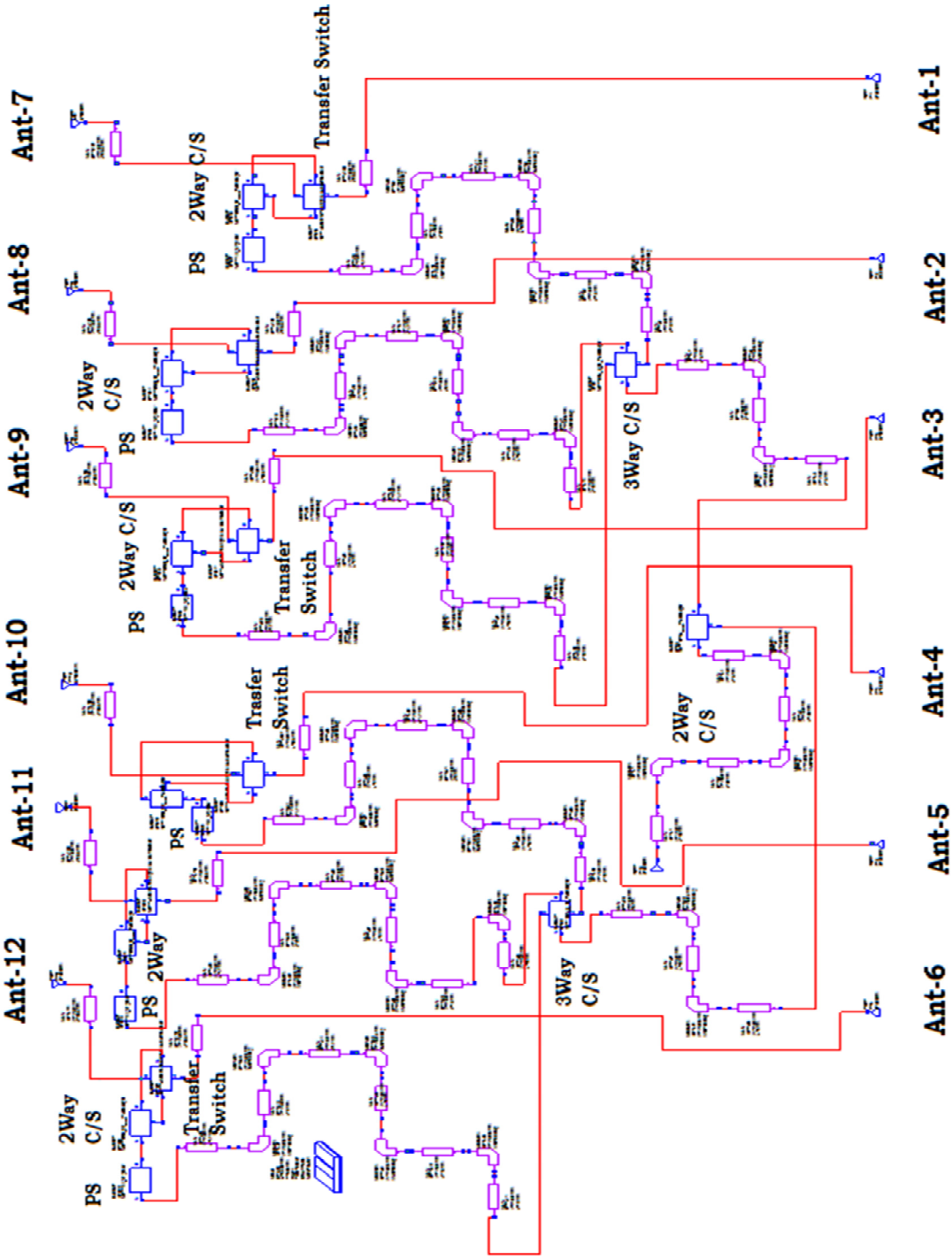

Figure 6.40: Schematic diagram for the MWO model by using the fourth method

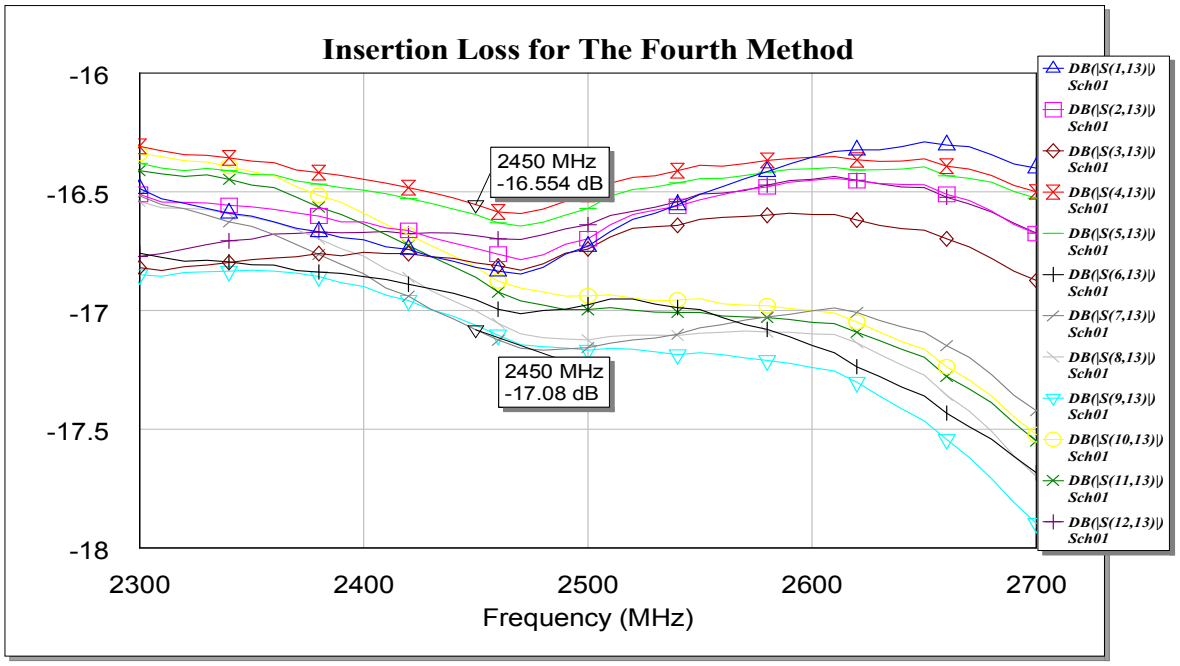

Figure 6.41: The Insertion Loss for The Fourth Method

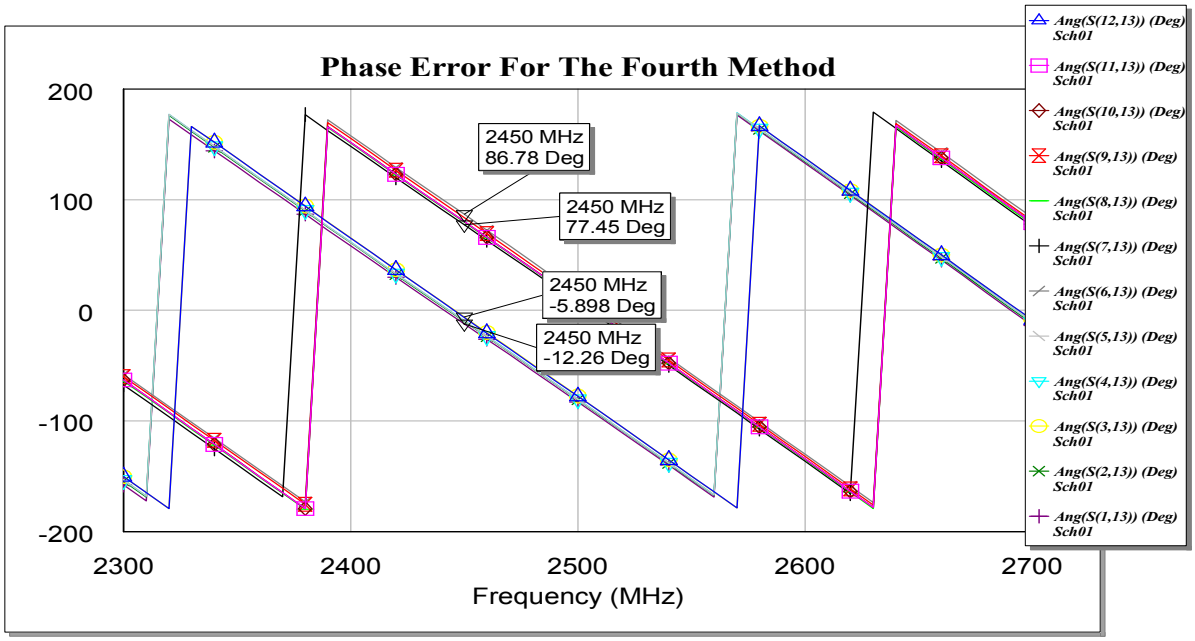

Figure 6.42: The Phase error between the input port and output ports

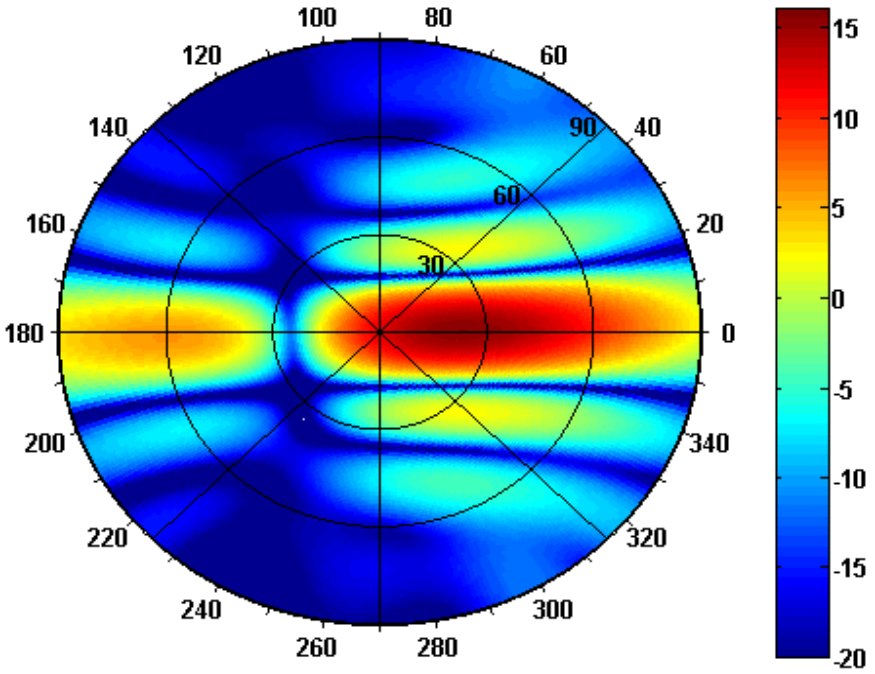

Figure 6.43: Simulated 3D pattern at θ=0,φ=0

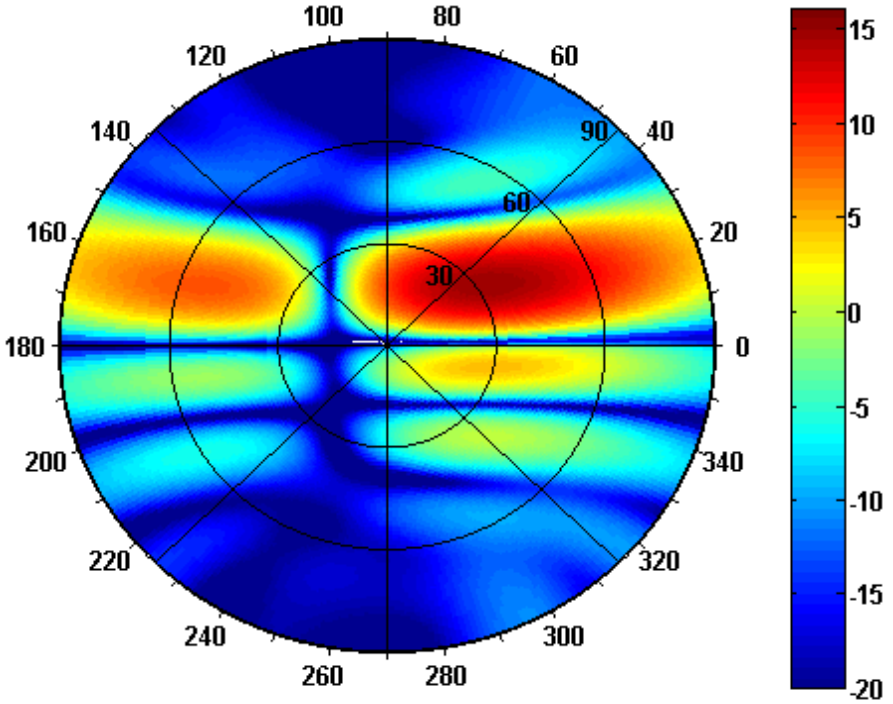

Figure 6.44: Simulated 3D pattern at θ=20,φ=90

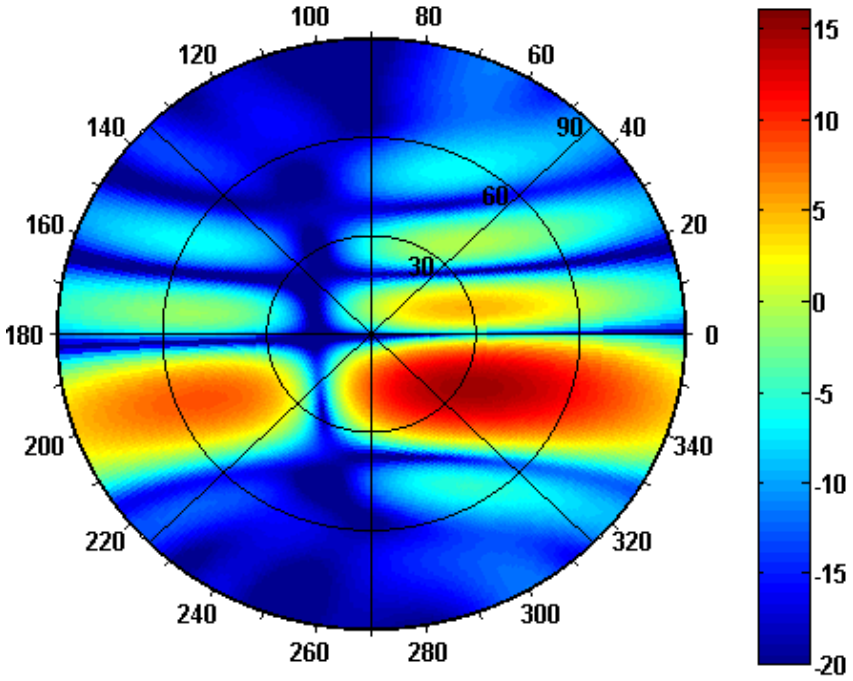

Figure 6.45: Simulated 3D pattern at θ=20,φ=270

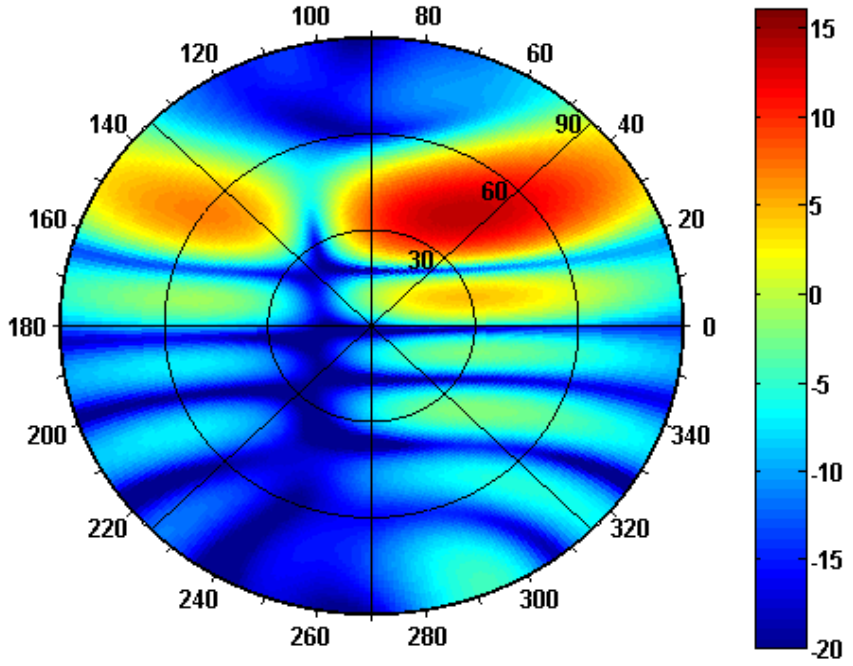

Figure 6.46 Simulated 3D pattern at θ=40,φ=90

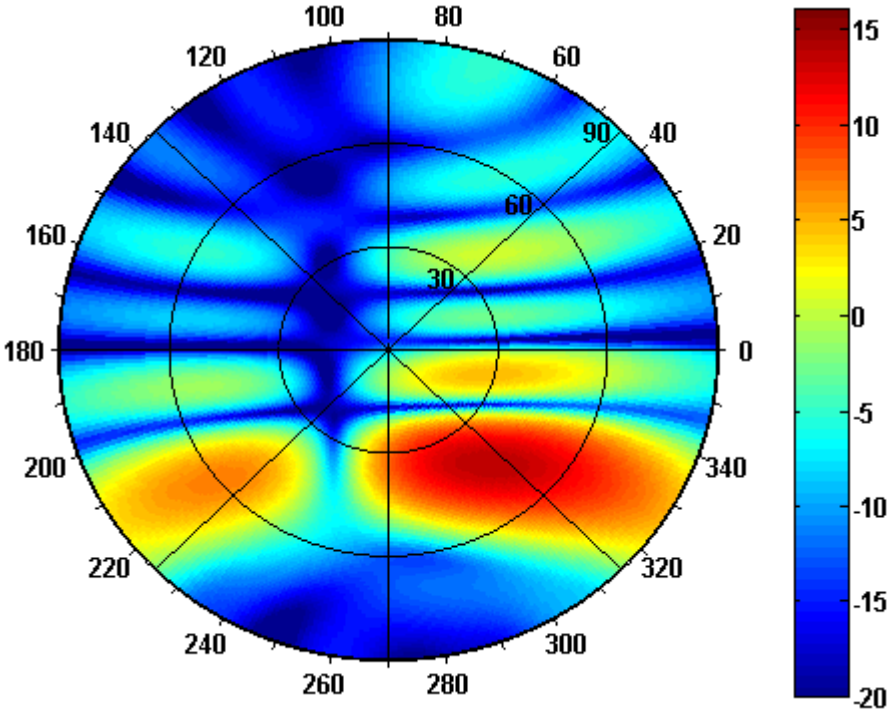

Figure 6.47: Simulated 3D pattern at θ=40,φ=270

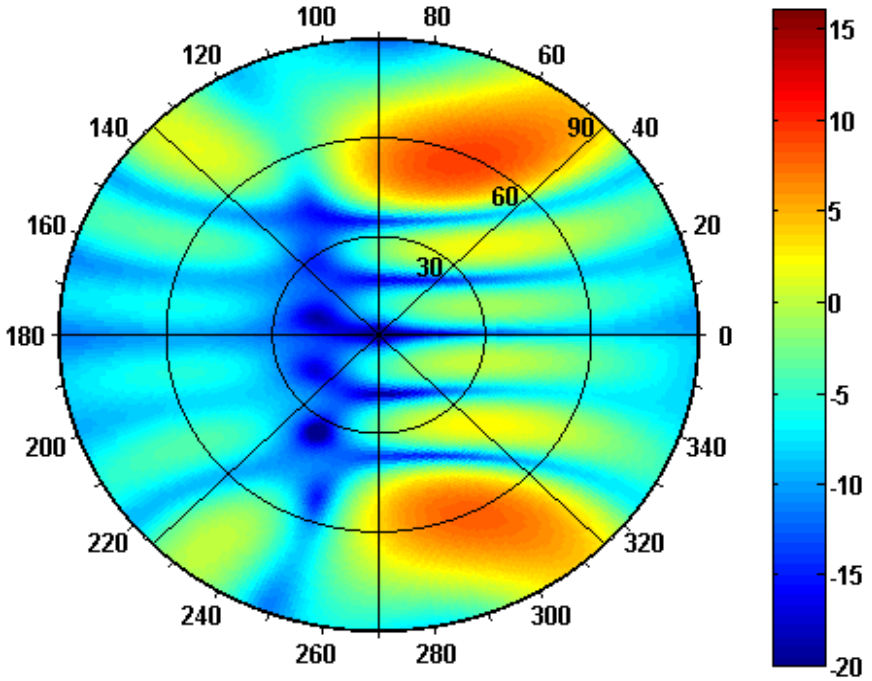

Figure 6.48: Simulated 3D pattern at θ=80,φ=90

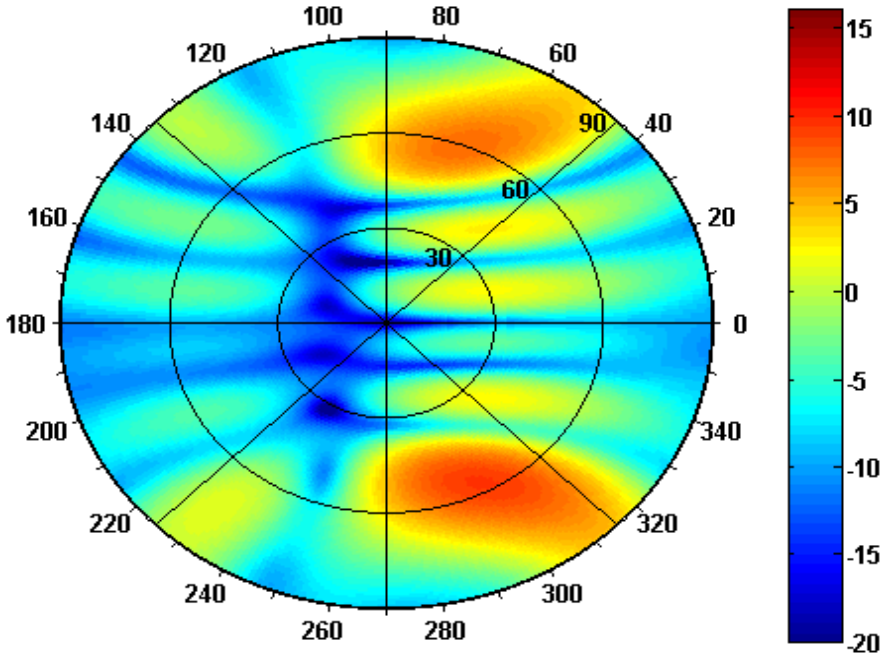

Figure 6.49: Simulated 3D pattern at θ=80,φ=270

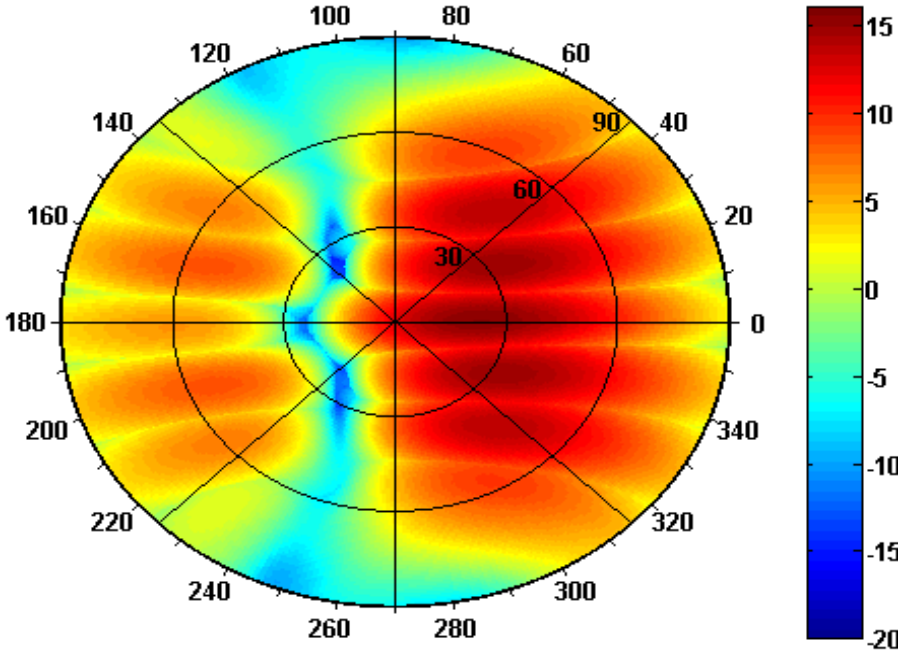

Figure 6.50: Total Coverage For Case-1 in Method 4

In case-1, simulations at ($\theta=0^o$ and $\varphi=0^o$), ($\theta=20^o$ and $\varphi=90^o$), ($\theta=20^o$ and $\varphi=270^o$), ($\theta=40^o$ and $\varphi=90^o$), ($\theta=40^o$ and $\varphi=270^o$), ($\theta=80^o$ and $\varphi=90^o$), ($\theta=80^o$ and $\varphi=270^o$) are shown. As can be shown from the simulations that beam steered towards $\theta=20^o$ and $\varphi=90^o$ is drifted toward right direction because of the 90^o phase difference between the adjacent antenna elements in the same row.

- **Case-2: Combiner Terminal With Leading Phase Connected to The Second Column Of the Array**

The second column of array is the one that contains antenna elements 7, 8, 9, 10, 11 and 12. When the leading terminal of the power combiner/splitter is connected to the second column of the array, then the progressive phases for this case will be as shown in Table 6.9

Table 6.9: The progressive phase for antenna elements in the second case

Antenna Element	Excitation Phase	Antenna Element	Excitation Phase
Ant-1	β_1	Ant-7	β_1+90^o
Ant-2	β_2	Ant-8	β_2+90^o
Ant-3	β_3	Ant-9	β_3+90^o
Ant-4	β_4	Ant-10	β_4+90^o
Ant-5	β_5	Ant-11	β_5+90^o
Ant-6	β_6	Ant-12	β_6+90^o

The gain contour plots for case-2 are shown in Figures 6.51to 6.58. Figure 6.58 shows the total coverage for case-2.

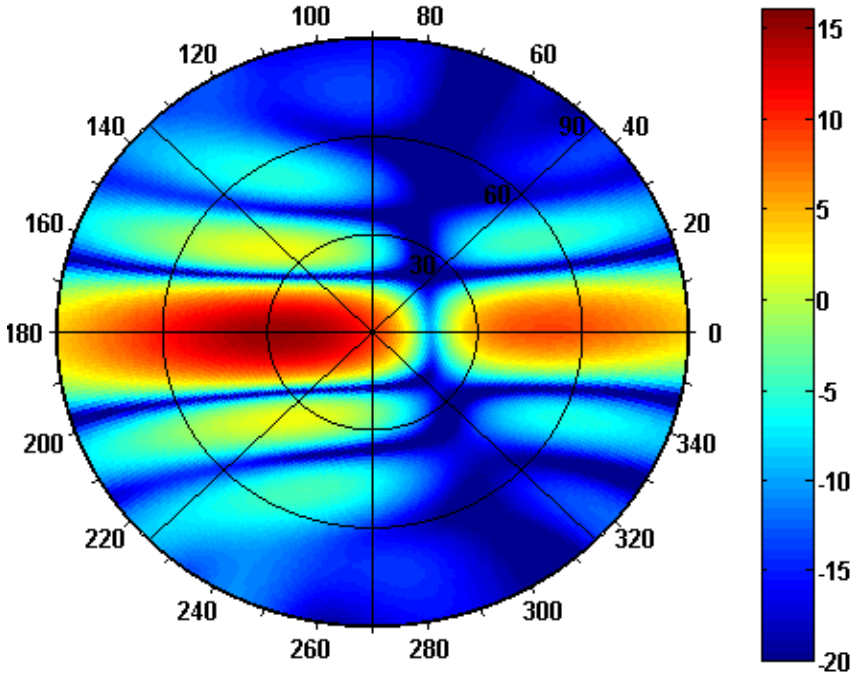

Figure 6.51: Simulated 3D pattern at θ=0,φ=0

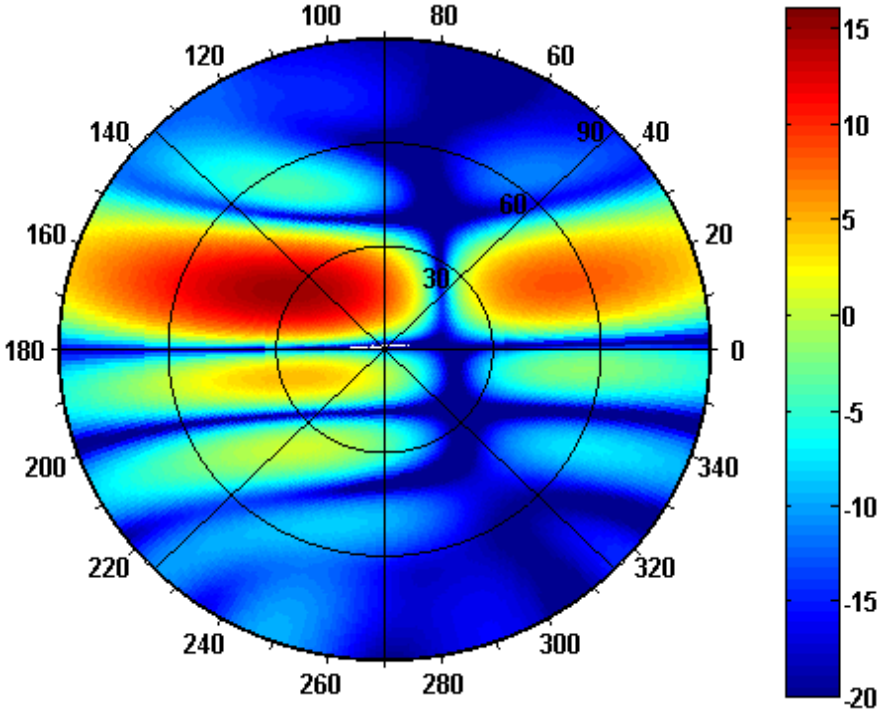

Figure 6.52: Simulated 3D pattern at θ=20,φ=90

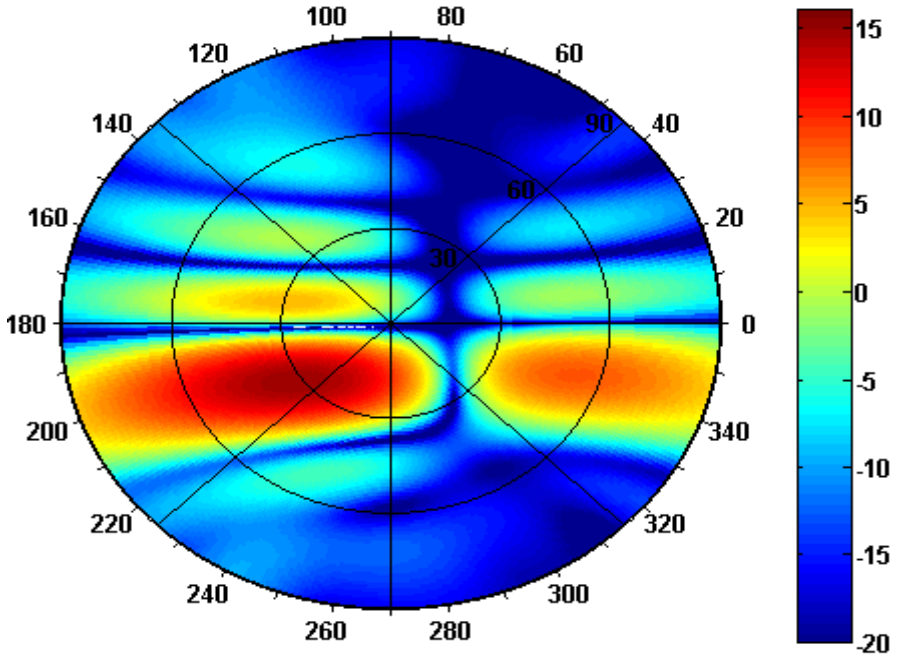

Figure 6.53: Simulated 3D pattern at θ=20,φ=270

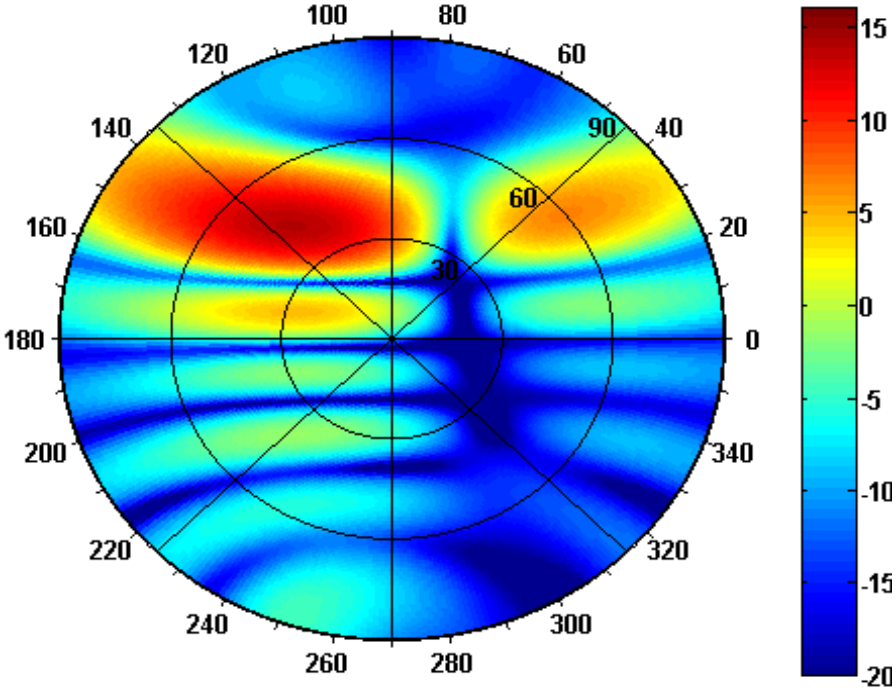

Figure 6.54: Simulated 3D pattern at θ=40,φ=90

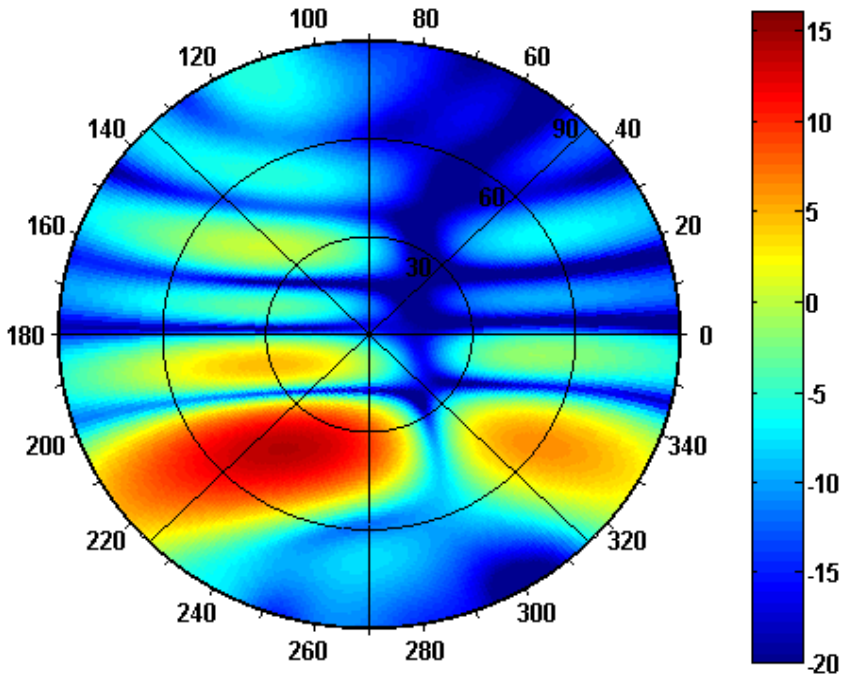

Figure 6.55: Simulated 3D pattern at θ=40,φ=270

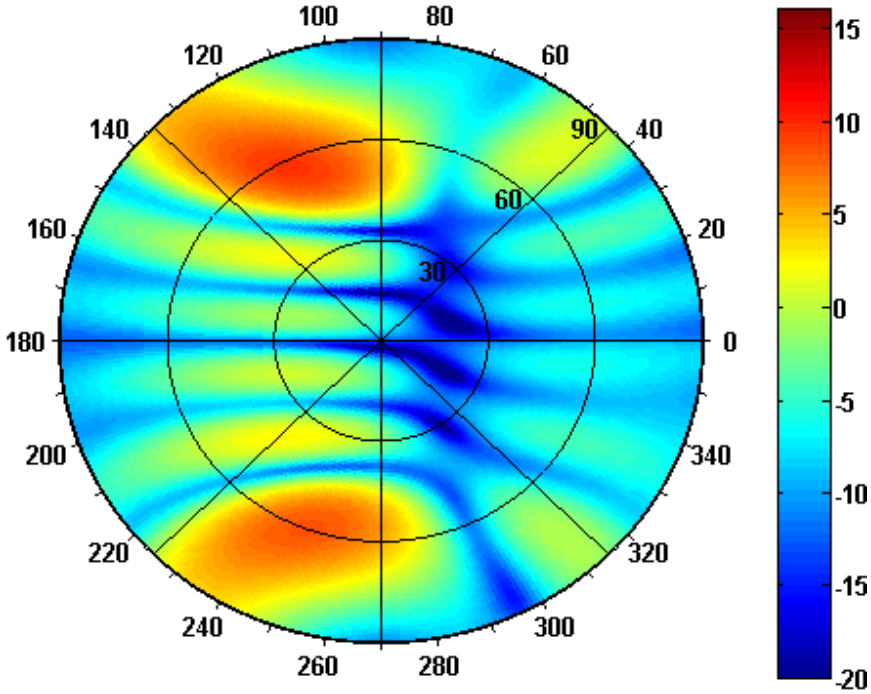

Figure 6.56: Simulated 3D pattern at θ=80,φ=90

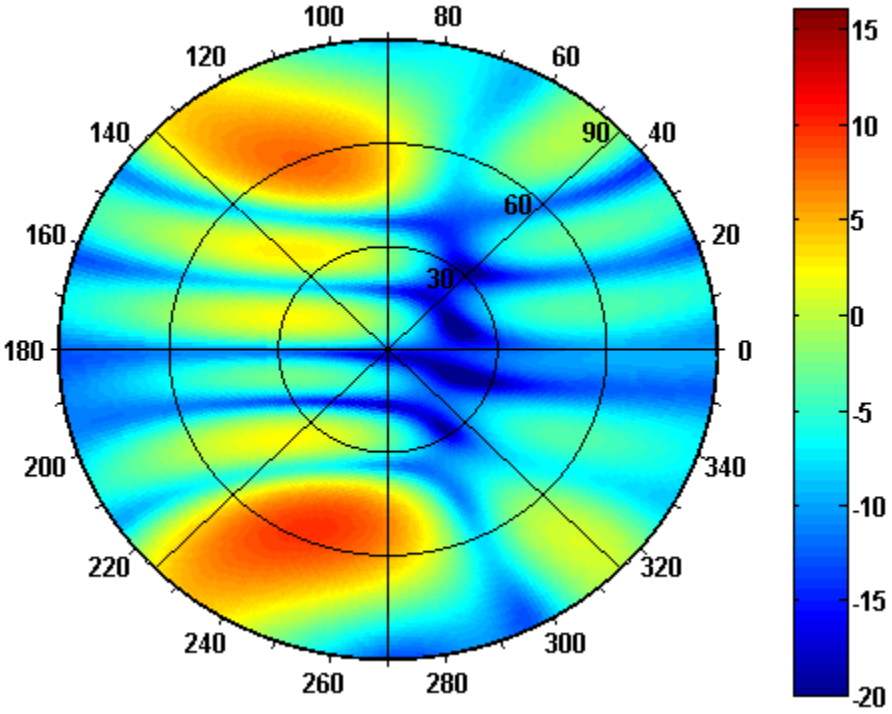

Figure 6.57: Simulated 3D pattern at θ=80,φ=270

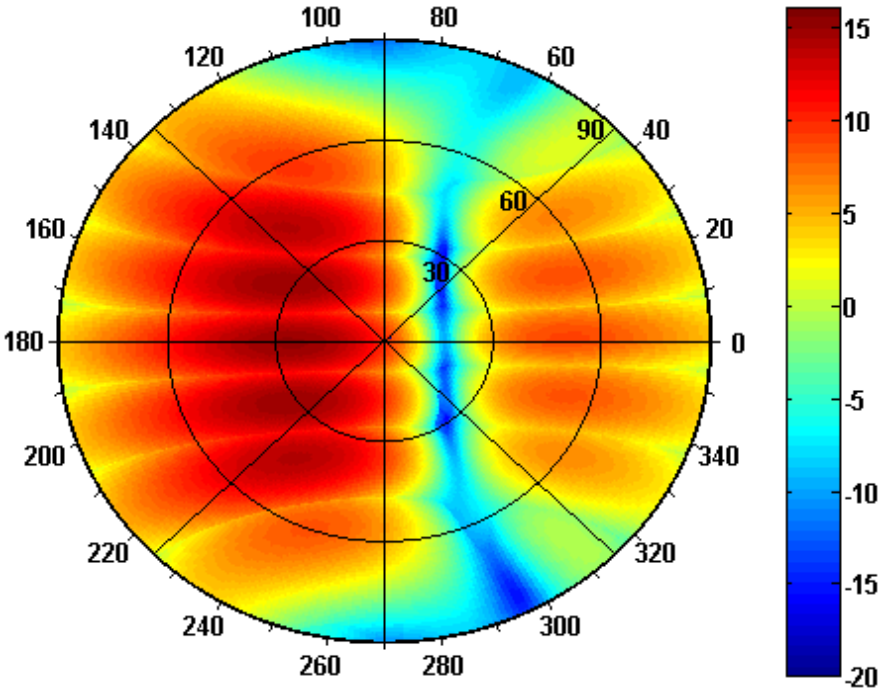

Figure 6.58: Total Coverage For Case-2 in Method 4

Combination between the case-1 and case-2 can be done by using a transfer switch (HMC427LP3/427LP3E) [45]. The transfer switch will take the order from the decision making block to switch to which case according to the location of the vehicle. Figures 6.59 and 6.60 shows the how the total coverage for case-1 and case-2 respectively.

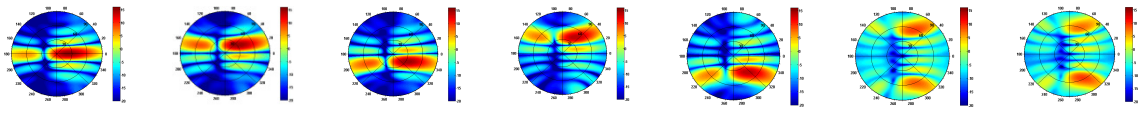

θ=0,φ=0 θ=20,φ=90 θ=20,φ=270 θ=40,φ=90 θ=40,φ=270 θ=80,φ=90 θ=80,φ=270

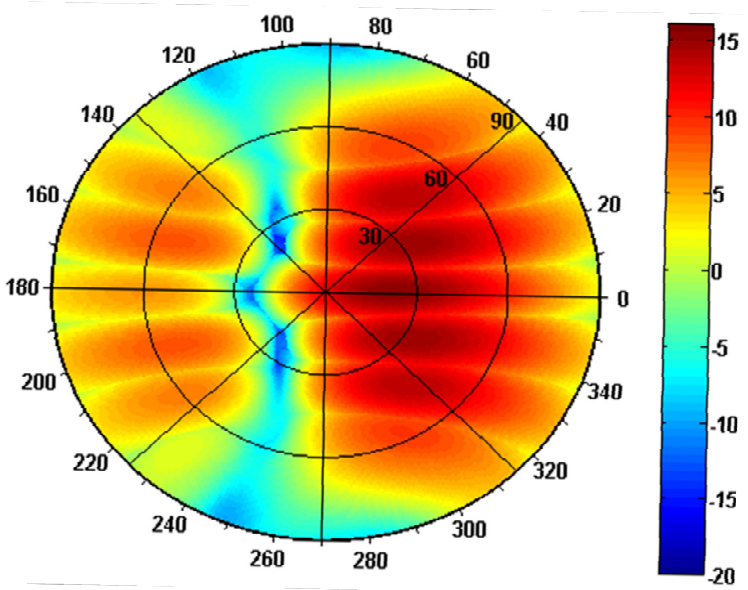

Figure 6.59: Total Coverage For Case-2 in Method 4

The shown Figures 6.48 to 6.55, the beam toward θ=20^{o} and φ=90^{o} is drifted toward left because of the phase difference between the adjacent antenna elements .

Finally by merging Figure 6.59 and 6.60 then we have.

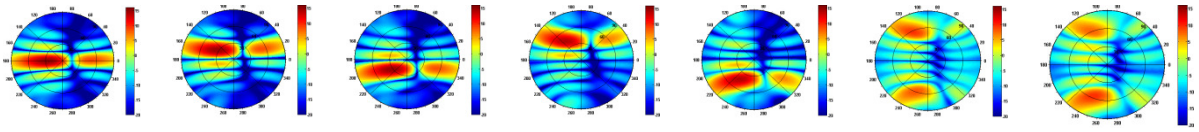

θ=0,φ=0 θ=20,φ=90 θ=20,φ=270 θ=40,φ=90 θ=40,φ=270 θ=80,φ=90 θ=80,φ=270

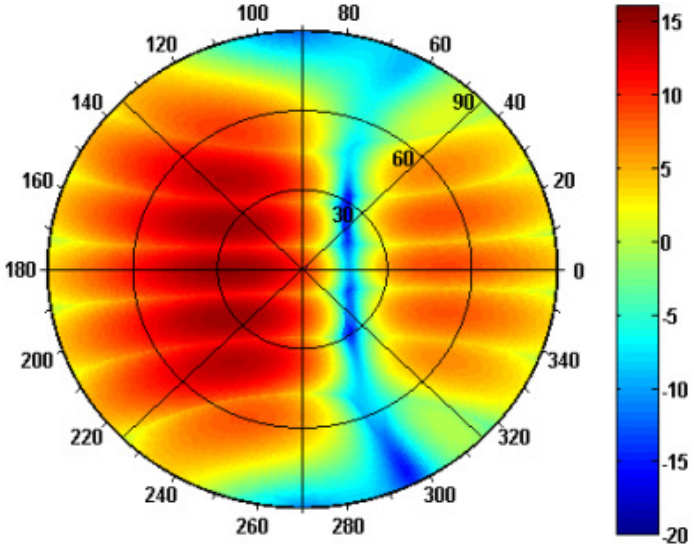

Figure 6.60: Total Coverage For Case-2 in Method 4

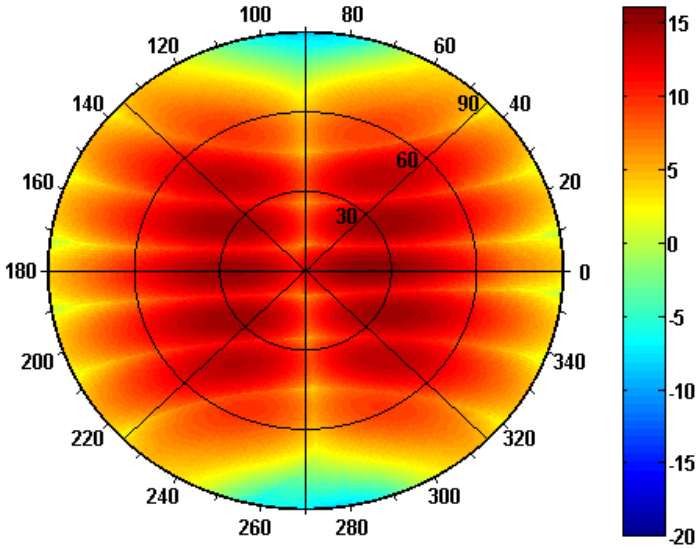

Figure 6.61: Total coverage in method 4

For the transfer switch used in Figure 6.62, the inputs (RF-1 and RF-2) are connected to the two-way power combiner, while the output ports are connected to antenna elements (RF-3 and RF-4). The switching between the two modes is shown in Table 6.10 and can be activated by the decision making block according the UAV location.

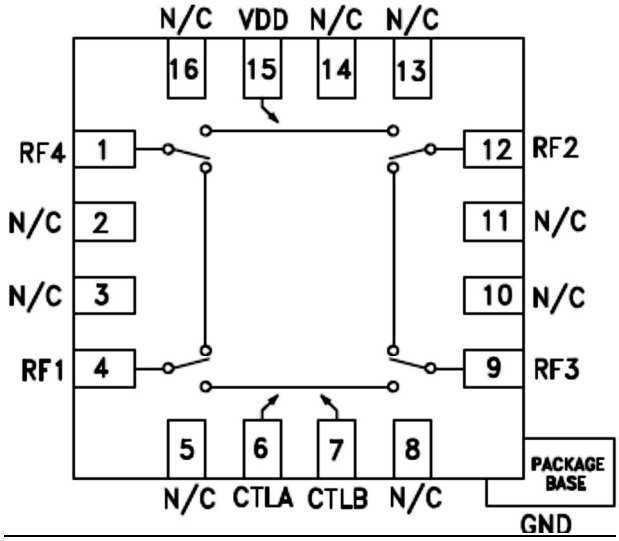

Figure 6.62: Pin diagram for transfer switch [44]

Table 6.10: The Single Path State For Transfer Switch [44]

Control Input		Signal Path State			
A	B	RF4 to RF2	RF1 to RF3	RF4 to RF1	RF2 to RF3
Low	High	On	On	Off	Off
High	Low	Off	Off	On	On

Table 6.11 shows the comparison between the four methods and original design. The reduction in number of phase shifters help in reducing the cost of implementing the feed network. Finally Comparison between the three proposed designs and the implemented design is shown in Table 6.11. The best beam coverage is provided in the fourth design which is also the original design that can provide full coverage, while the first method and third method have good coverage but less than the fourth one.

Table 6. 11: Comparison between the three proposed designs and the implemented design

	First Method	Second Method	Third Method	Fourth Method	Implemented design
Beam Coverage	All Thetas With φ=90,270 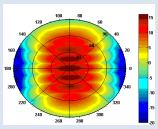	All Thetas With φ=0,180 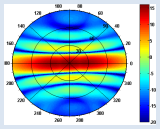	All Thetas With φ=0,90,180,270 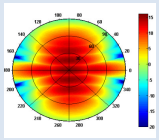	All Thetas With φ=90,270 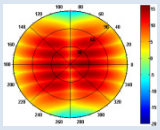	All Thetas and Phi
Average HPBW in Phi	77 Non Overlapped	51 Overlapped	63 Mixture of Overlapped and Non Overlapped	36 in each direction	69
Insertion Loss from feed network	15.8dB	15.5dB	19.5dB up to 26 dB	17dB	15.2dB
Components used	Six phase shifters+ Two 3 way combiner + 6 Two power combiner	Two phase Shifters + four three way combiner+ three two way combiner	Six phase shifter+ Four 3 way power combiner+ eight two way combiner +3 Switch matrix	Six Phase Shifters +One two way combiner + Six Two way hybrid Combiner +two three way combiner	Twelve Phase shifters +one three way power combiner +Three 4 way power combiner
No. Of Control lines	24	4	24+3 Bits for all the switch matrix ICs	24 + two control line	48
Cost	110.5$	48.97$	137.26$	339.1$	201.24$

The worst coverage was obtained using the second method. The insertion loss in the first and the second method is the minimum, while it is the worst in the third method. The first and the second methods have the same insertion loss as the original feed network that contains12 phase shifters. The second method is the least complex design. The first method is designed with simple structure when comparing with the original feed network which is constitute of 12 phase shifters. The third design is considered as the most complex design. The fourth design contains more

components than the first and the second design so it has 1 dB more insertion loss although the fourth method has more components than the first and second methods, the transfer switches can be controlled by two control lines because all the transfer switches have the same status at the same time. But the original feed network has at least 6 phase shifters more than any design. Each phase shifter has four dedicated digital lines that is used in controlling the phase shift state. Which means that the original design has at least 22 digital lines extra than fourth method and 24 extra digital lines that required for the first method. The costs for implementing the first method, second method and the third method are much lower than price for the original design. The cost for the fourth method is more than the implemented design. The cost for the fourth design is much more than original design with 12 phase shifters due to the high cost for the transfer switch (HMC427LP3/427LP3E). If the transfer switch (HMC427LP3/427LP3E) is replaced by transfer switch from anther manufacturer (AS218-000), then the cost will be reduced by 63%.

6.5 Conclusions

In this chapter, four methods for implementing feed network with minimum number of phase shifters were presented. These four methods are compared with the feed network that contains 12 phase shifters. The first method has good coverage with keeping the same insertion loss as the original design. The fourth method has the best coverage among the four methods, but the proposed circuit for this method is more complex than the first method with insertion loss increase by 1 dB.

CHAPTER 7

CONCLUSION S AND FUTURE WORK

7.1 Conclusions

A 12 elements planar antenna array integrated with microwave feed network for beam steering application in single metalized PCB is introduced in this report. This integrated array operated at 2.45GHz frequency with average bandwidth of 30MHz and it is intended for UAV applications due to its light weight (229g). The fabricated unit constituted of 3 layers, an upper one containing the feed network, middle layer acting as a ground plane while the bottom layer had the radiating part that contains the 12 radiating elements. The beam scanning capability of this unit can be achieved in two degrees of freedom ,for elevation and azimuth planes. The desired direction of the antenna beam can be controlled by changing phase shifter values digitally. But the result direction differs with some percentage of error due to approximation done for the value of excitation phase. That is because the 4 bit digitally controlled phase shifter has 22.5^{o} steps, so it is dealing with integer number of steps. The S-parameters of the fabricated prototype match the simulations. This work also includes a beam steering network with minimum number of phase shifters under the constraint of covering the majority of space below the array.

7.2 Future Work

Conduct gain measurements on the V2 array that was recently obtained and verify its new features. An actual implementation of the minimum phase shifting architecture and measure its performance to be done. Finally, to perform an actual system level fly verify that complete system works.

Reference

[1] M. S. Sharawi, D. N. Aloi, and O. A. Rawashdeh, "Design and implementation of embedded printed antenna arrays in small UAV wing structures," *IEEE Trans. On Antennas and Propagation.*, vol. 58, no. 8, pp. 2531–2538, 2010.

[2] "Signal Source Searching and Tracking via Antenna Array Beam Steering on Fixed Wing UAVs for Communication Link Enhancement," Thesis.

[3] C. A. Balanis, *Modern Antenna Handbook*. John Wiley & Sons, 2011.

[4] C. A. Balanis, *Antenna Theory: Analysis and Design*. John Wiley & Sons, 2012.

[5] E. O. Hammerstad, "Equations for Microstrip Circuit Design," in *Microwave Conference, 1975. 5th European*, 1975, pp. 268–272.

[6] D. M. Pozar, *Microwave Engineering*, 4 edition. Hoboken, NJ: Wiley, 2011.

[7] http://www.qsl.net/va3iul/

[8] P. Kishan, "Microwave ferrites for phase shifters," *Bulletin of Materials Science*, vol. 18, no. 6, pp. 679–692, Oct. 1995.

[9] M. Chua and K. Martin, "A 1GHz programmable analog phase shifter for adaptive antennas," *Proc. IEEE Custom Integrated Circuits Conference*, pp. 11-14, May 1998.

[10] M. Margolis, *Arduino Cookbook*. O'Reilly Media, Inc., 2011.

[11] M. Banzi, *Getting Started with Arduino*. O'Reilly Media, Inc., 2009.

[12] T. Lambard, O. Lafond, M. Himdi, H. Jeuland, S. Bolioli, and L. Le Coq, "Ka-Band Phased Array Antenna for High-Data-Rate SATCOM," *IEEE Antennas Wirel. Propag. Lett.*, vol. 11, pp. 256–259, 2012.

[13] N. Neveu, Y.-K. Hong, J. Lee, J. Park, G. Abo, W. Lee, and D. Gillespie, "Miniature Hexaferrite Axial-Mode Helical Antenna for Unmanned Aerial Vehicle Applications," *IEEE Transactions on Magnetics.*, vol. 49, no. 7, pp. 4265–4268, Jul. 2013.

[14] M. S. Sharawi, O. A. Rawashdeh, and D. N. Aloi, "Performance of an embedded monopole antenna array in a UAV wing structure," *in Proc. of 15th IEEE Mediterranean Electrotechnical Conference* (*MELECON 2010),* Valletta, Malta,Apr. 2010, pp. 835-838. - 2010 15th IEEE Mediterranean Electrotechnical Conference, 2010, pp. 835–838.

[15] M. Sazegar, Y. Zheng, H. Maune, C. Damm, X. Zhou, J. Binder, and R. Jakoby, "Low-Cost Phased-Array Antenna Using Compact Tunable Phase Shifters Based on Ferroelectric Ceramics," *IEEE Trans. Microw. Theory Tech.*, vol. 59, no. 5, pp. 1265–1273, May 2011.

[16] M. A. Y. Abdalla, K. Phang, and G. V. Eleftheriades, "A Planar Electronically Steerable Patch Array Using Tunable PRI/NRI Phase Shifters," *IEEE Trans. Microw. Theory Tech.*, vol. 57, no. 3, pp. 531–541, Mar. 2009.

[17] M. Tsuji, T. Nishikawa, K. Wakino, and T. Kitazawa, "Bi-directionally fed phased-array antenna downsized with variable impedance phase shifter for ISM band," *IEEE Trans. Microw. Theory Tech.*, vol. 54, no. 7, pp. 2962–2969, Jul. 2006.

[18] T.-Y. Yun and K. Chang, "A low-cost 8 to 26.5 GHz phased array antenna using a piezoelectric transducer controlled phase shifter," *IEEE Trans. Antennas Propag.*, vol. 49, no. 9, pp. 1290–1298, Sep. 2001.

[19] J. Cha, Y. Kuga, A. Ishimaru, and S.-W. Lee, "A 20 GHz Steerable Array Antenna Using 3-bit Dielectric Slab Phase Shifters on a Coplanar Waveguide," *IEEE Trans. on Antennas and Propag.*, vol. 55, no. 2, pp. 290–297, Feb. 2007.

[20] W. Gautier, A. Stehle, C. Siegel, B. Schoenlinner, V. Ziegler, U. Prechtel, and W. Menzel, "Hybrid Integrated RF-MEMS Phased Array Antenna at 10GHz," in *38th European Microwave Conference (EuMc),* Oct.27–31, 2008, pp. 139–142.

[21] Y. Li, M. F. Iskander, Z. Zhang, and Z. Feng, "A New Low Cost Leaky Wave Coplanar Waveguide Continuous Transverse Stub Antenna Array Using Metamaterial-Based Phase Shifters for Beam Steering," *IEEE Trans. Antennas and Propagation.*, vol. 61, no. 7, pp. 3511–3518, Jul. 2013.

[22] T. Ji, H. Yoon, J. K. Abraham, and V. K. Varadan, "Ku-band antenna array feed distribution network with ferroelectric phase shifters on silicon," *IEEE Trans. Microw. Theory Tech.*, vol. 54, no. 3, pp. 1131–1138, Mar. 2006.

[23] J. H. Kim and W. S. Park, "A Hadamard Matrix Feed Network for a Dual-Beam Forming Array Antenna," *IEEE Trans. Antennas and Propagation.*, vol. 57, no. 1, pp. 283–286, Jan. 2009.

[24] T.-Y. Kim, Y.-M. Yoon, G.-S. Kim, and B.-G. Kim, "A Linear Phased Array Antenna Composed of Inductive Loaded Patch Antennas," *IEEE Antennas Wirel. Propag. Lett.*, vol. 10, pp. 1051–1054, 2011.

[25] Y.-M. Yoon, H.-M. Koo, T.-Y. Kim, and B.-G. Kim, "Effect of Edge Reflections on the Mutual Coupling of a Two-Element Linear Microstrip Patch Antenna Array Positioned Along the E-Plane," *IEEE Antennas Wirel. Propag. Lett.*, vol. 11, pp. 783–786, 2012.

[26] P. S. Apostolov, "Linear Equidistant Antenna Array With Improved Selectivity," *IEEE Trans. Antennas and Propag.*, vol. 59, no. 10, pp. 3940–3943, Oct. 2011.

[27] Y. Liu, Z. Nie, and Q.-H. Liu, “Reducing the Number of Elements in a Linear Antenna Array by the Matrix Pencil Method,” *IEEE Trans. Antennas and Propagation.*, vol. 56, no. 9, pp. 2955–2962, Sep. 2008.

[28] W. Zhang, L. Li, and F. Li, “Reducing the Number of Elements in Linear and Planar Antenna Arrays With Sparseness Constrained Optimization,” *IEEE Trans. Antennas and Propagation.*, vol. 59, no. 8, pp. 3106–3111, Aug. 2011.

[29] M. S. Sharawi, M. Ibrahim, S. Deif, and D. N. Aloi, “A PLANAR PRINTED ANTENNA ARRAY EMBEDDED IN THE WING STRUCTURE OF A UAV FOR COMMUNICATION LINK ENHANCEMENT,” *Progress in Electromagnetic. Research, PIER*, vol. 138, pp. 697–715, 2013.

[30] M. Ibrahim, S. Deif, and M. S. Sharawi, “A 14-element printed planar antenna array embedded within a UAV structure,” in *Antennas and Propagation Conference (LAPC), 2012 Loughborough*, 2012, pp. 1–4.

[31] O. H. Karabey, A. Gaebler, S. Strunck, and R. Jakoby, “A 2-D Electronically Steered Phased-Array Antenna With 2 2 Elements in LC Display Technology,” *IEEE Trans. Microw. Theory Tech.*, vol. 60, no. 5, pp. 1297–1306, May 2012.

[32] R. Gomez-Garcia, M. Sanchez-Renedo, and J.-M. Munoz-Ferreras, “A Type of Planar Array-Antenna Feeding Network With Single/Multiband Filtering Capability,” *IEEE Antennas Wirel. Propag. Lett.*, vol. 9, pp. 1271–1274, 2010.

[33] W. Lee, Y.-K. Hong, J. Lee, D. Gillespie, K. G. Ricks, F. Hu, and J. Abu-Qahouq, “Dual-Polarized Hexaferrite Antenna for Unmanned Aerial Vehicle (UAV) Applications,” *IEEE Antennas Wirel. Propag. Lett.*, vol. 12, pp. 765–768, 2013.

[34] Z.-Q. Liu, Y.-S. Zhang, Z. Qian, Z. P. Han, and W. Ni, “A Novel Broad Beamwidth Conformal Antenna on Unmanned Aerial Vehicle,” *IEEE Antennas Wirel. Propag. Lett.*, vol. 11, pp. 196–199, 2012.

[35] Altium designer," 2011. [Online]. Available: www.altium.com

[36] M.-C. Inc., \Ultra-small ceramic, surface mount power splitter/combiner, scn-3-28," 2013. [Online]. Available: http://http://www.mini-circuits.com/.

[37] 4-way surface mount power splitter/combiner, bp4u1+," 2013. [Online]. Available: //http://www.mini-circuits.com

[38] 4-Bit digitally controlled phase shifter, MAPS-010144 Available online : //http:// http://www.macom.com/.

[39] //http://www.emtalk.com

[40] M. I. Montrose, *EMC and the Printed Circuit Board: Design, Theory, and Layout Made Simple*. John Wiley & Sons, 2004.

[41] Ansoft HFSS version 13.

[42] "MATLAB - The Language of Technical Computing." [Online]. available: http://www.mathworks.com/products/matlab/. [Accessed: 26-Nov-2012].

[43] Microwave office," 2009. [Online]. Available: http://www.awrcorp.com

[44] Switch Matrix (HMC276LP4 / HMC276LP4E) Hittite microwave," http://www.hittite.com/. [Online]. Available: http://www.hittite.com/

[45] Transfer Switch (HMC427LP3/427LP3E), Hittite microwave," http://www.hittite.com/. [Online]. Available: http://www.hittite.com/

Vitae

Name :Saeed Ahmed AL Dweik

Nationality :Jordan

Date of Birth :7/21/1985

Email :aldweik_63@hotmail.com

Address : Hebron, Palestine

Academic Back ground : B.Sc. in Electrical Engineering(Ajman University of Science and technology.

Work Experience :Electromechanical Engineer and inspector [2010/2012].

Emirates Integrated Telecommunications Company 'du'

:Electrical Engineer: Ittihad Electric Company [2008 / 2010].

Dubai, UAE

List of Publications

1. S. Dweik, S. Deif, W. Sadeh, O. A. Rawashde D. N. Aloi, M. S. Sharawi, "A Planar Antenna Array with Integrated Feed Network for UAV Applications," in 8th European Conference on Antennas and Propagation (EuCAP) , The Hague, The Netherlands, 6-11 April 2014.
2. Saeed. A. AL. Dweik. and. M. S. Sharawi, "Investigating Two Minimized Phase Shifter Methods for a Planar Phased Array," in Loughborough Antennas & Propagation Conference, Loughborough , UK, 2014.